

POLITECNICO DI TORINO

College of Chemical Engineering and Materials

Master of Science in Chemical and Sustainable Processes Engineering

Master Thesis Degree

Enhancement of the mechanical properties of 3D-printable objects by dual curing procedures.



Supervisors:

Prof. Sangermano Marco (Polytechnic of Turin)
Prof. Angels Serra Albet (Rovira i Virgili University)
Prof. Fernández-Francos Xavier (Polytechnic University of Catalonia)
Prof. Ramis Xavier (Polytechnic University of Catalonia)

Candidate
Di Donato Fabio

March 2019

Table of contents

TABLE OF CONTENTS.....	3
PREFACE.....	5
ACRONYMS AND ABBREVIATION	6
RIASSUNTO IN ITALIANO	8
SUMMARY	23
1 INTRODUCTION	24
1.1 Classification of polymers materials.....	24
1.2 Thermosets.....	25
1.3 Photopolymerization	37
1.4 Dual-Curing	39
2 MATERIALS, CHARACTERIZATION AND METHODS.....	42
2.1 Materials	42
2.2 Preparation of formulations.....	43
2.2.1 Base individual system	43
2.2.2 Dual curing system	43
2.3 Experimental characterization techniques	44
2.3.1 Differential Scanning Calorimetry (DSC).....	44
2.3.2 Dynamic Mechanical Analysis (DMA).....	46
2.3.3 Fourier-transform infra-red spectroscopy (FTIR/ATR)	48
2.3.4 Thermogravimetric analysis (TGA)	49
2.3.5 Soluble fraction analysis.....	50
2.3.6 Storage stability analysis	51
2.4 Kinetics methods and models.....	52
3 RESULT AND DISCUSSION	54
3.1 Base systems analysis	54
3.1.1 Spot-HT	54
3.1.2 Cationic epoxy formulation	57
3.1.3 Feasibility of the dual-curing system.....	63

3.2	Analysis of dual systems	64
3.2.1	Analysis of photo-curing stage.....	64
3.2.2	Analysis of thermal curing stage.....	72
3.2.3	Analysis of storage stability	83
4	CONCLUSION	85
5	BIBLIOGRAPHY	86
6	ACKNOWLEDGEMENTS	91
	LIST OF FIGURES	92
	LIST OF TABLES	95

PREFACE

Components produced by additive manufacturing face a number of drawbacks derived from the difficulty in controlling accurately the shape while ensuring uniform mechanical properties. With this thesis it is intended to design a family of materials that can be used in 3D-printing by MIP-SL, with enhanced assets, overcoming these drawbacks, based on dual-curing chemistry.

Understanding the structure-properties relationships in thermosets is essential in order to understand their applicability to different processing or end-use scenarios. The target of this thesis is to analyze how the intermediate and final material, obtained through the dual-curing polymerization, and their applications in the area of 3D-printing, are affected by the structure and properties of the thermosets. The work presented in this thesis has been carried out within a research group with extensive experience on the analysis and characterization of thermosetting systems and leading an active research line focused on development of dual-curable systems.

ACRONYMS AND ABBREVIATION

$\left(\frac{dm}{dt}\right) * \left(\frac{1}{m_0}\right)$	Mass loss rate
$\frac{d\alpha}{dt}$	Rate of degree of conversion
$\frac{dh}{dt}$	Reaction Heat Flow
$\frac{m}{m_0}$	Mass loss
α	Degree of conversion
α_t	Total degree of conversion
η	Viscosity
Base-3D	Spot-HT
CI	Cationic initiator (antimony hexafluoride-based catalyst)
DMA	Dynamic mechanical analysis
DSC	Differential scanning calorimetry
E'	Storage Modulus
E''	Loss Modulus
E_a	Activation Energy
EL	Cycloaliphatic epoxy, bis[(3,4-epoxycyclohexyl)methyl]adipate
ES	Cycloaliphatic epoxy, 3,4-epoxycyclohexylmethyl - 3',4'- epoxycyclohexanecarboxylate
FTIR	Fourier transform infrared spectroscopy
HEMA	2-hydroxyethyl methacrylate
k_a	Rate constant for monomer association
k_d	Dissociation rate constant

k_p	Propagation rate constant
k_{tc}	Combination termination rate
k_{td}	Disproportionation termination rate
k_{tr}	Transfer termination rate
PC	Propylene carbonate
Tan δ	Loss factor, ratio between the loss modulus and storage modulus
TEA	Triethanolamine
T_g	Glass transition temperature
$T_{g,gel}$	Temperature which gelation and vitrification coincide
$T_{g\infty}$	Glass transition temperature of the fully cured network
T_{g0}	Glass transition temperature of the unreacted material
TGA	Thermogravimetric analysis

RIASSUNTO IN ITALIANO

I. Introduzione

Al giorno d'oggi, i polimeri termoindurenti trovano impiego in un numero significativo di applicazioni per prodotti come adesivi, tessuti, pneumatici, e packaging ma sono anche usati come materiali compositi per i rivestimenti nel settore automotive, navale, ed aerospaziale. Uno dei campi di maggior rilievo, trattati in questa tesi, è quello del 3D-printing process.

Con questo progetto, l'obiettivo che ci si propone di raggiungere è il dual-curing di polimeri termoindurenti, volto all'ottenimento di materiali aventi proprietà che risultano essere ottimizzate rispetto a quelle iniziali. Questo trattamento rende il prodotto finale adatto ad un vasto campo di applicazioni tecnologiche ad alto valore aggiunto.

La strategia adottata è stata quella di controllare la prima reazione di curing, tramite la quale è possibile ottenere una formulazione stabile e successivamente, influenzare il secondo trattamento termico al fine di progettare un materiale con funzionalità termiche e meccaniche potenziate.

Il sistema di dual-curing, su cui abbiamo focalizzato il nostro lavoro, è il risultato di una combinazione tra una formulazione UV-polimerizzabile a base di acrilati, usata nei processi di stampa 3D, e l'aggiunta di una componente epossidica attivabile per via termica. Nel primo stage, la fotopolimerizzazione degli acrilati è innescata mediante l'attivazione del foto iniziatore attraverso l'irradiazione di luce ultravioletta. Diversamente accade per la reazione di omo-polimerizzazione cationica in cui sono coinvolti i gruppi epossidici, che si sviluppa solo dopo aver stimolato termicamente l'iniziatore cationico.

II. Materiali e metodi

Il sistema reattivo impiegato, durante il processo di UV-curing, è basato su una omo-polimerizzazione radicalica di formulazioni bi-componente costituite da:

- *Spot-HT*, preparato fornito da Spot-A Materials (Barcellona, Spagna) e composto da una miscela di acrilati con foto iniziatore avente una banda di assorbimento compresa nella regione dello spettro UV-visibile.
- *Resina epossidiche*, procurate da The Dow Chemical Company che sono Cycloaliphatic epoxy, 3,4-epoxycyclohexylmethyl - 3',4'-epoxycyclohexanecarboxylate (ES, CYRACURE UVR-6105)
- Altri additivi sono stati utilizzati nella preparazione delle diverse formulazioni come *l'agente legante* (2-hydroxyethyl methacrylate (CA, HEMA), fornito da Sigma-Aldrich), *l'iniziatore cationico* (CI) K-PURE® CXC-1612 che è un catalizzatore a base esa-fluoruro di antimonio utilizzato nella polimerizzazione cationica attivata termicamente e *l'agente stabilizzante* Triethanolamine (TEA), fornito da Sigma Aldrich ed usato così come ricevuto.

Poiché tutti i reagenti (Spot-HT, resine epossidiche ed altri componenti) sono liquidi, la preparazione dei campioni avviene nella seguente maniera. Una volta preparate, le fiale contenenti le formulazioni vengono incartate ed avvolte in una pellicola di alluminio al fine di evitare l'attivazione prematura da parte della luce solare ed infine immagazzinate nel congelatore a basse temperature. Le formulazioni, generalmente, contengono i seguenti componenti:

- Resina epossidica (ES o EL): 0, 10, 20, 30, 40 wt. %
- Agente legante (CA): 0, 1, 2, 5 wt. %
- Spot-HT: fino a saturazione del 100 wt. %
- Iniziatore cationico (CI), 1 phr (parts per hundred) in soluzione al 50 wt. % in solvente PC, contenente anche l'agente stabilizzante (TEA) con un rapporto in massa rispettivamente del 5%, 10%, 20% rispetto al CI.

Un sistema di codifica è stato impiegato per sottolineare le diverse quantità e proporzioni dei reagenti utilizzati nelle differenti formulazioni:

$ES_xCA_yCI_{z-t}$ o $EL_xCA_yCI_{z-t}$

Dove:

- x è la percentuale in massa wt. % della componente epossidica
- y è la percentuale in massa wt. % dell'agente legante
- z è il phr dell'iniziatore CI
- t è il rapporto in massa dell'agente stabilizzante TEA rispetto all'iniziatore CI

Mediante la variazione sistematica dei parametri appena descritti, che caratterizzano le formulazioni studiate, è stato possibile valutare gli effetti che tali cambiamenti provocano sulle cinetiche di reazione di foto e termo-polimerizzazione, e su campioni dove il processo di dual-curing è stato prima parzialmente e poi totalmente completato.

Le tecniche di misurazione adoperate per caratterizzare la stabilità dei materiali prodotti e le proprietà acquisite con la reazione di dual-curing sono state la differential scanning calorimetry (DSC), thermo-gravimetric analysis (TGA), dynamic mechanical analysis (DMA), and the Fourier transformed infrared radiation (FTIR). Analisi aggiuntive come la misurazione della frazione solubile e test di storage stability sono stati realizzati. Includendo poi, anche dei test specifici, su campioni differenti, è stato possibile sviluppare un modello predittivo e monitorare l'intero processo di indurimento.

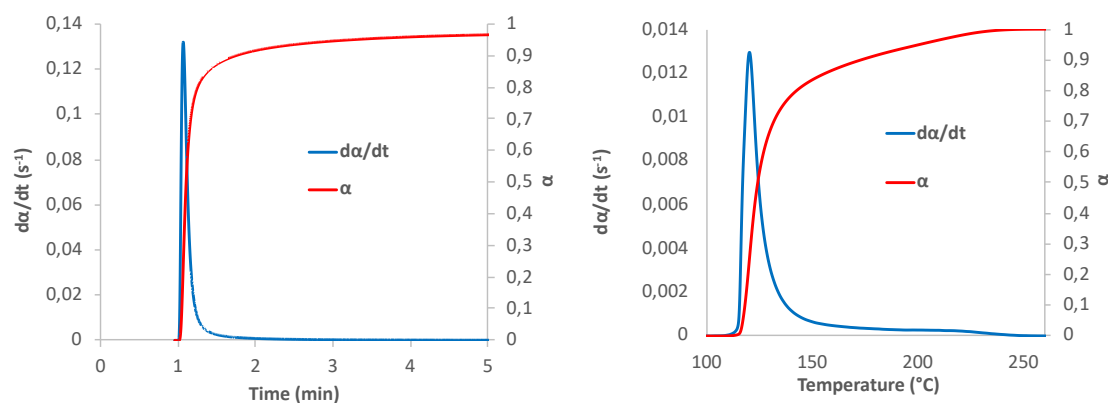
III. Risultati e discussioni

Analisi preliminari

Prima di tutto, sono state analizzate le reazioni di polimerizzazione rispettivamente dello Spot-HT e della formulazione epossidica base ES100CI1-0.1, con l'intenzione di

comprendere le loro cinetiche e proprietà e quindi, in battuta finale, di analizzare la fattibilità del processo di dual-curing.

Il Graph A confronta i risultati delle analisi al DSC durante il processo di photo-curing dello Spot-HT a 30 °C e la fase dinamica di thermal-curing a 10 °C/min per l'ES100CI1-0.1. Come può essere visto, la reazione di photo-curing dello Spot-HT è decisamente rapida, essa si sviluppa in un tempo inferiore ad un minuto a temperatura ambiente. Contrariamente, il processo di thermal-curing di ES100CI1-0.1 è altrettanto veloce ma è innescato a temperature superiori ai 100 °C. Inoltre, la forma della curva è indice del fatto che è presente una latenza termica. Le diverse cinetiche e la possibilità di attivare in maniera indipendente entrambe le polimerizzazioni (radiazione-UV e temperatura) suggerisce che l'unione, nel processo sequenziale di dual-curing, tra gruppi acrilici e sostituenti epossidici, potrebbe essere efficace.



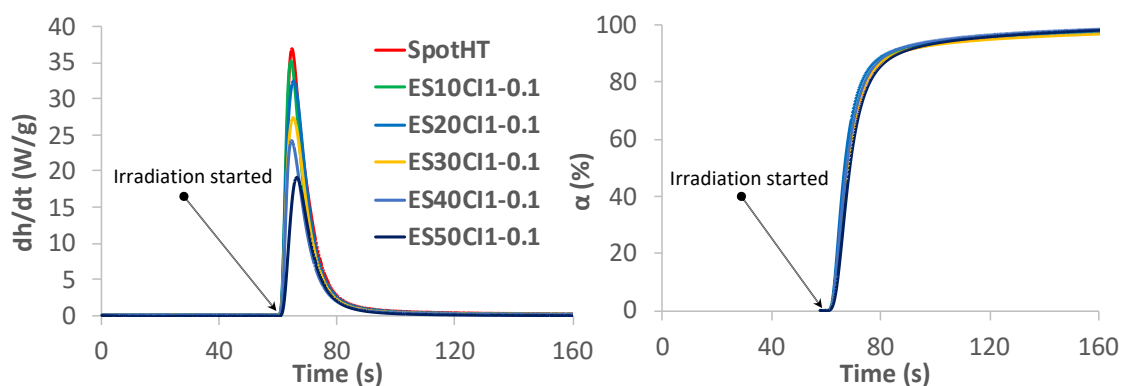
Graph A. Confronto della velocità di reazione e grado di conversione per il trattamento is termico di UV-curing a 30 °C per la formulazione base Spot-HT (sinistra) ed il curing dinamico a 10 °C/min per la formulazione epossidica ES100CI1-0.1 (destra).

Entrambe le reazioni di polimerizzazione sono altamente esotermiche. Il processo che coinvolge gli acrilati provoca il rilascio di 355 J/g mentre la susseguente reazione dei gruppi epossidici libera 620 J/g. Il valore ottenuto sperimentalmente dalla resina epossidica pura è in linea con i valori precedentemente riportati [1]. La combinazione tra l'alta velocità di reazione e la caratteristica esotermicità può portare ad avere delle difficoltà nel controllo nelle reazioni di curing. Comunque, il sistema di dual-curing è contraddistinto dall'aver un basso calore sviluppato per ogni fase di reazione, e questo rende più facile la gestione dell'intero processo. La T_g dello Spot-HT, determinata attraverso l'analisi al DSC, ha un valore di 49 °C. Non è stato possibile misurare la T_g del sistema epossidico a causa della alta densità di reticolazione del materiale indurito, ma attraverso le referenze individuabili nella letteratura scientifica, questa è stata stimata avere un valore di circa 200 °C [2].

UV-curing stage

Gli effetti dovuti alla variazione della concentrazione epossidica sulla cinetica della reazione di photo-curing vengono analizzati tramite analisi al DSC ed i risultati sono rappresentati nel Graph B. L'aggiunta di ES allo Spot-HT produce una diminuzione della velocità di reazione (es. flusso di calore, lato sinistro del Graph B) durante la fase di photo-curing, la quale diventa

poi proporzionale alla quantità di Spot-HT. Comunque, l'intero grado di conversione, relativo alla totale estensione del processo di photo-curing (lato destro del Graph B) mostra che la reazione viene terminata nello stesso tempo indipendentemente dalla quantità di ES.



Graph B. UV -curing (flusso di calore a sinistra, grado di conversione a destra) per la formulazione ESxCI1-0.1 analizzata con photo-DSC a 30 °C.

Era possibile aspettarsi questi risultati considerando che solamente gli acrilati potevano prendere parte al photo-curing stage, diversamente dai gruppi epossidici che sarebbero rimasti inalterati ovvero non avrebbero reagito. Comunque, l'effetto di diluizione causato dalla aggiunta della componente epossidica trova spiegazione in basi teoriche. Un possibile aspetto che la diluizione di acrilati e foto-iniziatore, potrebbe avere, è la forte decelerazione della velocità di reazione, che trova conferma nel modello fotopolimerizzazione radicalica descritto da Decker [3], assumendo una irradiazione continua, uno stato di pseudo stazionarietà della concentrazione di iniziatore e una terminazione bimolecolare:

$$-\frac{dM}{dt} = k_p \cdot \left(\frac{\phi_i \cdot I_a}{k_t} \right)^{1/2} \cdot M$$

Dove k_p e k_t sono le costanti della velocità della reazione di propagazione e di terminazione, M è la concentrazione del monomero (acrilato), e $\phi_i \cdot I_a$ è il rate di iniziazione espresso in termini di quantum yield del processo di fotolisi (ϕ_i) e della intensità adsorbita I_a . Dato che la diluizione dello Spot-HT facilita la penetrazione della radiazione luminosa [4], le velocità relative ai processi di fotolisi e di foto-iniziazione sono incrementate compensando quindi la diminuzione della concentrazione di foto-iniziatore.

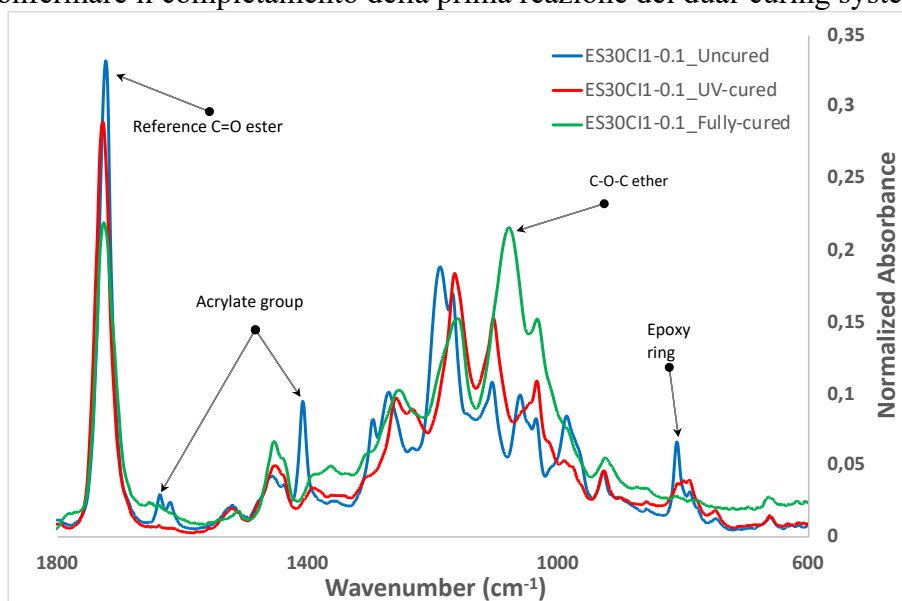
Come può essere visto dalla Table A, il calore di reazione rilasciato nel primo curing stage decresce mentre il calore prodotto durante il secondo curing stage aumenta con l'aumentare della quantità della componente epossidica. Questo andamento era atteso prendendo in considerazione le composizioni delle diverse formulazioni ed i risultati delle analisi preliminari. La Table A mostra, inoltre, l'evoluzione della temperatura di transizione vetrosa dopo il processo di photo-curing ($T_{g,1}$). Si evince che la $T_{g,1}$ diminuisce con l'aumento della concentrazione di gruppi epossidici, come era possibile aspettarsi dato che la temperatura di transizione vetrosa del monomero non reagito ES è di gran lunga inferiore alla temperatura ambiente. Questo implica che i materiali aventi una alta concentrazione di ES saranno

rilassati a temperatura ambiente dopo il photo-curing in contrasto con il reagente puro Spot-HT.

Table A. Sommario delle analisi al DSC per la formulazione ESxCII-0.1. Δh_{1st} è il calore rilasciato nella prima fase isotermica di UV-curing, Δh_{2nd} è il calore prodotto nella successiva fase dinamica di riscaldamento a 10 °C/min e Δh_{total} è il calore totale di reazione sviluppato. $T_{g,1}$ (°C) è la temperatura di transizione vetrosa del materiale parzialmente polimerizzato, misurata dopo il processo di UV-curing del campione trattato nel forno UV, $T_{g,2}$ (°C) è la temperatura di transizione vetrosa del materiale completamente polimerizzato, misurata dopo aver effettuato il trattamento termico.

Formulation	Δh_{1st} (J/g)	Δh_{2nd} (J/g)	Δh_{total} (J/g)	$T_{g,1}$ (°C)	$T_{g,2}$ (°C)
Spot-HT	346,9	8,2	355,1	51	52
ES10CI10.1	323,7	63,5	387,2	31	65
ES20CI10.1	293,5	129,7	423,3	-9	78
ES30CI10.1	273,7	191,6	465,3	-25	92
ES40CI10.1	224,5	256,3	480,8	-36	97
ES50CI10.1	200,1	310,7	510,8	-42	110

Mediante l'analisi agli infrarossi è stato possibile determinare lo spettro IR del materiale prima del processo di dual-curing, e quello relativo al trattamento post photo-curing. Il Graph C mostra i risultati della formulazione studio ES30CI1-0.1. Attraverso il confronto tra gli spettri del materiale non reagito e di quello foto-polimerizzato, è possibile osservare le bande di assorbimento caratteristiche del doppio legame C=C, tipico del gruppo acrilato, a 800, 1400 and 1620 cm^{-1} [5,6] scomparire dopo la reazione di photo-curing. Questo risultato va quindi a confermare il completamento della prima reazione del dual-curing system.



Graph C. Risultati della spettroscopia infrarossa FTIR per la formulazione ES30CI1-0.1 nei casi di pre-curing, UV-curing, e fully-curing. I dettagli delle bande di adsorbimento a 600-1800 cm^{-1} vengono riportati.

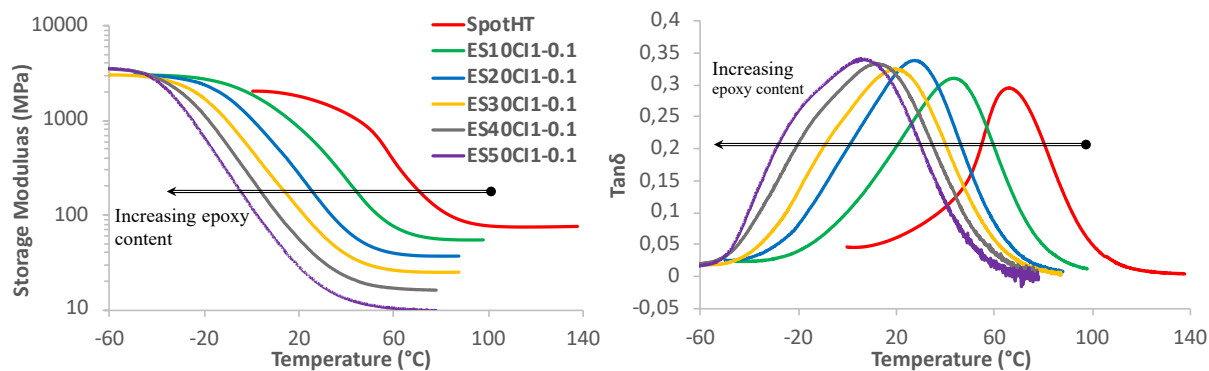
Ulteriori analisi sono state effettuate al fine di verificare il grado di avanzamento della reazione di indurimento ed analizzare le proprietà del materiale dopo il processo di photo-

curing. Prima di tutto, sono stati condotti dei test volti alla determinazione della frazione solubile delle formulazioni fotopolimerizzate usando diclorometano come solvente al punto di ebollizione in condizioni operative di riflusso totale. I risultati di queste analisi vengono mostrati nella Table B dove può essere osservato che la frazione in massa residua della componente insolubile decresce con l'aumentare del contenuto di epossidi. I risultati ottenuti sono in linea con le aspettative, e questo perché la frazione epossidica non partecipa alla fase di photo-curing. Questo trend va a confermare che la reazione degli acrilati nel photo-curing stage è di tipo quantitativo. I risultati ottenuti per via sperimentale sono coerenti con le frazioni in massa residue teoriche calcolate tenendo conto della composizione della formulazione analizzata, come può essere visto dalla tabella. I risultati, suggeriscono inoltre, che la frazione solubile sperimentale è inferiore a quella teorica, e questo è dovuto al fatto che una porzione dei monomeri acrilici non reagisce per via di restrizioni topologiche. Le frazioni solide ottenute sono state poi analizzate attraverso analisi al DSC e FTIR, le quali hanno confermato le ipotesi iniziali.

Table B. Confronto tra la frazione in massa residua sperimentale e la frazione in massa teorica attesa per il materiale intermedio.

Formulation	Experimental Residual weight (%)	Theoretical Residual weight (%)
Spot-HT	96.9	100
ES10CI1-0.1	85.5	88.2
ES20CI1-0.1	76.5	78.4
ES30CI1-0.1	69.9	68.6
ES40CI1-0.1	57.4	58.8
ES50CI1-0.1	48.1	49.0

Con l'obiettivo di studiare la struttura e le proprietà meccaniche del materiale sottoposto al trattamento di fotopolimerizzazione, sono state eseguite delle analisi al DMA. I risultati dei test dinamici sono stati riassunti nel Graph D e nella Table C. Come si evince da Graph D, lo storage modulus ed il $Tan\delta$ rispetto alla temperatura sono riportati per lo Spot-HT e la formulazione intermedia ESxCI1-0.1. È possibile osservare che il rilassamento meccanico dei diversi materiali (dato dalla rapida diminuzione dello storage modulus e dal picco del $\tan\delta$) trasla verso temperature inferiori con l'aumentare della concentrazione epossidica. Questo andamento è in completo accordo con le temperature di transizione vetrosa riportate in Table A.



Graph D. Risultati delle analisi dinamiche al DMA condotte a 3 °C/min, 1 Hz e con una tensione del 0.05 % per lo Spot-HT e la formulazione intermedia ESxCI1-0.1. Lo storage modulus è mostrato nel lato sinistro del grafico, ed il $Tan\delta$ sul rispettivo lato destro del grafico.

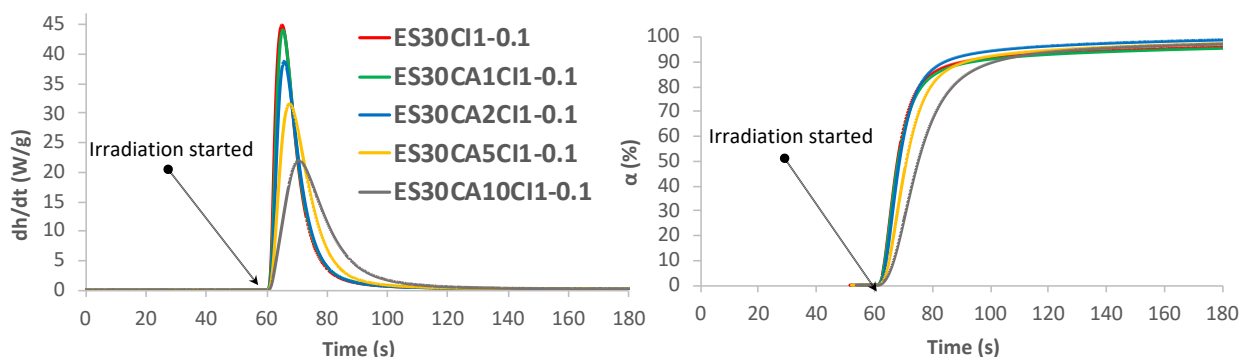
Inoltre, è possibile dedurre che il relaxed storage modulus dei diversi materiali diminuisce significativamente con l'incremento della componente epossidica e questo può essere spiegato dalla possibile presenza di monomeri epossidici, che non reagendo, promuovono il rigonfiamento del network di acrilati. La diminuzione del modulus è strettamente connessa con il fenomeno di diluizione degli acrilati da parte della resina epossidica, ma è correlato anche alla variazione che subisce il processo di sviluppo del network acrilico durante la reazione di omo-polimerizzazione, come riportato dalla letteratura [7]. Materiali con un contenuto di epossidi superiore al 30 wt.% sono quasi completamente rilassati a temperature inferiori rispetto a quella ambiente, con un modulus compreso in un range tra 10-30 MPa (vedi Table C). Questo indica che i materiali saranno teneri ed in uno stato rilassato dopo l'operazione di stampa 3D e durante il trattamento termico necessario per attivare la seconda fase del processo di curing. Il Graph D e la Table C mostrano anche che il fenomeno relativo al rilassamento diventa più esteso con l'aumento della concentrazione di epossidi, come è comunemente riportato per network che manifestano rigonfiamento [7].

Table C. Riassunto delle analisi al DMA per lo Spot-HT ed una formulazione intermedia ESxCI1-0.1. Gli andamenti rispettivamente dello storage modulus (E'), loss modulus (E''), ed il $Tan\delta$ sono tabellati.

Formulation	E' relaxed (MPa)	$Tan\delta$ peak T(°C)	$Tan\delta$ \uparrow height (°C)	$Tan\delta$ \leftrightarrow width (°C)	E'' peak T(°C)
Spot-HT	74	66.5	0.269	34.5	40.9
ES10CI1-0.1	53	43.7	0.295	50.6	6.5
ES20CI1-0.1	37	21.2	0.322	52.5	-9.3
ES30CI1-0.1	25	19.5	0.314	59.4	-19.2
ES40CI1-0.1	17	11.5	0.317	63.5	-30.1
ES50CI1-0.1	8	5,1	0.335	65.4	-35.1

È stato, inoltre, analizzato l'effetto promosso dall'agente legante sul processo di dual-curing. Il Graph E mostra il flusso di calore (dh/dt) e il grado di conversione (α) del dual-system di riferimento ES30CAxCI1-0.1 rispetto al tempo. Il risultato della variazione della quantità di agente legante sulla cinetica di photo-curing porta ad avere un calo della quantità di calore di reazione liberata in corrispondenza dell'aumento della concentrazione di CA. La stessa tendenza generale, ma con la conversione, è diagrammata nel lato destro del grafico. Era possibile aspettarsi questo comportamento considerando che l'agente legante utilizzato, HEMA, è a base di metacrilati e la velocità di reazione di questi ultimi è inferiore rispetto a

quella dei gruppi acrilici. Questo, è dovuto alla elevata stabilità (e bassa reattività) del radicale terziario che si viene a formare durante la omo-polimerizzazione metacrilica, in netto contrasto con la spiccata attività che caratterizza il radicale secondario formato con la reazione di omo-polimerizzazione acrilica.



Graph E. Curing dinamico condotto a 10 °C/min (flusso di calore sulla sinistra, grado di conversione a destra) per una formulazione ES30CAxCII-0.1.

La Table D mostra i risultati derivanti dal cambiamento del contenuto di CA nelle differenti formulazioni ES30CAxCII-0.1 rispetto alle quantità di calore rilasciate relativamente alla prima e la seconda fase di curing. Da un punto di vista pratico, questa modifica non produce nessuna trasformazione apprezzabile. Tenendo conto di quanto appena detto e gli effetti che si hanno sulla cinetica di reazione, i quali potrebbero essere dannosi per il processo di stampa 3D, abbiamo deciso di non usare HEMA nei test coinvolti nel progetto.

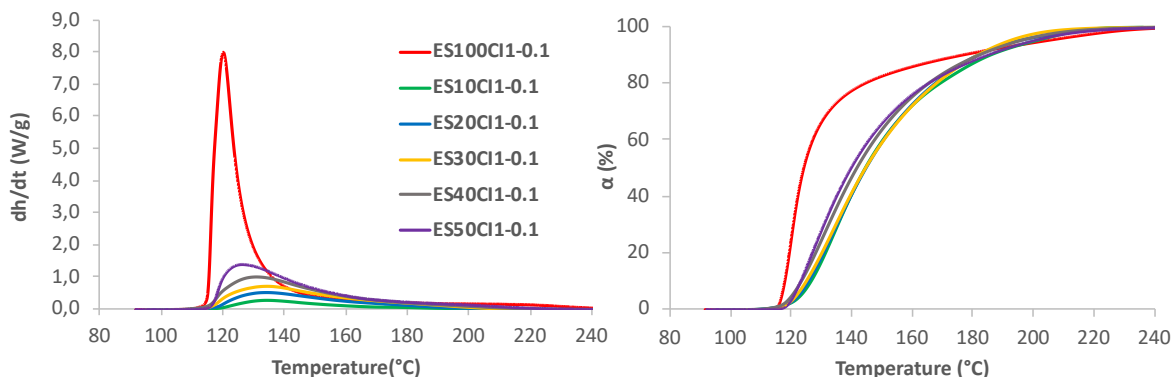
Table D. Sommario delle analisi al DSC per formulazioni a CA variabile ES30CAxCII-0.1. Δh_{1st} è il calore rilasciato dal primo trattamento isoterico di fotopolimerizzazione, Δh_{2nd} è il calore liberato nel successivo riscaldamento dinamico a 10 °C/min e Δh_{total} è il calore totale sviluppato dalla intera reazione.

Formulation	Δh_{1st} (J/g)	Δh_{2nd} (J/g)	Δh_{total} (J/g)
ES30CI1-0.1	276,0	186,9	462,9
ES30CA1CI1-0.1	273,2	182,4	455,6
ES30CA2CI1-0.1	263,6	181,1	444,6
ES30CA5CI1-0.1	274,8	182,5	457,2
ES30CA10CI1-0.1	268,3	188,7	456,9

Thermal curing stage

Come può essere visto dal Graph F, il flusso di calore che si sviluppa durante la polimerizzazione termica aumenta con l'incremento della concentrazione di epossidi. Il valore massimo del calore di reazione rilasciato corrisponde alla formulazione epossidica pura, questo comportamento era previsto tenendo conto della composizione della formulazione ed i risultati delle analisi preliminari. Lo stesso andamento può essere osservato nel lato destro del Graph F dove è riportato l'avanzamento del grado di conversione (α) rispetto alla temperatura durante il curing dinamico. È possibile raggiungere un miglioramento del grado di conversione attraverso l'aumento della concentrazione della componente epossidica. La diminuzione della velocità di reazione che si ottiene con l'incremento dell'effetto di diluizione della formulazione di Spot-HT può essere spiegata, in prima battuta, dalla diluizione dei gruppi epossidici all'interno della formulazione stessa.

Comunque, viene ipotizzato che la presenza significativa di gruppi esterei all'interno della formulazione, provenienti dalla struttura dello Spot-HT o da altre specie, è in grado di rallentare il processo di curing. Crivello ha indagato circa l'interazione negativa che i gruppi estere provocano [8]. Strutture a base polieteree sono anche note per via del ritardo che inducono nella reazione di indurimento, e a causa della formazione di specie inattive [9].



Graph F. Curing dinamico a 10 °C/min (flusso di calore sulla sinistra, grado di conversione sulla destra) per le formulazioni ESxCI1-0.1.

La Table E mostra gli effetti, che ha il cambiamento della concentrazione di epossidi, sul calore di reazione liberato durante il secondo ed ultimo curing termico. Come può essere osservato, maggiore è la concentrazione epossidica e maggiore è il calore prodotto. In effetti, il valore riportato in J/g è strettamente proporzionale alla percentuale in massa wt.% di epossidi contenuti nella formulazione. Il calore di reazione calcolato su base equivalente del gruppo epossidico è stato stimato avere un valore che si aggira attorno ai 82-85 kJ/eq, il quale è del tutto simile ai valori riportati precedentemente per la omo-polimerizzazione cationica del monomero epossidico [1].

Table E. Confronto tra valutazioni al DSC per il sistema epossidico puro ES100CI1-0.1 e le formulazioni ESxCI1-0.1. Δh_{exp} (J/g) è il calore rilasciato durante il riscaldamento dinamico a 10 °C/min basato sulla massa del campione. Δh_{exp} (kJ/eq) è il calore liberato ma calcolato su base equivalente di epossidi pari a 130 (g/eq).

Formulation	Δh_{exp} (J/g)	Δh_{exp} (kJ/eq)
ES100CI1-0.1	620	82
ES10CI1-0.1	63,5	84
ES20CI1-0.1	129,7	86
ES30CI1-0.1	191,6	85
ES40CI1-0.1	256,3	85
ES50CI1-0.1	310,7	82

Tutti i campioni prodotti, dopo il trattamento termico, sono stati caratterizzati mediante analisi di spettroscopia infrarossa FTIR. Il completamento del processo di indurimento (es. completa scomparsa dei gruppi epossidici ed acrilici) è stato verificato in tutti i casi. Il Graph C mostra la prova riscontrata per la formulazione studio ES30CI1-0.1.

La Table A mostra che, aumentando la concentrazione della componente epossidica, la T_g dei materiali aumenta significativamente dopo il processo di curing termico. Questo comportamento era atteso tenendo conto che la T_g della formulazione epossidica pura

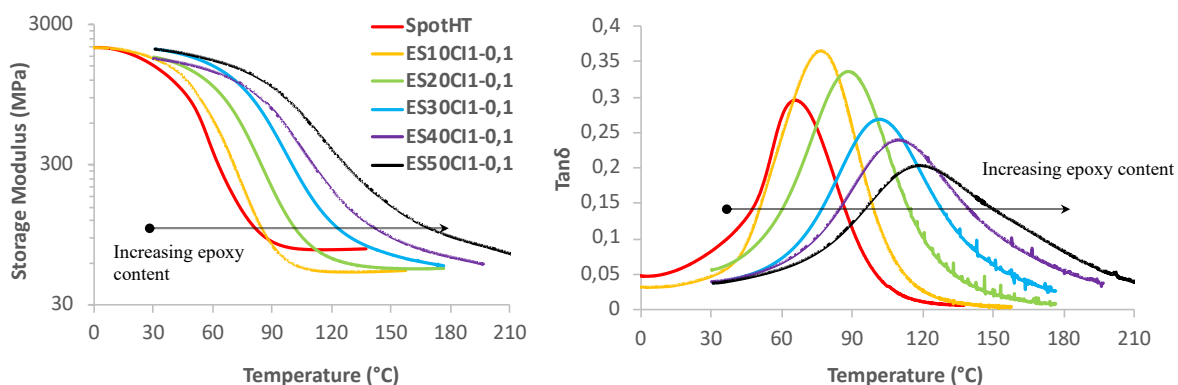
ES100CI1-0.1 era molto vicina ad una temperatura di 200 °C [2], la quale è decisamente superiore a quella riportata per lo Spot-HT. Di conseguenza, il materiale completamente polimerizzato dovrebbe mostrare un aumento del valore della T_g in corrispondenza dell'aumento del contenuto di epossidi.

È stata, inoltre, determinata la frazione solubile del materiale fully-cured usando come solvente il diclorometano portato all'ebollizione ed in condizioni di reflusso totale. Come è possibile vedere dalla Table F, la frazione insolubile è piuttosto vicina all'unità in tutti i casi analizzati ed è possibile osservare che questa aumenta con la concentrazione dei gruppi epossidici. Quindi, incrementando il contenuto epossidico, il risultato che si riscontra sui materiali completamente polimerizzati è quello di avere una molto piccola o comunque bassa frazione in massa della componente solubile ed un minor rischio di emissioni VOC, il che rende il loro utilizzo sicuro dal punto di vista ambientale.

Table F. Confronto tra la frazione in massa residua sperimentale e la frazione in massa residua teorica attesa per il materiale fully-cured.

Formulation	Experimental Residual Weight (%)	Theoretical Residual Weight (%)
Spot-HT	96.9	100
ES10CI1-0.1	96.7	100
ES20CI1-0.1	98.1	100
ES30CI1-0.1	98.3	100
ES40CI1-0.1	99.5	100
ES50CI1-0.1	99.8	100

I risultati delle analisi meccaniche al DMA dei materiali completamente polimerizzati sono riassunti nel Graph G e nella Table G. In questo caso, l'aumento della concentrazione di epossidi contenuti nella formulazione conduce ad avere una traslazione del fenomeno di rilassamento meccanico verso temperature maggiori, contrariamente a quanto ottenuto per i materiali UV-polimerizzati. Questo trend assume un significato logico prendendo in considerazione che la omo-polimerizzazione di tipo cationico, dei gruppi epossidici, porta ad avere un network saldamente reticolato con una alta temperatura di transizione vetrosa. [2]. In aggiunta, il rilassamento meccanico risulta essere ampliato in corrispondenza dell'aumento della concentrazione di epossidi, il che è tipico per i materiali con una elevata densità di reticolazione [10].

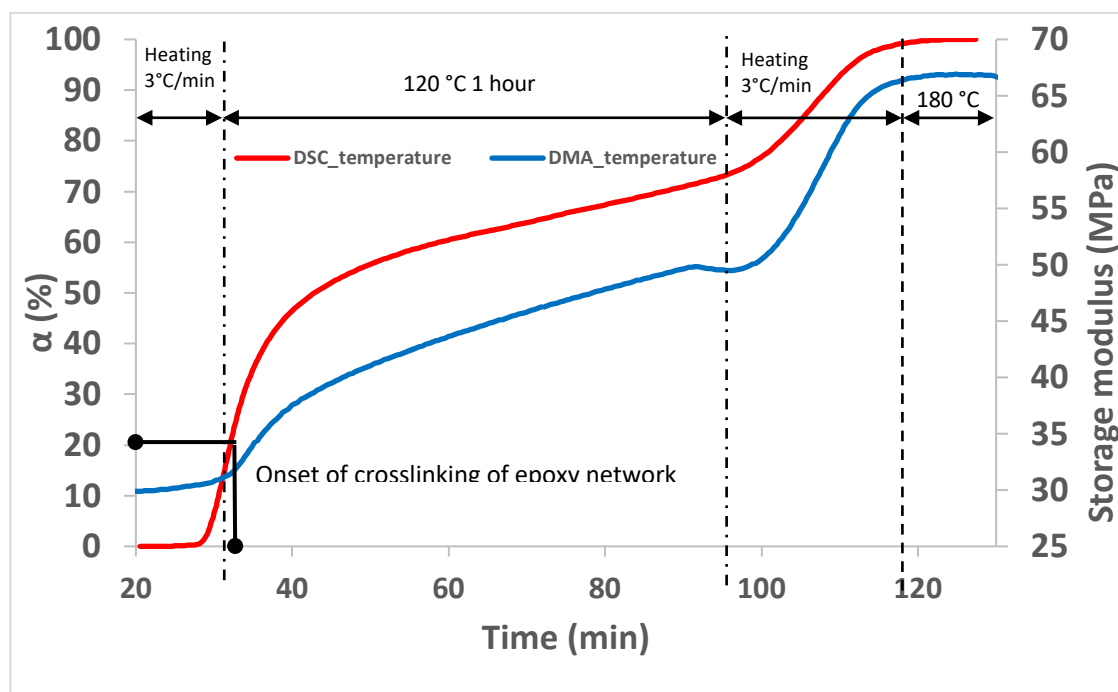


Graph G. Analisi dinamiche al DMA condotte a 3 °C/min (Storage Modulus sulla sinistra, Tan δ sulla destra) per un campione di Spot-HT e la formulazione finale ESxCI1-0.1.

Table G. Sommario delle analisi al DMA per lo Spot-HT e per la formulazione fully-cured ESxCI1-0.1.

Formulation	E' relaxed (MPa)	Tan δ peak T(°C)	Tan δ \uparrow height (°C)	Tan δ \leftrightarrow width (°C)	E'' peak T(°C)
Spot-HT	75	66.5	0.269	34.5	40.9
ES10CI1-0.1	52	77.1	0.349	39.6	56.7
ES20CI1-0.1	59	88.8	0.301	42.5	68,7
ES30CI1-0.1	74	101,3	0.237	48.2	81.5
ES40CI1-0.1	96	109.5	0.201	56.7	88.9
ES50CI1-0.1	104	118.0	0.170	72.3	96.9

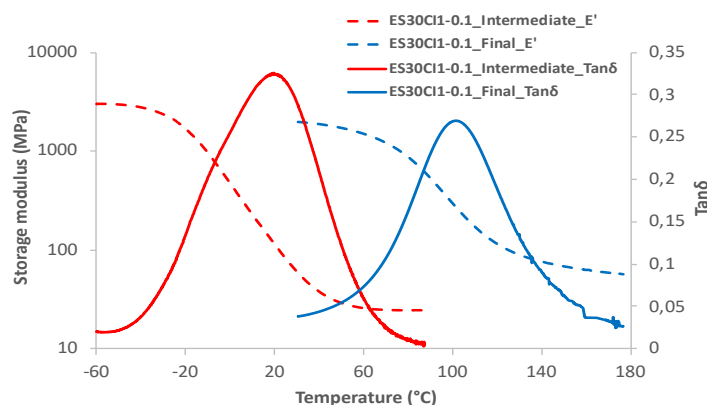
Il processo di crosslinking, durante la fase del trattamento termico per la formulazione studio ES30CI1-0.1, è stato monitorato rispettivamente mediante una analisi meccanica al DMA e confrontato con il curing svolto al DSC. Il Graph H pone a confronto l'evoluzione dello storage modulus ed il grado di conversione ottenuto al DSC mediante un programma di riscaldamento pianificato come segue: heating rate di 3 °C/min fino al raggiungimento di 120 °C, 60 minuti a 120 °C, riscaldamento a 3 °C/min fino a 180 °C, trattamento isothermico a 180 °C. È possibile osservare che l'evoluzione del modulus segue un andamento del tutto simile a quello dal grado di conversione ottenuto mediante l'analisi al DSC, congruentemente con le aspettative attese. Lo sviluppo del modulus presenta, comunque, un ritardo rispetto all'inizio del processo di curing. L'inizio della crescita del modulus si sviluppa quando la conversione assume un valore corrispondente a circa il 20-25 %. Questa fase è strettamente correlata al punto di gelificazione del network epossidico, il che risulta essere in totale accordo con i risultati riportati dagli autori [11] per lo stesso sistema preso in esame.



Graph H. Analisi al DMA e DSC con lo stesso programma di riscaldamento programmato. Grado di conversione e E' vs. tempo per una formulazione finale ES30CI1-0.1 vengono graficati.

I risultati indicano che il modulus non è mai soggetto ad una diminuzione al di sotto del valore di rilassamento determinato con l'analisi al DMA durante il processo di riscaldamento e ciò implica che non si presenterà nessun ulteriore fenomeno di intenerimento. Di conseguenza, se il materiale è meccanicamente stabile dopo l'operazione di stampa 3D, sottoporlo ad un riscaldamento in forno, al fine di innescare la seconda reazione di curing, non provocherebbe nessuna perdita in termini di consistenza dimensionale e meccanica.

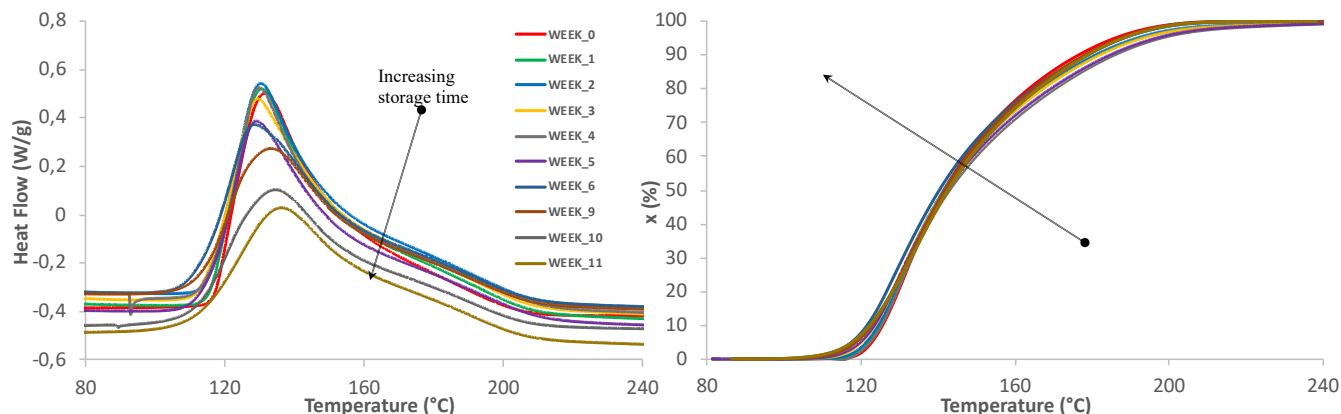
Al fine di sottolineare i cambiamenti prodotti in termini di proprietà termiche e meccaniche, il Graph I pone a confronto la variazione dello storage modulus (E') e del $Tan\delta$ dopo il primo processo di UV-curing e dopo il secondo step termico per la formulazione di riferimento ES30CI1-0.1. Come si può osservare, si riscontra una traslazione di entrambe le proprietà, le quali trovano inizio in corrispondenza di temperature basse per l'UV-curing stage, fino ad arrivare a temperature decisamente superiori per il trattamento termico. Il trend ottenuto rispetta le previsioni, e ciò è dovuto al fenomeno di crosslinking che promuove la formazione del network attraverso il processo di dual-curing. I risultati ricavati con l'analisi al DMA sono completamente connessi con i valori di T_g tabellati nella Table A.



Graph I. Confronto tra lo storage modulus (E') e il $Tan\delta$ per la formulazione ES30CI1-0.1 UV-cured e fully-cured.

Storage stability

Con l'obiettivo di determinare l'applicabilità delle formulazioni prodotte dal processo dual-curing, è stato essenziale condurre delle prove di storage stability su sistemi base e su quelli sottoposti ad UV-curing. Per cominciare, lo storage stability del componente acrilato dovrebbe essere garantito per un tempo corrispondente a quello in cui la miscela viene tenuta al buio, es. evitando l'esposizione alla luce. Per quanto riguarda il costituente epossidico, bisognerebbe accertarsi che il catalizzatore termico sia stabile ed abbia un periodo di latenza sufficientemente esteso da permetterne l'utilizzo pratico. Con questo proposito, sono state realizzate delle analisi a carattere settimanale su campioni stoccati ad una temperatura costante di 35 °C ed in condizioni opportune (es. protetti dalla luce solare nel caso di formulazioni base ancora non UV-polimerizzate).



Graph J. Curing dinamico settimanale al DSC condotto a 10 °C/min (flusso di calore sulla sinistra, conversione sulla destra) per la formulazione di riferimento ES30CI1-0.1.

Il Graph J mostra le scansioni dinamiche condotte per campioni UV-polimerizzati e stoccati ad una temperatura di 35 °C. Può essere osservato come difficilmente, in 5 settimane, si sia modificato il carattere esotermico della reazione promossa dalla componente epossidica. L'inizio della reazione di curing è leggermente traslato a temperature inferiori ma emerge, comunque, che l'attivazione della reazione avviene al di sopra dei 100 °C. Questi risultati sono in totale accordo con quelli ottenuti dalle valutazioni precedenti di Isarn et al. [2], il quale riporta lo storage stability condotto per un periodo di 16 settimane su una formulazione epossidica in cui è stato utilizzato il medesimo sistema catalitico. È stato, inoltre, verificato come i processi di UV-curing e curing termico, delle formulazioni non polimerizzate, risultassero inalterati dallo stoccaggio in quelle precise condizioni operative durante le settimane iniziali. Ma al fine di indagare sul come evolverebbe la formulazione nelle fasi successive a quelle del curing, altro lavoro dovrebbe essere fatto.

IV. Conclusioni

Un nuovo sistema di dual-curing è stato sviluppato partendo da una miscela per il 3D-printing, disponibile in commercio, al fine di migliorare le proprietà dei componenti prodotti. Il dual-curing di polimeri termoindurenti presenta numerose e distinte caratteristiche che possono essere utilizzate in svariati campi aventi importanti applicazioni tecnologiche; un obiettivo importante, raggiunto con il sistema in questione, è stato il potenziamento e l'ottimizzazione delle caratteristiche termiche, meccaniche e reologiche.

Il processo preso in esame, di formazione del network polimerico, è suddiviso in due fasi differenti, la prima di UV-curing e la seconda distinta dal trattamento termico. L'associazione di differenti tipologie di polimerizzazione risulta essere un punto strategico nello studio e sviluppo della formazione di interpenetrated network (IPNs), dando la possibilità di adattare e manipolare la morfologia dei materiali prodotti a seconda di come evolva la polimerizzazione ed a seconda della presenza o meno di entrambi i tipi di network reticolati. Le proprietà dei materiali intermedi e finali, sottoposti al processo di dual-curing, hanno una forte dipendenza dal sistema di network che si viene a formare in corrispondenza del completamento di ogni polimerizzazione.

La struttura dei network prodotti nei diversi stadi è stata controllata attraverso la concentrazione di monomeri epossidici e di Spot-HT, iniziatore cationico, agenti leganti e stabilizzanti. Tramite la selezione e l'elaborazione di formulazioni caratteristiche è stato possibile superare i limiti intrinseci dei materiali base. Senza alcun dubbio, il dual-curing fornisce la possibilità di progettare formulazioni efficienti con una buona capacità di stoccaggio del sistema non polimerizzato, proprietà stabili del composto intermedio e un prodotto finale con capacità specifiche ed innovative che lo rendono utile in svariati campi applicativi. Ulteriori analisi sono richieste per stimare le performance e confermare l'applicabilità del sistema proposto nel processo di 3D-printing in uno scenario basato sulla MIP-SL.

BIBLIOGRAFIA

- [1] X. Fernandez, J.M. Salla, A. Serra, A. Mantecn, X. Ramis, Cationic copolymerization of cycloaliphatic epoxy resin with a spirobis lactone with lanthanum triflate as initiator: I. Characterization and shrinkage, *J. Polym. Sci. Part A Polym. Chem.* 43 (2005). doi:10.1002/pola.20801.
- [2] I. Isarn, F. Gamardella, L. Massagués, X. Fernández-Francos, A. Serra, F. Ferrando, New epoxy composite thermosets with enhanced thermal conductivity and high Tg obtained by cationic homopolymerization, *Polym. Compos.* (2018). doi:10.1002/pc.24774.
- [3] C. Decker, Kinetic Study and New Applications of UV Radiation Curing, *Macromol. Rapid Commun.* 23 (2002) 1067–1093. <http://dx.doi.org/10.1002/marc.200290014>.
- [4] G.A. Miller, L. Gou, V. Narayanan, A.B. Scranton, Modeling of photobleaching for the photoinitiation of thick polymerization systems, *J. Polym. Sci. Part A Polym. Chem.* 40 (2002) 793–808. <http://dx.doi.org/10.1002/pola.10162>.
- [5] G. González, X. Fernández-Francos, À. Serra, M. Sangermano, X. Ramis, Environmentally-friendly processing of thermosets by two-stage sequential aza-Michael addition and free-radical polymerization of amine-acrylate mixtures, *Polym. Chem.* 6 (2015) 6987–6997. doi:10.1039/c5py00906e.
- [6] A.O. Konuray, A. Ruiz, J.M. Morancho, J.M. Salla, X. Fernández-Francos, À. Serra, X. Ramis, Sequential dual curing by selective Michael addition and free radical polymerization of acetoacetate-acrylate-methacrylate mixtures, *Eur. Polym. J.* 98 (2018). doi:10.1016/j.eurpolymj.2017.11.003.
- [7] M. Dušková-Smrčková, H. Valentová, A. Ďuračková, K. Dušek, Effect of Dilution on Structure and Properties of Polyurethane Networks. Pregel and Postgel Cyclization and Phase Separation, *Macromolecules.* 43 (2010) 6450–6462. doi:10.1021/ma100626d.
- [8] J. V Crivello, U. Varlemann, Structure and Reactivity Relationships in the Photoinitiated Cationic Polymerization of 3,4-Epoxy cyclohexylmethyl-3 prime ,4 prime - epoxy cyclohexane Carboxylate, *ACS Symp. Ser.* 673 (1997) 82–94.
- [9] L. Matejka, P. Chabanne, L. Tighzert, J.P. Pascault, Cationic polymerization of diglycidyl ether of bisphenol a, *J. Polym. Sci. Part A Polym. Chem.* 32 (1994) 1447–1458. <http://dx.doi.org/10.1002/pola.1994.080320806>.
- [10] J.-P. Pascault, H. Sautereau, J. Verdu, R. J.J Williams, *Thermosetting polymers*, Marcel Dekker, 2002.
- [11] Y.-M. Kim, L. Kris Kostanski, J.F. MacGregor, Kinetic studies of cationic photopolymerizations of cycloaliphatic epoxide, triethyleneglycol methyl vinyl ether, and cyclohexene oxide, *Polym. Eng. Sci.* 45 (2005) 1546–1555. <http://dx.doi.org/10.1002/pen.20383>.

SUMMARY

In this thesis, it is proposed to modify a commercially available acrylate formulation (Spot-HTTM) used in 3D-printing by MIP-SL (masked image projection stereolithography) following a dual-curing scheme in order to overcome some processing drawbacks and enhance the quality and thermal-mechanical properties of the processed parts.

To the base formulation, an epoxy monomer and suitable co-reagents (i.e. initiator + stabilizing agent, coupling agent) are added. In the first stage, the photo-polymerization of the acrylates groups is triggered through the UV-activation of the photo-initiator while in the second pathway a cationic homo-polymerization of the epoxy groups occurs when thermally stimulated.

The measurement techniques used to characterize the material properties performed with the dual-curing reaction have been the differential scanning calorimetry (DSC), thermogravimetric analysis (TGA), dynamic mechanical analysis (DMA), and the Fourier transform infrared radiation (FTIR). Also, the soluble fraction and storage stability analyses are carried out.

The results show that the addition of epoxy monomer does not affect negatively the rate of the photopolymerization process. The intermediate materials have lower glass transition temperature (T_g) with increasing epoxy content due to the low T_g of the unreacted monomer, but final materials have higher T_g due to the tighter network structure and higher T_g of the epoxy homopolymer. As shown by DSC and DMA analyses, there is a substantial change in thermal-mechanical properties between the intermediate and final materials. Completion of both polymerization reactions and selectivity in each polymerization stage have been verified with DSC, FTIR and solubility measurements. Storage stability tests suggest that these curing systems could find application in real processing scenarios based on MIP-SL additive manufacturing.

The thesis is structured as follows: in the first part of the thesis, general concepts about polymers, thermosets and processing are introduced. Then, the experimental techniques and analysis methods are described. The results are then discussed and analyzed in a structured way. Finally, global conclusions of the research work are presented and future prospects are discussed.

1 INTRODUCTION

1.1 Classification of polymers materials

The word polymer is derived by the classical Greek words *poly* which mean “many” and *meros* that mean “parts”. A polymer could be defined as a long chain molecule that is composed by a huge number of repeating units of identical structure, these units are called monomer. All the polymers can be assigned to one of two groups based upon their processing characteristics. The main classification, based on their response to temperature, split the polymers in two categories:

Thermoplastics, which can be heat-softened in order to be processed into a designed form and shape. This class of material can be refabricated and reshaped by application of heat and pressure. The fluid state can be reached apply heating, this is possible because that class of materials is composed by linear or branched macromolecules held together by secondary forces (van der Waals, dipole-dipole, hydrogen bonding). These materials, in the solid state, may be either amorphous or semicrystalline glasses. For the amorphous thermoplastic, flow will take place by heating beyond the glass transition temperature (after the devitrification) while for the semicrystalline thermoplastic it is necessary to heat beyond the melting temperature to reach the fluid state. The principal example of a commercial thermoplastic is the polystyrene but there are polyolefins which are widely treated too. (e.g., polyethylene and polypropylene). Plastics find significant applications for products such as textiles, tires, and packaging but are also applied for composite in automotive, marine, and aerospace industries.

On the other hand, *thermosets* are polymers whose singular chains have been coupled by covalent bonds during the polymerization or by chemical or thermal treatment (usually called *curing*) during the fabrication. Once formed, these crosslinked networks oppose resistance to the softening, creep and solvent attack, but they cannot be thermally processed. Thermosets can be molded when initially constituted but reheating a cured sample serves only to degradate the artefact. This happen because the covalent bonds are destroyed by the action of high temperature, the thermosetting polymers will not flow.

Key examples of thermosets include epoxy resins, formaldehyde-based resins, and unsaturated polyesters. Such properties make thermosets suitable materials for composites, coatings, and adhesive uses.

The difference between the thermal behavior of thermoplastics and thermosets is illustrated by Figure 1. Polymers have different thermal transitions according to the activation of different levels of mobility due to the increase in free volume with increasing temperature. If the free volume of the chain increases, the ability to move in various direction also increases [1]. Moving from low temperature, where the molecules are compressed, to higher temperature, the first change are the solid-state transitions.

This process is shown in Figure 1. As the material warms and expands, the free volume increases so bond movements (bending and stretching) and side-chain can occur; this is the gamma transition, T_γ . As the temperature and the free volume continue to increase, the whole side chain begins to have enough space to move and the material starts to develop some toughness. This is the beta transition, T_β , and is related to the T_g of secondary component in a blend. As heating continues, the glass transition appears when large segment of the chain start to move. The T_g represents a major transition for many polymers, as the physical

properties change drastically as the material goes from a hard glassy to a rubbery state. It usually defines the end or the start of the temperature range over which the polymer can be used, often called the operating range of the polymer. If the polymer is a thermoset, the relaxed modulus will remain stable upon heating, up to the degradation temperature, where thermal breakage of bonds and destruction of the polymer structure takes place. For thermoplastics, either amorphous or semi crystalline, heating above the glass transition will lead eventually to flow. T_g values reported for thermosets are of meaningful practical importance because in their proximity a catastrophic alteration takes place. In particular, the elastic modulus drops by 2 – 3 orders of magnitude, from the range of gigapascal to the range of megapascal.

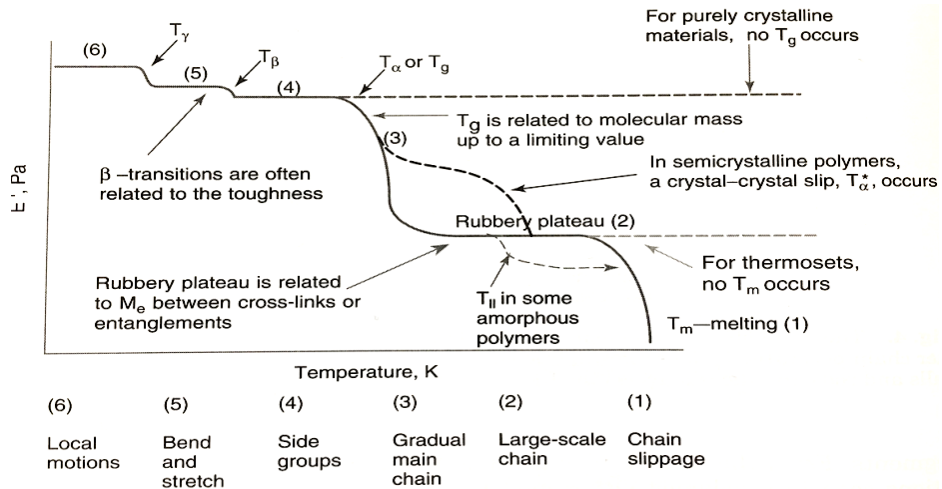


Figure 1. Temperature scan versus Storage Modulus E' . Adapted from [2]

Many thermoplastics/thermosets are managed at temperatures far below their glass transition temperatures to obtain the high mechanical properties and characteristic of the glassy state (i.e. as adhesives, structural composites, kitchenware...). In contrast, cross-linked polymers that are used at temperatures far above T_g are usually classified as rubbers (i.e. rubber bands, tires). Nevertheless, there are some applications which are carried at temperatures close to T_g . This is the situation for the shape-memory polymers whose responds depends on a thermal cycle that goes above and below the T_g [3].

In the following section, it is intended to discuss in more detail the thermosets and dual-curing processing.

1.2 Thermosets

A thermoset [4,5] can be defined as a polymer network highly cross-linked by a covalent chemical bond that percolates the whole mass. This class of polymers is obtained by chemical reaction of different monomers which have distinctive reactive groups. The process that involves the reaction of the monomers to produce the thermoset is usually called *curing*. This is a complex process in which the properties of the system experience significant changes,

ranging from those of a low-molecular weight liquid to a tightly crosslinked network structure.

As shown in the Figure 2 [4], starting from the singles monomers Figure 2-(a) the chemistry of curing process begins by the development and linear growth of chains that quickly begin to branch below the gel point Figure 2-(b); the reaction continues with the gelation but with a low cross-linking degree Figure 2-(c) till the end with the fully cured thermoset Figure 2-(d). During the reaction, the rise in molecular weight accelerates and several chains become linked together into a network of infinite weight.

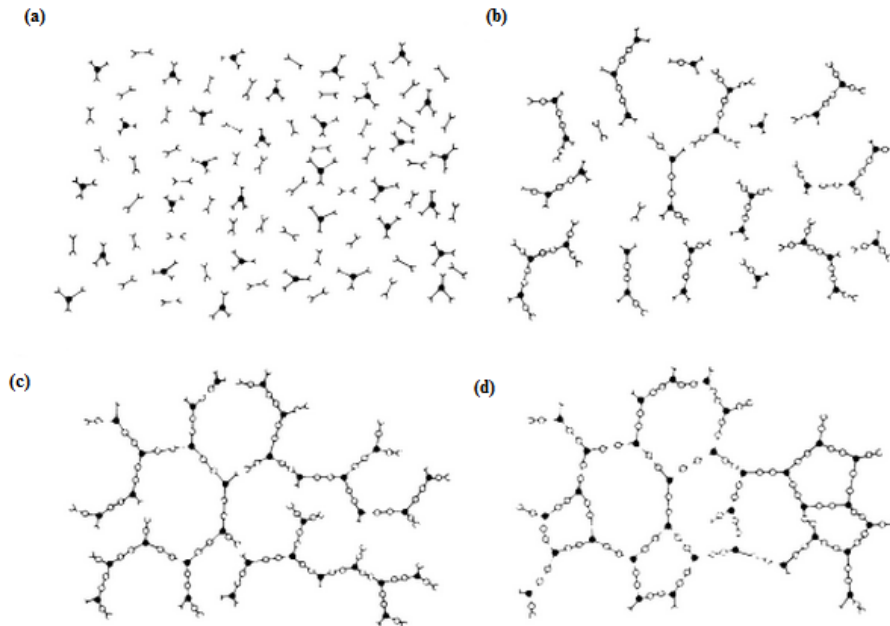


Figure 2. Scheme of cross-linking network formation. Image adapted from [4]

A characteristic highlight during the network formation is the presence of a critical transition from a viscous liquid to an elastic gel or rubber, this point is called *gel point*. Gelation occurs in a particular conversion during the polymerization when one of the reactive growing species reaches a mass so large that interconnects every boundary of the system. In this condition, the polymer gel has a macroscopic manifestation as an abrupt increase in viscosity that transform the polymerization mass from liquid to solid. This evolution assumes a fundamental importance during the development of a thermosetting formulation. The critical aspect is that the gelation must occur in a mold with the final required shape of the product, because no reshaping is possible after the gel point; in thermosetting polymers this phenomenon is irreversible.

This also illustrated by Figure 3, which shows the evolution of the viscosity and the elastic modulus as function of the conversion of reactive groups. At $x = x_{gel}$ the viscosity become infinite, the buildup of elastic modulus follows.

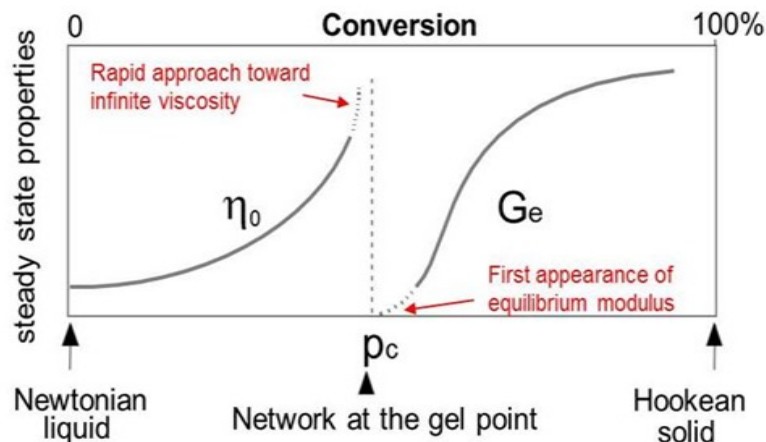


Figure 3. Viscosity (η) and Modulus vs. degree of conversion (α). Adapted from [5]

Gelation can also be described from the evolution of relevant statistical averages [5] connected with the polymer structure that is developing during the reaction:

- M_n number-average molar mass defined in terms of the number contribution of every species in the whole population (with molar fraction used as weight factor).
- M_w the mass-average molar mass expressed in terms of the mass contributions of every species to the total mass (with mass fraction used as weight factor).

When gelation takes place during the reaction of thermosetting polymer, there is only one huge macromolecule present into the system. This means that its contribution to the total number of molecules is negligible and this consequence is reflected by the fact that M_n is unaffected by gelation. The situation is completely different for M_w because the mass fraction of the giant species is more significant than the contributions of the smaller pieces. This means that when $x = x_{gel}$, M_w diverges. From the mathematical point of view the gelation states is defined as $M_w \rightarrow \infty$ at $x = x_{gel}$

An accurate experimental determination of gelation is performed measuring the evolution of $\tan\delta$ (ratio between loss and elastic modulus) using a rheometer [6,7]. At the gel point, as is shown in the Figure 4, the value of $\tan\delta$ is independent of the frequency (iso-conversional transformation) used in the experimental test and the gel time could be converted into the gel conversion exploiting the conversion-time curve determined at the equivalent temperature. This parameter cannot be identified with the procedures sensitive only to the chemical reaction as DSC and TGA [5]. Every kind of polymerization has a specific gel conversion with a very low sensitivity respect to the reaction temperature.

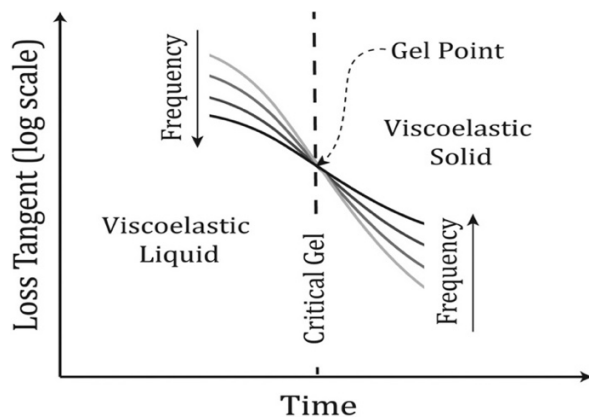


Figure 4. $\text{Tan}\delta$ vs. time (t). Adapted from [6]

A different phenomenon, dissimilar from the gelation, may appear during the curing process; the *vitrification* of the polymer network. This phenomenon is connected with the fact that the T_g of the system is increasing throughout the curing process due to the reaction and crosslinking. Before gelation, the polymerization process leads to an increase in molecular weight leading to a decrease in the available free volume. After gelation, reduction in free volume continues but, in addition, the crosslinking process leads to a significant decrease in the mobility of the system. Both factors contribute to increase the glass transition temperature of the system during the curing process [8].

A huge number of equations have been proposed as a model to explain the evolution of the glass transition temperature with the conversion (x) [8–10]. One example of equation that can be used to fit experimental values of several thermosetting polymers is the following [5,10]:

$$\frac{T_g - T_{g0}}{T_{g\infty} - T_{g0}} = \frac{\lambda \cdot x}{1 - (1 - \lambda) \cdot x}$$

Equation 1. Evolution of the glass transition temperature T_g with the conversion x [5,10].

Where λ is the ratio between the increase in specific heat at the glass transition temperature for the fully reacted network (Δcp_∞) and for the initial mixture (Δcp_0), and $T_{g\infty}$ and T_{g0} are the values of the glass transition temperature and initial mixture, respectively [5,10]. Both parameters T_g and Δcp can be predicted with a calorimetric determination for the initial mixture and for the fully reacted thermoset. The Figure 5 shows an example of the fitting of the Equation 1 to experimental values.

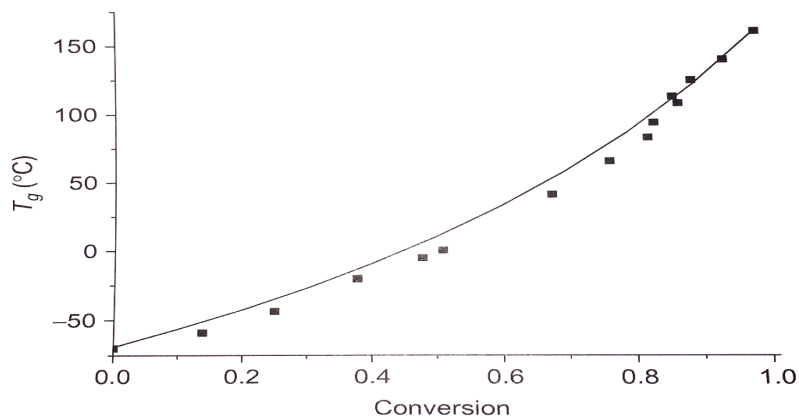


Figure 5. Glass transition temperature vs. degree of conversion (α). Adapted from [4]

The vitrification (hardening) process can be defined like an evolution from liquid or rubber to the glassy state as direct effect of the network evolving. The transformation takes place when incessant rising of the glass transition temperature of these growing chains or network becomes equal to the cure temperature, $T_g = T_{\text{cure}}$. The glass transition temperature of the initial mixture, $T_{g0} = T_g(x = 0)$, is located below the polymerization temperature T . If the reaction temperature is lower than the value of T_g at full conversion, $T_{g\infty} = T_g(x = 1)$, when $T_g(x)$ gets close to T , the curing process will change from chemical to diffusion control, slow down and eventually halt. As a consequence of this phenomenon, the curing process will not reach completion. The only way to carry the polymerization to conclusion is to heat the system to a temperature close or higher than $T_{g\infty}$, considering that overcome the $T_{g\infty}$ lead to the product degradation process [4,5].

Contrasting with the gelation, that is an iso-conversional transformation (independent from the frequency), the vitrification is a frequency-dependent process therefore can be detected by a DSC analysis [4,11,12]. This fact finds an explanation into the polymerization reaction rate; in the glassy state, the rate fall (by 2 – 3 order of magnitude) because the reaction becomes controlled by the diffusion of reactants [12,13]. Any amorphous material undergoes a reversible hard-to-soft transition, the chemical control may be reestablished during the heating step to devitrify (softening) the partially cured thermoset.

Curing processes can be represented in different types of diagrams. The two most important representation are the conversion-temperature-transformation (CTT) diagram [4,5], Figure 6, and the time-temperature-transformation (TTT) diagram [12,14,15], Figure 7. The main difference between the CTT and the TTT diagram is the introduction of the factor of the isothermal curing time in the latter. Therefore, iso-conversional lines are vertical in the CTT diagram, while they are time-dependent in the TTT diagram due to the influence of curing temperature on reaction kinetics.

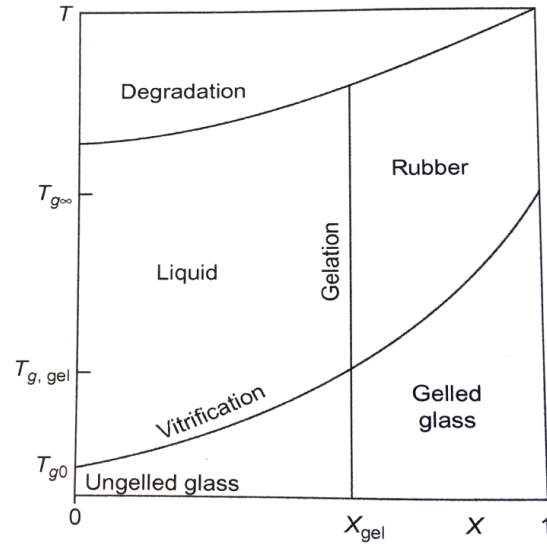


Figure 6. CTT diagram. Adapted from [4]

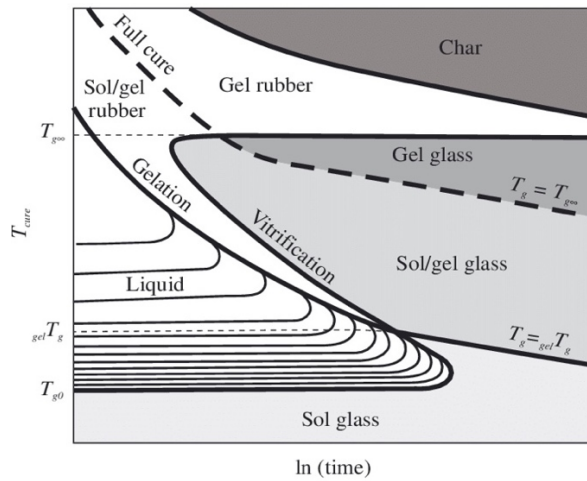


Figure 7. TTT diagram. Adapted from [6]

All the principal transformation which take place during the polymerization (vitrification, gelation, complete cure and degradation) may be represented in different transformation diagrams. The key parameters, used in both transition diagram, are:

- T_{g0} (glass transition temperature of the unreacted material)
- $_{gel}T_g$ (temperature which gelation and vitrification coincide)
- $T_{g\infty}$ (glass transition temperature of the fully cured network)

As described before, the gelation process does not depend on temperature. In consequence, gelation line is plotted usually as an iso-conversional line, which is vertical in the CTT diagram. The glass transition temperature increases with the conversion as described before, and the degradation temperature is assumed to increase with the conversion. Below the degradation temperature, the progressing material may be placed in four different areas:

- Un-gelled glass
- Liquid
- Rubber
- Gelled glass

An advantage of the TTT diagram is that it provides useful information in terms of gelation and vitrification times during isothermal cure versus temperature. This is of special importance because many curing processes are designed as sequences of isothermal curing steps. Polymer reactions are highly exothermic ($\Delta H < 0$) and therefore it is frequent that temperature deviations from the prescribed curing programme occur, especially in the case of the processing of thick components [16]. Control of processing conditions is essential to ensure that the reaction process produces the material with the expected thermal, mechanical and dimensional properties.

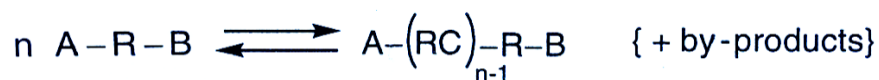
The thermal process used in the curing process of a thermosetting polymer must begin in the liquid region and end in the rubber area at a temperature close to or higher than the glass transition temperature of the fully cured thermoset. Several thermosets are formed in two different stages. In the first step, the polymerization is carried in the liquid state to a conversion below the gelation, and the material is cooled the un-gelled glass region where it can be stored indeterminately (according with the predictive model and the experimental analysis evaluated in the following section). The partially reacted thermosetting polymer is usually termed as the B-stage polymer. In the second and final step, the material is reheated to the liquid region and the polymerization is completed.

Thermosetting polymers may be designed in two different pathways:

1. By polymerizing (step/chain mechanisms) monomers where at least one of them has more than two functional groups in the molecule.
2. By chemical way which produce crosslinks between previously formed linear or branched macromolecules (e.g. vulcanization for the natural rubber).

The way in which the network structure is developed depend predominantly on the mechanism of polymerization reaction that is involved [5]. The process of network formation, during the cross-linking reaction, occasionally occurs as a combination of step-growth and chain-growth polymerization. It is common practice to start from small molecular weight monomers, but the use of the so-called telechelic oligomers [17,18] in crosslinking processes, i.e. unsaturated polyester resins, is frequent.

Based on the classical definitions given in organic chemistry, the step-growth polymerization process is defined as a random reaction of two molecules that may be a combination of monomer, oligomer or a long-chain molecule. This polymerization can involve either condensation or addition steps. The former proceeds with elimination of by-product while the latter takes place without this behavior. This is illustrated in the following scheme:



The polymer network is generated by the reaction of functional groups of type A present in the monomer (A_f , with f functional group in the molecule), with functional groups of type B present in the comonomer (B_g , with g functional group in the molecule), converted in a linked unit C . In order to form a network, f and/or g must be higher than 2. In contrast, for classical linear polymers correspond to $f = g = 2$. The network is produced in successive steps starting from the mixture of monomers and generating branched structures of increasing size as reaction progresses. Any A -functional group can react with any B -functional group independently of the size of the species on which they are situated. This leads to the formation of polymer network. The molar mass distribution of the product grows gradually, and the molar mass distribution becomes continuously broader. High-molecular-weight polymer is formed only near the end of the process when most of the monomer has been depleted. Step-growth polymerization process in thermosets have very well defined network build-up processes [5], although nonidealities may appear.

Many different reactive processes are available, based on step-growth kinetics. An important type are *phenolic resins* [6], which can be divided into two different types:

- one-step phenolics (Resoles) formed by reaction of phenol (A_3) with formaldehyde (B_2), characterizing by a self-curing process due to the presence of reactive side groups
- Two-step phenolics (Novolacs), which occur when one of the initial reactants is a multifunctional oligomer or polymer including functional groups on its backbone. The process is constituted by a first stage where the phenol and formaldehyde are polymerized using a defect of formaldehyde leading to a distribution of oligomers called Novolacs, including few phenolic rings per chain. In a second phase, Novolacs are cross-linked with the addition of a hardener which the most common is hexamethylenetetramine (HMTA). These resins are not self-reactive and need a cross-linking agent to fully polymerize.

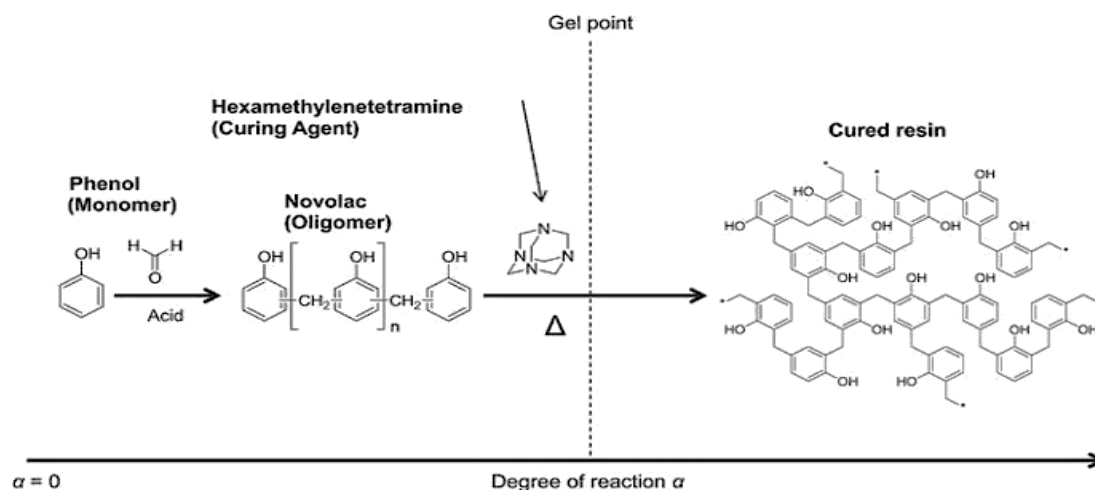


Figure 8. Details of phenolic resins reaction. Adapted from [19]

This phenolic resin was the first totally synthetic coating material. It was commercialized in 1909 as Bakelite, a replacement for the cellulose nitrate. Nowadays it is widely used for the production of molded products including billiard balls, laboratory countertops, and as

coatings and adhesives. Although molded products no longer represent their most important application, through their use as adhesives they still represent almost half of the total production of thermosetting polymers. Phenol-formaldehyde polymers are usually used like adhesive for exterior plywood and as binders for similar wood product: oriented strand board, hardboard, particleboard and molded wood product. This behavior is due to the chemical bonds which this form with one wood component (lignin). For these applications, phenolic resins offer low cost and good compatibility with wood fibers. Phenolic resins are also used as binders with glass and mineral “wool” fibers to make products suitable for thermal and acoustic insulation. In this application, phenolic resins are chosen because of their low cost, good thermal resistance (high T_g), relatively good flame resistance.

Another well-known family are *polyurethanes* (PUR) which formed by addition polymerization of a poly-isocyanate ($A_f, f > 2$) with a diol (B_2).

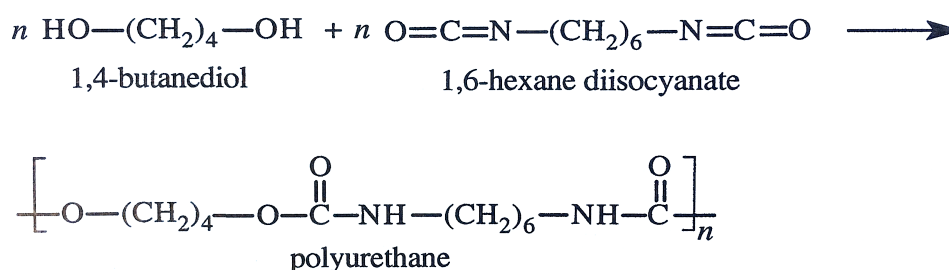


Figure 9. Polyurethanes scheme polymerization. Adapted from [20]

Polyurethanes were developed by Otto Bayer in 1937, they find huge application because of mechanical resilience and ease of manufacture of finished parts. These polymers have high strength, good resistance to gas, oil, and aromatic hydrocarbons, high abrasion resistance, and excellent resistance to oxygen and ozone, but they are susceptible to microbial attack. Application include shoe soles, solid tires, and impellers. The majority of the polyurethane usage is for rigid and flexible foam. Flexible foams are used in mattresses and furniture, including automotive seating, insulation and household uses such a caulk. Rigid foams are used for thermal and sound insulation, especially for appliances such as refrigerators.

Thermosets based on *epoxy-amine* chemistry are highly popular [5,12,21,22] and a key example of step-growth reaction. As shown in the Figure 10, this reaction involves epoxy groups reacting with primary and secondary amines. These are the most commonly curing agent/hardeners for epoxides. As seen on the figure, one epoxy ring reacts with each amino-proton:

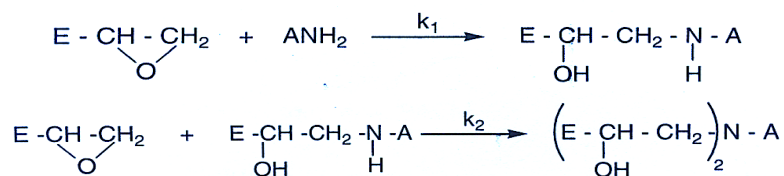


Figure 10. Epoxy-Amine pathway reaction. Adapted from [5]

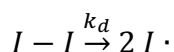
The reactivity of the amine increases with its nucleophilic character: aliphatic > cycloaliphatic > aromatic. Usually when the concentration of epoxy groups is equal or lower than the concentration of NH groups, side reactions do not take place. The two amino hydrogens have initially the same reactivity but once the first one has reacted, the secondary amine formed may be less reactive. For aliphatic amines both primary and secondary amino hydrogens have approximately the same reactivity. But for aromatic amines, the reactivity of the secondary amine is typically 2 to 5 times less than the reactivity of a primary amino hydrogen. This change in reactivity is called the “substitution effect”.

Epoxy resins are versatile monomers [6] used in several applications as adhesives, coatings (both “liquid” and powder), composites, and castings. Due to the formation of the hydroxyl groups during cure with most hardeners, epoxy thermosets have good adhesion to metals and reinforcing fibers as glass or carbon. Common adhesive applications are for automotive, aerospace, appliance, and electronics. Epoxy coating are used as primer coats for automotive applied in water suspension, marine coating, and as powder coatings for automotive and furniture. Particular formulations are used with reinforcing fibers to make composites for windmill blades, printed circuit boards, pressure vessels, and aerospace. Epoxies are also used as casting resins for transformer and electric motor. For large parts, care must be taken to avoid overheating during the molding process because the heat release during the cure can be substantial. The price is the major factor that limits more widespread use of epoxies.

Other significant step-wise processes that can be used for the production of thermosets include epoxy-acid [23], epoxy-phenol [24], thiol-ene [25], thiol-epoxy [26] and Michael-type reactions [27,28], among others.

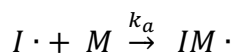
A significant number of thermosets are produced, however, by *chain-growth polymerization*. This process requires the presence of an initiating molecule that can be used to attach a monomer molecule at the start of the polymerization. The chain-growth of a particular monomer can occur by one or more mechanisms (i.e., free radical, anionic, or cationic), it depends, in part, on the chemical nature of the substituent group. The general reactive pathway includes initiation, propagation and termination/transfer steps.

In the case of *free radical polymerization* of double-bonds, the initiation step consists of two stages: (a) dissociation of the initiator to form two radical species and (b) association of a single monomer molecule to the initiating radical. The dissociation of the initiator ($I \sim I$) to form two free-radical initiator species ($I \bullet$) can be represented as:



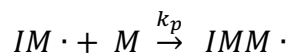
where k_d is the *dissociation rate constant*. Initiators for free-radical polymerization include any organic compound with a labile group, such as an azo ($-N \equiv N-$), disulfide ($-S-S-$), or peroxide ($-O-O-$) compound. The labile bond of the initiator can be broken by heat or irradiation, such as UV- or γ -irradiation.

In the second phase of the initiation, a monomer is attached to the radical initiator. This addition step may be represented as:



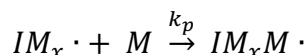
Where k_a is the rate constant for monomer association.

Propagation occurs by growth of the active (free radical) chain by sequential addition of monomers:

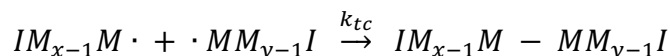


Where k_p is the *propagation rate constant*. For the styrene addition with benzoyl peroxide initiation, the first propagation step is:

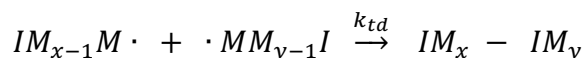
Additional monomers are added sequentially during the propagation steps, as represented by the general equation:



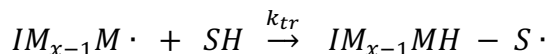
Propagation will continue until some termination process takes place. One termination process follows when two propagating radical chains of arbitrary degree of polymerization of x and y meet at their free-radical ends. Termination in this sense occurs by *combination* to give a single terminated chain degree of polymerization $x + y$ through the formation of a covalent bond between the two combining radical chains, as illustrated by the next scheme:



Termination also can take place by a *disproportionation* reaction to give two terminated chains, as illustrated below. In this case, one terminated chain will have an unsaturated carbon group while the other terminated end is fully saturated. In both termination (combination and disproportionation), one end or both ends contain the initiating free-radical group of the initiator molecule. This indicates a significant difference between an initiator, which becomes part of the terminated chain, and a polymerization catalyst, which promotes the reaction but is fully recovered at the end of the polymerization.



In addition to the two previous termination mechanism, another pathway can be developed, the *chain transfer*. This termination occurs by hydrogen abstraction from the initiator, monomer, polymer, or solvent molecule. In general terms, this process may be represented as:



where SH represents a solvent or any other molecule with an abstractable hydrogen atoms. As illustrated, the radical site is transferred to the chain transfer agent ($S \cdot$), which can add monomer units to continue the polymerization process.

Differently from the step-growth polymerization, in this mechanism, the functional groups can only react with the active sites situated at the end of the growing chains and the high-molecular-weight polymer is formed in the early stages of the chain-growth polymerization.

Relevant examples of free-radical polymerization processes in thermosets involve the reaction of acrylates [29], methacrylates [30], unsaturated polyester [31] or vinyl esters [32], among others.

Another significant process based on chain-growth polymerization is *the cationic ring-opening polymerization of epoxides* [33–35]. The basic mechanism is illustrated in the following scheme

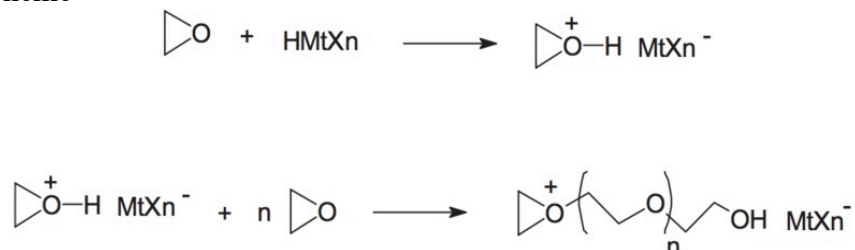


Figure 11. Mechanism of the cationic ring-opening polymerization of epoxide. Adapted from [35]

This process is highly sensitive to the presence of proton-donor compounds, resulting in chain-transfer reactions between the propagating oxonium cation and unreacted epoxy monomer, producing a significant effect in terms of network build-up and crosslinking [33]. Termination reactions generally include reaction of the propagating oxonium cation with an ether bond instead of an epoxy monomer leading to inactive tertiary cations [34]. Connected with this, inhibition by excessive content of environmental moisture has been reported [36]. Oxetanes are another example of cyclic monomer that can undergo cationic ring-opening polymerization [37].

An alternative polymerization mechanism is based on the anionic ring-opening polymerization of epoxides [38,39]. This process is also sensitive to the presence of proton donors [40]. Typical initiators include metal alkoxides and also nucleophilic tertiary amines [38–40]. The reaction mechanism can be quite complex, including a variety of termination and regeneration reactions [39–41].

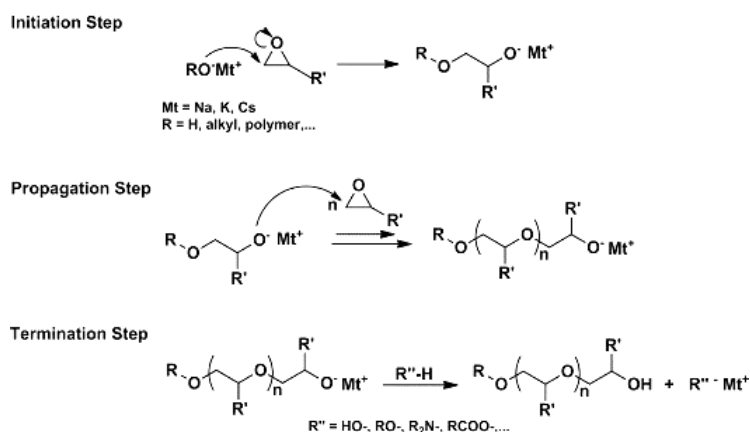


Figure 12. Epoxy anionic polymerization steps. Adapted from [42]

1.3 Photopolymerization

Radiation curing interests is growing rapidly on the industrial scale because of its vast applicability in several fields such as wood products, coatings on a large variety of substrates, adhesives, dental materials, printing inks and composites [43,44]. These techniques use the light to irradiate the photochemical initiator which permit the polymer network formation through a polymerization of the reactive monomer. The UV-curing technology is continuously growing because it shows a great number of advantages in comparison with the classic thermal curing, such as: decreasing of the curing time, low energy necessities, room-temperature system, non-polluting and solvent-free formulations, and low materials cost [35]. Therefore, UV- curing technology can be considered the most rapid and effective way of transforming a solvent-free liquid monomer into a crosslinked polymer at room temperature [29]. A large number of new applications are currently emerging in the graphic arts and in the coatings industry that demand ever-higher performance characteristics. For instance, one very promising area, opened up by the commercial development of various powerful lasers, is concerned with the use of laser-induced polymerization in monomeric and polymeric materials in photoimaging, microelectronics, and holographic image recording and data storage [35].

A typical formulation includes three main components:

- 1) The photo-initiator, which absorbs the light and creates the active species. This is able to start the polymerization of the reactive monomer, commonly by addition to a multiple bond (acrylates, meth-acrylates, unsaturated polyester and styrene systems) or by a ring-opening (epoxies) process [45].
- 2) A reactive multifunctional monomer or oligomer, or combination of both that gives rise to a crosslinking polymerization. The backbone of the oligomer can be planned to give specific mechanical and physical properties to the final product.
- 3) The diluent, which function is to modify the viscosity of the mixture to a tolerable level for the substrate applications; sometimes it is associated to the polymerization.

In a photoinduced polymerization reaction, the kinetics rate can be approximately described by Equation 2 [29,46]:

$$R_p = K_p [M] \left(\frac{\Phi I_a}{K_t} \right)^{\frac{1}{2}}$$

Equation 2. Polymerization rate (R_p).

The light intensity I_a can be substituted by the Lambert–Beer law and the rate can be reformulated as reported in the Equation 3:

$$R_p = K_p [M] \left(\frac{\Phi \varepsilon [A] I_o 10^3 e^{-\varepsilon [A] D}}{K_t} \right)^{\frac{1}{2}}$$

Equation 3. Final polymerization rate (R_p).

Where:

- I_a is the light intensity
- Φ is the quantum yield for initiation
- K_t and K_p are respectively the polymerization and termination constant
- $[M]$ and $[A]$ is the monomer and photo-initiator concentration $\left(\frac{mol}{L}\right)$
- I_o is the incident light intensity
- D sample thickness (cm)
- ϵ molar absorptivity $\left(\frac{L}{mol*cm}\right)$
- 10^3 is a conversion factor, which converts I_a from $\frac{mol}{cm^3*s}$ to $\frac{mol}{L*s}$

The molar absorption coefficient, ϵ , of the photoinitiator determines how strongly light of a given wavelength is absorbed, i.e., the required amount of energy to form the reactive species. The efficiency of the photo-initiator can be described by two quantum yields: the quantum yield of initiation (Φ_i), which represents the number of active species generated per number of photons absorbed, and the quantum yield for polymerization (Φ_m), which is the number of monomer units polymerized per number of photons absorbed [46].

Photo-initiators absorb light in the UV-visible spectra range, 250-450 nm. The photo-initiator, PI, is raised to an electronically excited state, PI*, by promotion of an electron to a higher-energy orbital, and then it converts this light into chemical energy in the form of reactive intermediates, such as free radicals or cations, which successively start polymerization of monomers.



After the formation of the radical initiator the reaction propagates with the same free-radical pathway described before.

The photo-polymerization process of monomer and oligomer readily occurs to generate a three-dimensional cross-linked network, but it presents the oxygen inhibition issue [29,47]. Molecular oxygen is known strongly to inhibit radical-induced polymerization because its reactivity toward radical species. This inhibition effect is particularly pronounced for photo-polymerization which usually occurs in thin film because of the limited penetration of the UV-light. Carry out the UV-curing process in airborne atmosphere present a number of problems such the latency period which cause the induction phase, substantial decrease of polymerization rate (R_p) and the final conversion (α) that produce an early termination of the polymer chain length and the formation of a sticky coating surface due to the liquid formulation which is not still fully-polymerized. This behavior is triggered to the molecular oxygen which easily react with any free radical species, including the initiator molecules. During the inhibition the initiator lose its radical and excited state, and this leads to a lower number of free radical produced, less initiated polymer chain and subsequently a smaller amount of final polymer chain produced.

However, in order to overcome the oxygen inhibition of the UV-curing product many methods have been developed:

1. Changing in formulations: the free radical curing adhesives and sealants can be formulated to contain thiols, amines, or ethers, all of which contain abstractable hydrogen atoms that can simply react with the peroxy radicals formed by the oxygen molecules through the scavenging. Other options include the use of waxes, which migrate to the surface to form a barrier. The disadvantage is the influence on the coating's final properties. A valid alternative has been found through the increasing photo-initiator concentration which reduce certainly the oxygen inhibition but rise the amounts of by-products.
2. Particular production technique: in this pathway, the oxygen concentration can be depleted by the environmental variable's regulation and manipulating the UV-light intensity and the UV-wavelengths. O_2 can be removed from the UV-curing area carrying out the process in an inert atmosphere (non-reactive gas such N_2). Rising the UV-light intensity and the wavelength induce a higher free radical concentration which compete to the oxygen inhibition.
3. Cationic photo-polymerization: cationic polymerization products are synthesized in the same free radical pathway, but the difference is that the process starts with a monomer attacked by the cation and the subsequently growth of the cation chain. In this case O_2 does not interfere the reaction because the counterion produces by the initiator is not nucleophilic.

The cationic photo-polymerization [35] present several advantages, in particular, the lack of the oxygen inhibition, post-polymerization in the dark, low shrinkage, and good adhesion to various substrate. The most commercially important class of cationically photocurable monomers is the epoxides. In the presence of a photogenerated protonic acid, the ring protonic polymerization of epoxy monomers proceeds through an oxiranium ion intermediate. When difunctional epoxides or epoxy-substituted polymers are used as the starting materials, the crosslinking of the polymer network occurs.

A relevant application of photopolymerization is 3D-printing, either by stereolithography [48] or digital light processing [49,50]. This is a promising alternative to conventional manufacturing process given the unique complex structures that can be achieved by processing components layer-by-layer. Given their fast reaction rate, free-radical photopolymerization of acrylates is mainly used [50]. However, 3D-printing faces a number of drawbacks derived from the difficulty in controlling accurately the shape while ensuring uniform mechanical properties [49,50].

1.4 Dual-Curing

The dual curing is given by two distinctive polymerization processes taking place in a consecutive pathway or concurrently during curing of resin and it can be triggered by analogous or different stimulus such as temperature or UV-light [51]. Dual-curing of thermosetting formulations present numerous distinctive characteristic that can be exploited in several field with important technological applications; an important objective reachable with this system is the enhancement of the thermal, mechanical and rheological properties. An example of industrial application of dual-curing is the combination of a thermal curing

process in a UV-curing process to ensure complete curing of shadowed, non-irradiated parts of a coating [52].

Sequential dual-curing can be regarded as an evolution the B-stage procedure used in the processing of adhesives or composites. To modify the extent of both curing reaction and the properties of the materials it is possible to manipulate the composition of the formulation. In the situation of the consecutive dual-curing, the material is not cured further after the end of the first polymerization and for this reason has stable and well-ordered properties until the second reaction is initiated. The intermediate and final properties of dual curing materials have a strong dependency from the network system at the completion of each polymerization process. Network structure of both stages is manipulated by monomer functionality, structure, and feed ratio. Sequential dual-curing is illustrated by the following scheme:

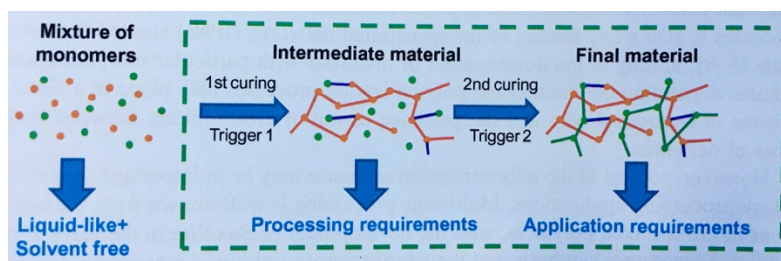


Figure 13. Dual-curing stages. Adapted from [51]

Dual-curing give also the possibility to design efficient formulation with good storage stability of the uncured system and stable intermediate properties and custom-tailored final material with specific and innovative skills that makes them useful in various field application. On the other hand, this methodology has the advantage to work in solvent free conditions, starting from liquid monomers, and mild performing conditions which is fundamental to reduce the VOCs emission and the processing cost.

Several reactions can be combined in the dual-curing process such the click polymerization reaction (stepwise) which is widely used because of their high selectivity and efficiency. The most widespread click-reaction that are used in the dual-curing system, as shown in the Figure 14, are thiol-click addition reaction such as thiol-ene, thiol-epoxy, and Michael addition reaction between Michael donors such as thiols, amines, acetoacetates and a variety of Michael acceptors, especially acrylates.

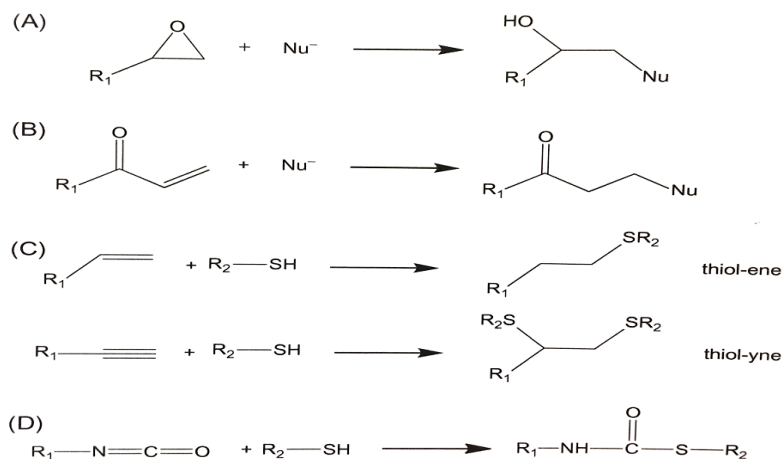


Figure 14. Reaction scheme of click reaction. (A) Nucleophilic ring opening reaction, (B) Michael addition reaction, (C) Photochemical additions of thiols to alkenes and alkynes, and (D) Carbonyl addition of thiols to isocyanates. Adapted from [51]

For various technological areas in which polymer networks have become fundamental, dual curing reactions are very strategic because these systems allow the development of two definite and widely sets of material assets. In this way it is possible to obtain one stable polymer network with designed physical properties holding the capacity, through the second curing stage, to react and complete the second final network with different (improved) material properties.

This type of polymerization has found different application starting from energy- absorbing device, impression materials, and microfluidics to the evolving shape memory effect and the conventional dental materials. Very recently, application of dual-curing to 3D-printing with the purpose of enhancing the properties of the resulting materials have been reported [53,54].

2 MATERIALS, CHARACTERIZATION AND METHODS

2.1 Materials

The base material used during the UV-curing processes is the Spot-HT, a preparation provided by Spot-A Materials (Barcelona, Spain). The formulation consists of a mixture of acrylates with a photo-initiator which has an absorption range in the UV-visible region of the spectrum. According to the product brochure, the formulation has been designed to obtain enhanced hardness, toughness, impact and abrasion resistance, weatherability, chemical and water endurance, as well as to withstand operating conditions as high temperature, above 100°C (212 F). The formulation was stored in the fridge, protected from visible light, before use.

The epoxy resin used is the cycloaliphatic epoxy, 3,4-epoxycyclohexylmethyl - 3',4'-epoxycyclohexanecarboxylate (ES), with an epoxy equivalent weight of 130 g/eq and supplied by Dow (CYRACURE UVR-6105). The epoxy monomer was dried under vacuum at 80°C for two hours and stored in to the desiccator after to use. 2-hydroxyethyl methacrylate (HEMA, M=130.14 g/mol), supplied by Sigma-Aldrich and used as received, was tested as coupling agent (CA). K-PURE® CXC-1612 (King Industries Inc., kindly donated by Protex), which was identified as N-(4-methoxybenzyl)-N,N-dimethylanilinium [55,56] (CI), was used as initiator for the epoxy homopolymerization. It was prepared as a catalyst solution 50 wt.% in propylene carbonate (PC, M=102.09 g/mol). Triethanolamine (TEA, M=149.19 g/mol), supplied by Sigma Aldrich, was also incorporated into the catalyst solution at different wt.% [55].

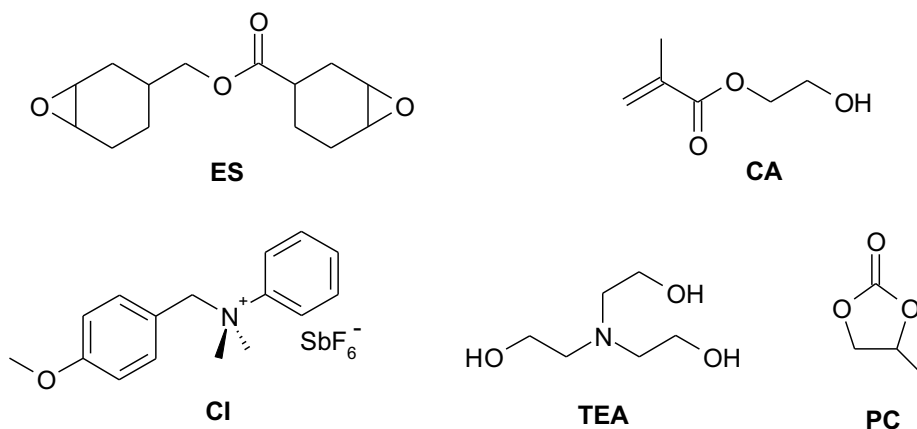


Figure 15. Chemical structures of reagents ES and CA, and of components of catalyst solution CI, TEA and PC.

2.2 Preparation of formulations

2.2.1 Base individual system

All the base system, such the Spot-HT and the epoxy, used to perform the preliminary analysis are liquid and for this reason the sample formulations can be simply prepared by filling a glass vial and stirring with the spatula.

After the preparation, the sample is labeled, specifying the date and eventually the formulation used, and wrapped in to the aluminum paper to prevent a premature activation by the sun light. The samples were stored in the freezer at $-18\text{ }^{\circ}\text{C}$.

2.2.2 Dual curing system

Formulations generally contain the following components:

- Epoxy co-monomer (ES or EL): 0, 10, 20, 30, 40 *wt. %*
- Coupling agent (CA): 0, 1, 2, 5 *wt. %*
- Base formulation: up to 100 *wt. %*
- Cationic initiator (CI), 1 phr (parts per hundred) as a 50 *wt. %* solution in solvent *PC*, containing also a stabilizing agent (TEA) in a weight ratio of 5%, 10%, 20% respect to *CI*.

A *codification system* is been applied to identify the formulations, $ES_xCA_yCI_{z-t}$ or $EL_xCA_yCI_{z-t}$, where:

- x is the *wt. %* of epoxies
- y is the *wt. %* if the coupling agent
- z is the *phr* of initiator *CI*
- t is the weight ratio of stabilizing agent *TEA* respect to the initiator *CI*

The variations of all the different composition parameters are been evaluated in order verify the effects on the photo and thermal post-curing kinetics, partially and fully cured samples.

Given that all the components are fluid, formulation can be easily prepared by mixing all the elements in the suitable proportions in a glass vial and homogenization by hand stirring using a spatula. In the same way as before, it is useful wrap and store at lower temperature the formulation in order to withstand the pre-polymerization process. The unique case where the sample is not stored in safe conditions in the storage stability tests as shown in the following part.

2.3 Experimental characterization techniques

2.3.1 Differential Scanning Calorimetry (DSC)

Differential scanning calorimeters are the most widely used thermal analysis techniques for characterizing thermosetting materials. The calorimeters used to detect thermal phenomena are the Mettler DSC-821e and DSC-822e as shown in the following picture.



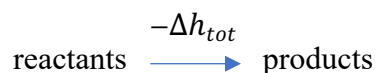
Figure 16. Mettler DSC-821e (left) and DSC-822e (right)

DSC measurement includes:

1. Degree of Conversion α and Reaction Rate (da/dt)
2. Reaction Heat Flow (dh/dt)
3. Glass transition temperature (T_g)

Both equipment has been calibrated with Indium (temperature and heat) and Zinc (temperature) standards. DSC-821e is air-cooled and equipped with a Hamamatsu LC-5 light source (Hg-Xe medium pressure lamp) and fiber-optics light guides to irradiate sample and reference pans and carry out photo-curing experiments. DSC-822e is cooled with liquid nitrogen (N_2) and is equipped with a robotic arm for automatic sampling. Photo-curing experiments are carried out at room temperature (i.e. $30\text{ }^\circ\text{C}$) while for the thermal post-curing trial are been used isothermal conditions at higher temperature (i.e. $100\text{ }^\circ\text{C}$) or under constant heating rate (i.e. 1, 2, 5, $10\text{ }^\circ\text{C}/\text{min}$) in order to analyze curing kinetics.

The thermosetting curing process is characterized by the liberation of heat:



where Δh_{tot} is the exothermic heat determined experimentally. Sometimes the reaction heat is known, and it can be used to quantify the extent to which complete reaction take place or as a reference for the isothermal kinetic trials. The basic assumption which allow to use the DSC to the thermoset cure is that the measured heat flow (dh/dt) is proportional to the

reaction rate ($d\alpha/dt$), and that the degree of cure is proportional to the heat released up to a given time, Δh_t .

$$\frac{d\alpha}{dt} = \frac{dh/dt}{\Delta h_{tot}} \quad \alpha = \frac{\Delta h_t}{\Delta h_{tot}}$$

Equation 4. Relationship conversion α , rate $d\alpha/dt$ and heat released (dh/dt and Δh)

Dynamic curing experiments have the advantage that the curing process always reaches completion. However, from a kinetics point of view, isothermal curing experiments are more reliable. In isothermal experiments, there might be some heat loss depending on the calorimeter sensitivity and some maximum rate of heat production, and due to the time to heat and establish instrument equilibrium to the desired reaction temperature. At higher temperature an important portion of the reaction take place before the calorimeters equilibrates. In order to correct this unrecorded heat is possible rerunning the experiment on the reacted sample, under the same conditions, to obtain the base line as illustrated in the following picture:

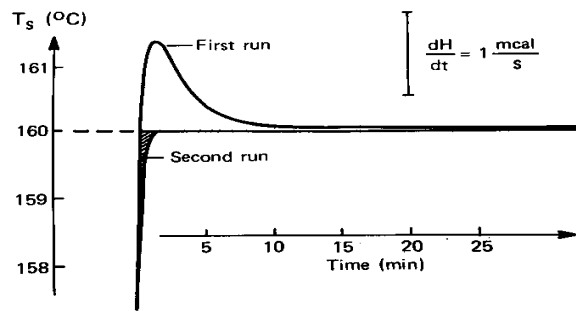


Figure 17. DSC double scan details. Adapted from [4]

Moreover, under isothermal conditions the curing process might not be complete due to vitrification [4], so that the reaction heat determined is lower than the total reaction heat. A subsequent dynamic scan can be performed to determine the residual heat Δh_{res} , and this can be used to determine the degree of cure in an isothermal experiment as

$$\alpha = 1 - \frac{\Delta h_{res}}{\Delta h_{tot}}$$

Equation 5. Degree of conversion determined from the residual heat.

The glass transition temperature T_g of different samples was determined as the midpoint in the heat capacity step Δc_p that takes place during the glass transition.

The samples for DSC analysis were placed into aluminum crucibles, with capacity of 40 μL . As shown in the following picture, the components used are a pan, the lid and, optionally, a polypropylene (PP) cover for some photo calorimetric experiments:



Figure 18. Sample preparation details.

For normal DSC experiments (i.e. dynamic curing, isothermal curing, T_g) liquid samples of about 2-10 mg were prepared. The samples were placed in the pan and covered with the lid and sealed before analysis. A small hole was pierced on the lid to allow the release of volatile components that might be formed.

For photo-DSC analysis, samples of 1.6 mg (+/- 0.1 mg) were prepared. A PP cover was placed over the liquid sample in order to obtain a sample with controlled thickness. For the analysis of thermal treatment (dynamic or isothermal) after the photocuring stage, samples of about 4-6 mg were prepared without any PP cover, irradiated, and subsequently covered with normal lid before the thermal treatment.

Samples cured in the UV-oven, of about 15-25 mg, were also analyzed with DSC. Sample preparation was identical to liquid samples for thermal analysis only.

2.3.2 Dynamic Mechanical Analysis (DMA)

The dynamic mechanical analysis (DMA) [4] is the technique that allows the determination of the mechanical response of a polymer under a given temperature and strain/stress programme. In oscillatory experiments, a sinusoidal strain is applied, and a sinusoidal stress is also obtained. From the amplitude of these signals and their relative phase angle δ , relevant parameters indicative of the viscoelastic behaviour of the polymer are obtained: the storage modulus E' , the loss modulus E'' and the loss factor $\tan \delta = E''/E'$. E' represent the elastic component of the mechanical response (recoverable energy), E'' represent the viscous component (lost energy) and the loss factor $\tan \delta$ is a measure of the relative amount of energy lost/stored.

DMA is very sensitive to the motions of the polymer chains and it is a powerful tool for localize and measure the transition which sometimes is not possible identify with the classical differential scanning calorimetry. As shown in the Figure 19 there are several methods to determine the T_g 's value:

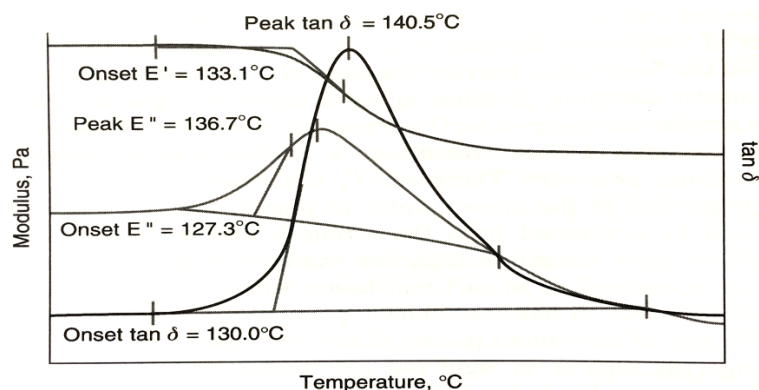


Figure 19. DMA typical scan. Adapted from [2].

It is possible to analyze the peak or onset of the $\tan \delta$ curve, the onset of the E' drop, or the onset or peak of the E'' curve. The value obtained from these methods can differ up to 25°C from each other on the same run. In addition, a $10 - 20^{\circ}\text{C}$ difference from the DSC is also seen in many materials and for this reason it is essential to specify how the T_g is detected. This is translated in establishing the heating rate, applied stress or strain, the frequency used, and the method of determining T_g .

A dynamic mechanical analyzer (DMA) TA instrument DMA Q800 is used, in the following conditions, to carry out the analysis: run the sample at a fixed heating rate of $3^{\circ}\text{C}/\text{min}$ under 0.05% strain at 1 Hz in nitrogen purge $20\text{ cc}/\text{min}$ and the T_g is determined from the peak of the $\tan \delta$ curve.



Figure 20. Dynamic mechanical analyzer TA instrument DMA Q800.

The DMA sample preparation is characterized by a standard procedure which permits to obtain a solid sample in a desired condition. It is possible to analyze photo-cured samples or fully-cured samples after thermal treatment. The first step is the preparation of the investigated formulation with a specific coding; this liquid is used to fill a mold through a syringe. The mold is formed by two glass slides divided by the rectangular shape, held together by pliers. The glass slides were previously coated with silicone grease to prevent sticking of the sample.

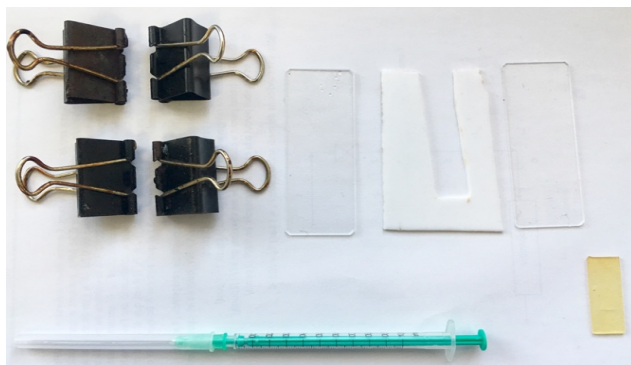


Figure 21. Sample's accessories preparation.

Then, for the photo-curing process, is used the Vilber Lourmat UV-oven, equipped with UV lamps emitting at 365 nm . The samples were irradiated at different irradiation steps: 0.1, 0.2, 0.5, 1.0, 2.0 *min*. Each irradiation step was applied on both sides of the sample before moving onto the following irradiation step.



Figure 22. Vilber Lourmat UV-oven.

The solid UV-cured sample can be analyzed in the DMA after a polishing and resizing operation in order to obtain a given length, depth and width. The same modality is used in the case of fully-cured sample, the only difference in the thermal treatment applied in the oven after the photo-curing.

2.3.3 Fourier-transform infra-red spectroscopy (FTIR/ATR)

The most widely used method to characterized polymer structure is the infrared spectroscopy (IR), particularly the Fourier transform infrared spectroscopy (FTIR) which is a technique based on the vibrations of atoms of a molecule [2]. An FTIR spectrum is obtained by passing IR radiation through a sample and determining what fraction of the incident radiation is absorbed at a particular energy. The energy at which any peak in an absorption spectrum appears corresponds to the frequency of a vibration of a part of a sample molecule and for this reason, the peak is considerate such a fingerprint of a specific group of the molecule. FTIR has improved the quality of the spectra and minimized the time required to obtain data, it is based on the idea of radiation interference between two beams to yield an interferogram. An interferogram is a signal produced as a function of the change of the pathlength between the two beams. The two domains of distance and frequency are interconvertible by the mathematical method of Fourier transformation.

In order to carry out the spectroscopy analysis of partially and fully cured samples is been used a Bruker Vertex 70 FTIR spectrometer equipped with an attenuated total reflection accessory with thermal control and a diamond crystal (Golden Gate Heated Single Reflection Diamond ATR) and a mid-band liquid nitrogen-cooled mercury-cadmium-telluride (MCT) detector. The same device can be used for the monitoring of photo-curing (in association with a Hamamatsu LC-5 light source) and thermal post-curing process under isothermal or constant heating rate.



Figure 23. Vertex 70 spectrometer Brukers and detail of ATR device.

All the IR-spectrum are recorded at 35°C in absorbance mode with a resolution of 4 cm^{-1} and a wavelength range from 400 to 4000 cm^{-1} , averaging 20 scans for each spectrum. The samples used during the experiment do not need prior preparation and they can be directly arranged on the diamond head of the ATR device. In order to acquire data from FTIR spectra it is necessary to normalize all spectra using a reference signal of some group that remain unaffected during curing process. The carbonyl ester group is been used as a reference corresponding to the band at 1720 cm^{-1} . After the scan, the characteristic peaks are displayed in the normalized FTIR spectra corresponding to different functional groups present in the formulations.

2.3.4 Thermogravimetric analysis (TGA)

The thermogravimetric analysis (TGA) is based on the continuous mass detecting, through a micro-balance, versus temperature or time while the sample is heated in a furnace with a controlled environment [4]. The sample may be heated at the constant rate or held at an isothermal temperature. One of the meaningful practical application of the TGA analysis is the measurement of the thermal stability in an inert atmosphere with nitrogen gas (N_2).

In order to exanimate the polymer degradation process, Mettler TGA/SDTA-851e Ultra-micro Balance is used to define the mass loss (m/m_0) and mass loss rate $(dm/dt) * (1/m_0)$ versus temperature of partially and fully cured sample under a constant heating rate experiment, $10^{\circ}\text{C}/\text{min}$.



Figure 24. Mettler TGA/SDTA-851e Ultra-micro Balance.

The TGA sample is composed by a portion of the solid investigated formulation arranged in the silicon oxide crucibles and heated starting from 30°C to 800°C.

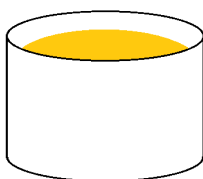


Figure 25. Crucibles for thermogravimetric analysis.

2.3.5 Soluble fraction analysis

In order to determine the extent of the polymerization process after each curing stage a soluble fraction analysis is carried out. The objective of this investigation is to evaluate the insoluble/soluble fractions of the partially and fully cured materials through reflux boiling in suitable solvent such dichloromethane which present the higher solubility rate respect to the interested formulation. The solubility process requires several hours and can be divided in different steps:

1. Sample boiling at solvent evaporation temperature (dichloromethane boiling point 39.6°C)
2. Separation of soluble/insoluble fraction by vacuum pump filtration
3. Drying in a vacuum oven to remove trapped solvent

During the last stage, every hour the sample is removed, weighed and taken back to the vacuum oven, until weight stability is reached. The liquid filtrate and dried sample obtained are analyzed by FTIR to identify their main components.



Figure 26. ES50CI1-0.1 after and before the soluble fraction analysis.

2.3.6 Storage stability analysis

The storage stability of selected liquid and partially cured materials was analyzed, in order to establish their useful pot life. The strategy adopted to verify the product stability is:

- Preparation of liquid formulation using the assumed reference
- Molding of a solid sample as same composition as the liquid
- Storage of uncured systems in oil-bath (Figure 27) at constant temperature (35°C)



Figure 27. Detail of the storage oil-bath.

Subsequently, a weekly analysis is scheduled in these modalities:

1. Solid sample: DSC dynamic analysis ($10\text{ }^{\circ}\text{C}/\text{min}$) with range temperature ($30 - 300\text{ }^{\circ}\text{C}$)
2. Liquid sample: Photo-DSC analysis carried out at $30\text{ }^{\circ}\text{C}$ with 9% light intensity of the UV-lamp and an (1-6-1_0,1) scansion program where 1 is the time without irradiation and 6 the irradiation time and 0,1 is the collecting data time of the device. Two scansion are carried out, the first to analyze the photo-curing and the first to draw the base line.

Crucibles sealed and pierced are used for the dynamic analysis while for the photo-DSC it is necessary to differentiate the analysis in two stages. In the first moment the photo-polymerization is analyzed with a crucible normally filled without the lid but for the thermal subsequently scan it is necessary close the sample as the same mode as before.

2.4 Kinetics methods and models

The kinetics of the epoxy reaction in the pure epoxy and the second stage of dual systems was analyzed using the isoconversional methodology [57]. The basis for this methodology is the assumption that the reaction rate can be expressed as separate functions of conversion α and temperature T as:

$$\frac{d\alpha}{dt} = k(T) \cdot f(\alpha)$$

Equation 6. Rate equation.

Where $k(T) = k_0 \cdot \exp(-E/RT)$ is the kinetic constant, A is the preexponential factor, E is the activation energy, R is the gas constant and $f(\alpha)$ is the model representing the reaction mechanism governing the curing process. Assuming that the reaction mechanism is not affected by the temperature schedule of the curing process, the apparent activation energy at a given degree of conversion E_x can be calculated as:

$$\frac{d\ln(d\alpha/dt)}{dT^{-1}} = \frac{d\ln(f(\alpha))}{dT^{-1}} + \frac{d\ln(k(T))}{dT^{-1}} \equiv -\frac{E_x}{R}$$

Equation 7. Definition of apparent activation energy.

Rearrangement and integration of the rate expression, Equation 6, leads to:

$$g(\alpha) = \int_0^x \frac{d\alpha}{f(x\alpha)} = k_0 \cdot \int_0^t \exp(-E/R \cdot T) \cdot dt$$

Equation 8. Integration of rate equation.

Under isothermal conditions, and taking natural logarithms:

$$\ln t = \ln\left(\frac{g(\alpha)}{k_0}\right) + \frac{E}{R \cdot T}$$

Equation 9. Integral equation for isothermal experiments.

Representation of $\ln t$ against $(R \cdot T)^{-1}$ for different experiments at a given degree of conversion α yields a straight line with slope E_x and intercept at the origin $\ln(g(\alpha)/k_{0,\alpha})$. In the case of dynamic curing experiments, integration of Equation 8 under constant heating rate leads to:

$$\frac{g(\alpha)}{k_0} = \frac{1}{\beta} \cdot \int_0^T \exp(-E/R \cdot T) \cdot dT = \frac{1}{\beta} \cdot \frac{E}{R} \cdot p(y)$$

Equation 10. Integration of rate equation under dynamic (constant heating rate) conditions.

Where β is the heating rate, and $y = E/R \cdot T$ and $p(y)$ is a numerical approximation of the solution of the temperature integral. It is used the general set of solutions proposed by Starink [58]. After rearrangement, the following expression is used [59]:

$$\ln \frac{\beta}{T^k} = \left[\ln \frac{k_0}{g(x)} + (1 - k) \cdot \ln \frac{E}{R} + B \right] - \frac{A \cdot E}{R \cdot T}$$

Equation 11. Integral equation for dynamic experiments.

Representation of $\ln(\beta/T^k)$ against $-A \cdot (R \cdot T)^{-1}$ for a number of dynamic experiments at given degree of conversion α should produce a straight line with slope E_α and an intercept at the origin from which one obtain the term $\ln(g(\alpha)/k_{0,\alpha})$. This factor, along with E_α , is used in Equation 9 for the simulation of isothermal processes starting from dynamic data. The parameters used in Equation 11 are $A = 1.0008$, $B = -0.312$ and $k = 1.92$ [58,59].

3 RESULT AND DISCUSSION

3.1 Base systems analysis

3.1.1 Spot-HT

First of all, the curing of Spot-HT systems was studied, with the purpose of understanding its kinetic and properties and therefore analyze the feasibility of the dual-curing process. Figure 28 and compares the DSC results of the photocuring process of Spot-HT formulation at 30 °C. The blue curve shows the reaction rate, while the red curve is referred to the conversion. As can be seen, the photocuring process of Spot-HT is very fast, taking place in less than a minute at room temperature.

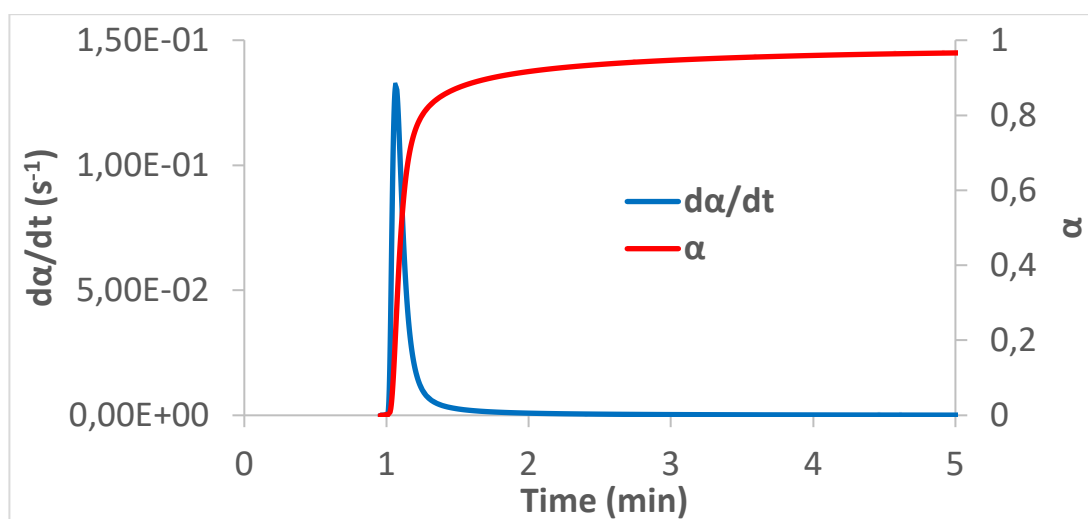


Figure 28. Isothermal DSC analysis (30°C) for the Spot-HT system. Degree of conversion (α) and rate of degree of conversion ($d\alpha/dt$) are charted respect the time.

Figure 29 shows the results of the DSC dynamic scans at 10 °C/min after photocuring of the Spot-HT system. The first dynamic scan (blue curve) shows that there is a little exotherm starting at ca. 45 °C, which suggests that the material vitrifies during the photocuring stage. Indeed, the second scan shows that the final T_g of the fully cured material is about 49 °C, which is higher than room temperature. Integration of the experimental exotherms during the photocuring stage and the subsequent dynamic scan produced values of 347 and 8 J/g, respectively, indicating that the material was almost fully cured at the end of the photocuring stage and that the reaction was incomplete most probably due to vitrification.

Figure 30 shows the dynamic scan at 10 °C/min of the Spot-HT formulation without previous UV-irradiation. It can be observed that high temperatures can lead to the formation of free radicals, therefore producing the acrylate homopolymerization. However, the thermal reaction is triggered at temperatures higher than 180 °C. In consequence, Spot-HT can be regarded as a thermally latent curing system, with a high stability at common storage conditions, and, from a practical point of view, it can be stated that the reaction will only take place under exposure to UV/visible light.

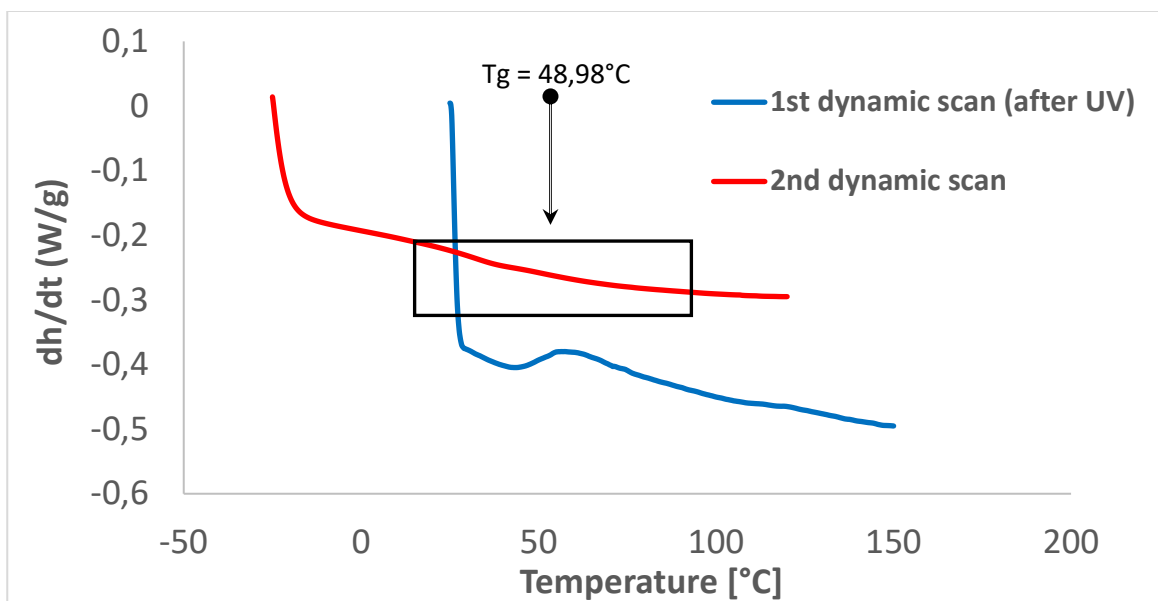


Figure 29. Dynamic DSC curves (10 °C/min) for investigated Spot-HT system. The blue curve is referred to the residual reaction heat after the dynamic-curing process. On the red curve is shown the T_g of Base-3D sample photo-cured in the UV-oven.

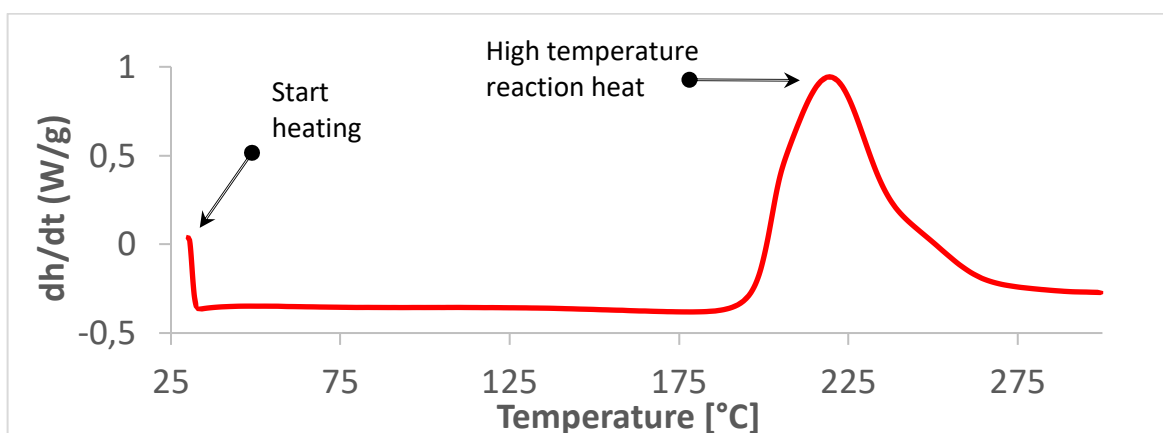


Figure 30. Dynamic DSC measurement (10 °C/min) for Spot-HT system. As can be seen by the plotted peak, the reaction is triggered by the high temperature at 200°C to end at 250°C.

Table 1. Comparison of DSC evaluation of net epoxy system ES100CI1-0.1 and Spot-HT formulation. Δh (J/g) is the heat released in the dynamic heating 10°C/min based on the sample's weight. Δh (kJ/eq) is the heat liberated but calculated with an epoxy equivalent of 130 (g/eq).

Formulation	Δh (J/g)	Δh (kJ/eq)	T_g (°C)
Spot-HT	355,2	n/d	49
ES100 CI1-0,1	617,0	80,2	n/d

The FTIR spectra of the uncured and photo-cured Spot-HT system are shown in Figure 31. The red spectrum, corresponding to the unreacted Spot-HT formulation, shows typical signals corresponding to an acrylate formulation: a strong peak at ca. 1730 cm^{-1} of the

carbonyl ester groups, a double peak around 1620 cm^{-1} characteristic of C=C bonds of the acrylate group, and sharp peaks around 1400 and 800 cm^{-1} also characteristic of acrylate C=C bonds [27,60]. The blue spectrum, corresponding to the reacted Spot-HT formulation, shows that the signals that are characteristic of acrylate C=C bonds have disappeared (taking into consideration that there might be some overlapping signals and noise in the signal), therefore indicating quantitative conversion and therefore completion of the homopolymerization of acrylate groups.

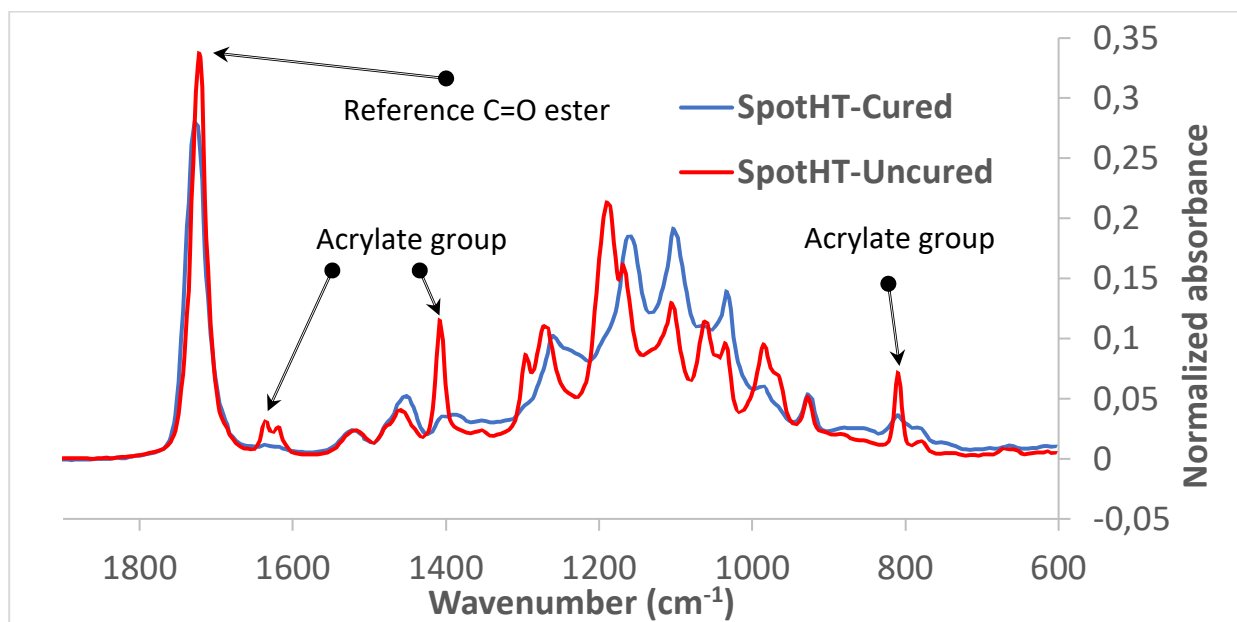


Figure 31. FTIR spectrometry results of Spot-HT sample. The red curve is referred to the uncured formulation. The blue curve represents the cured formulation. Detail of $600\text{-}1800\text{ cm}^{-1}$ absorption band are plotted.

The UV-cured Spot-HT material was analyzed by DMA and the results are shown in Figure 32. It can be observed that the relaxation of the network structure is rather broad, taking place between $20\text{-}90\text{ }^{\circ}\text{C}$. The storage modulus decreases from a value of ca. 2 GPa down to ca. 70 MPa, and the loss factor $\tan \delta$ has a well-defined peak at a temperature of $67\text{ }^{\circ}\text{C}$, which is higher than the T_g determined using DSC, as usual in DMA analysis. The loss modulus reaches a maximum at a temperature of ca $45\text{-}50\text{ }^{\circ}\text{C}$, which is closer to the T_g determined with DSC. The results indicate that, although the material is apparently vitrified at room temperature, mechanical relaxation can take place, therefore imparting flexibility and toughness to the cured material. While this is beneficial for some applications, it might be a serious limitation in other scenarios.

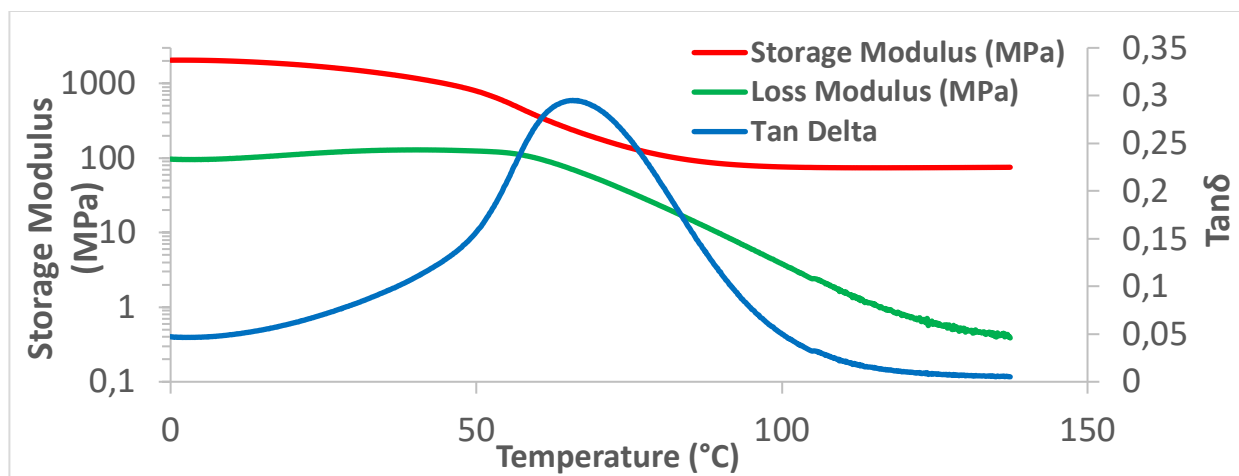


Figure 32. DMA analysis of UV-cured Spot-HT system at 3°C/min, frequency of 1 Hz and 0.05 % strain.

3.1.2 Cationic epoxy formulation

The curing of the neat ES formulation was analyzed. DSC analysis were carried out for the epoxy formulation with different stabilizing agent content ES100CI1-x (triethanolame, TEA) in order to understand the reactivity of the initiator system. TEA was added in a proportion x equal to 0.05, 0.1 and 0.2 (that is, weight ratios of CI:TEA of 1:0.05, 1:0.1 and 1:0.2). The results of this analysis are shown in Figure 33. An increase in the content of TEA produces a shifting of the curing exotherm to higher temperatures, that is, an increased latency. This could be expected, because carbocations formed by the thermal activation of the catalyst become blocked with available TEA molecules. When TEA is depleted, further formation of carbocations leads to the initiation of the cationic homopolymerization of epoxy groups. Table 2 compares the reaction heat determined for the different formulations. It can be observed that formulations with x equal to 0.05 and 0.1 the reaction heat is about 620 J/g or 82.3 kJ/eq, which are very similar to the reported values for the cationic homopolymerization of this epoxy monomer [61]. In contrast, formulation with x equal to 0.2 the heat releases is substantially lower, indicating that conversion of epoxy groups was not complete. This can be explained by the lower effective amount of available initiator for the reaction and the occurrence of termination reactions [34].

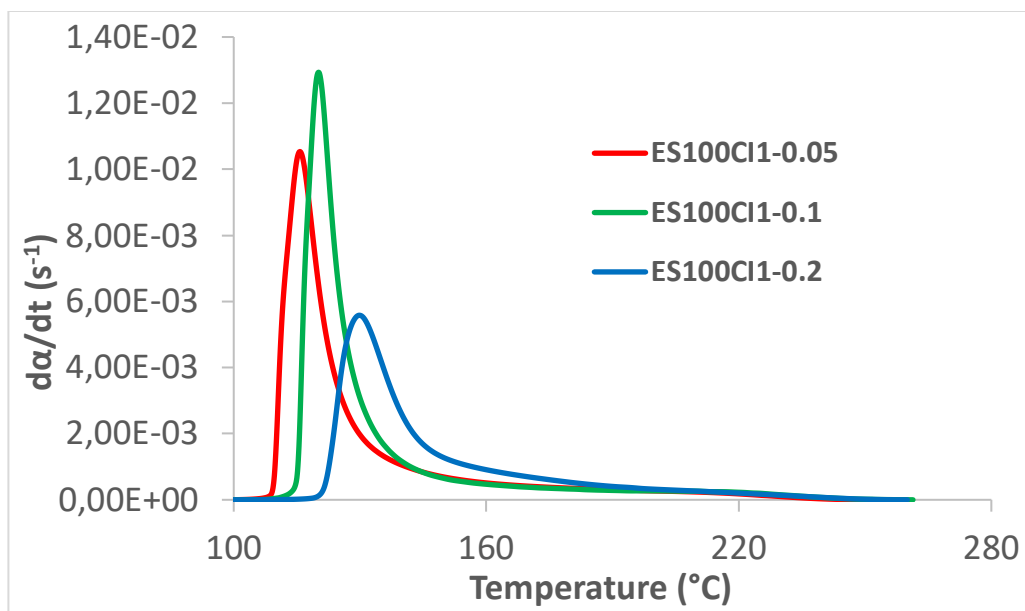


Figure 33. DSC measurement for the pure epoxy system. Rate of degrees of conversion (da/dt) versus temperature during the dynamic curing 10 ($^{\circ}\text{C}/\text{min}$) for different TEA content ES100CI1-x are shown.

Table 2. Summary of reaction heat Δh (in J/g and kJ/eq) for pure epoxy formulation with different TEA content ES100CI1-x.

Formulation	Δh (J/g)	Δh (kJ/eq)
ES100CI1-0,05	621	82.3
ES100CI1-0,1	621	82.3
ES100CI1-0,2	488	64.7

Therefore, it was decided to continue the analysis with a tea content of 0.1 in order to maximize thermal latency while ensuring completion of cure. The kinetics of the ES100CI1-0.1 formulation were analyzed in more detail in order to have a more detailed idea about the latency of this curing system and therefore analyze the viability of the dual-curing system. DSC runs were carried out at different heating rates and the results in terms of reaction rate and conversion are shown in Figure 34 and Figure 35 respectively. It is possible to observe that both rate and conversion curves are shifted to higher temperatures with increasing heating rates. Table 3 shows the reaction heat determined for all experiments. In all cases, the reaction heat is about 620 J/g or 82 kJ/eq, indicating completion of cure in all cases.

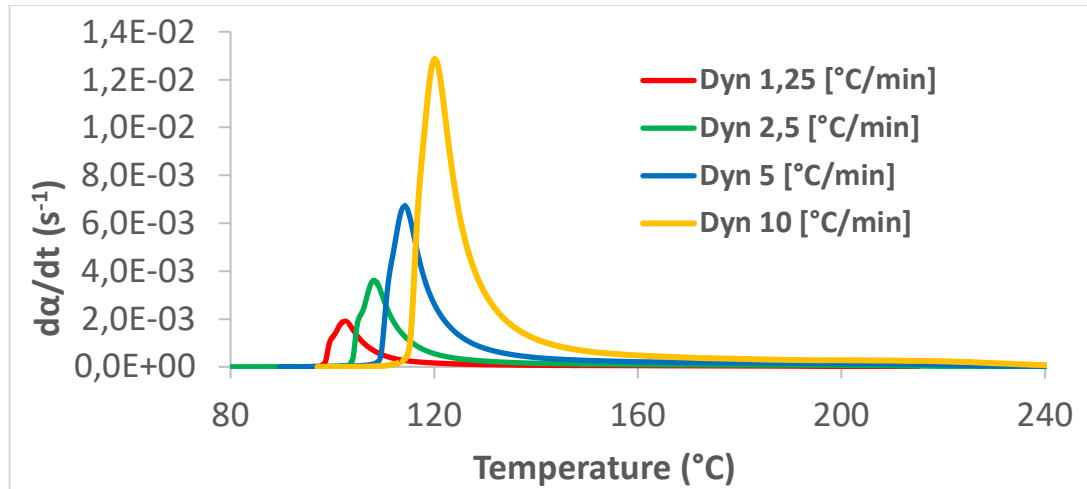


Figure 34. DSC dynamic measurement, for pure epoxy, at different heating rate of 1.25, 2.5, 5, 10 ($^{\circ}C/min$). Evaluation rate of degrees of conversion ($d\alpha/dt$) versus temperature are plotted.

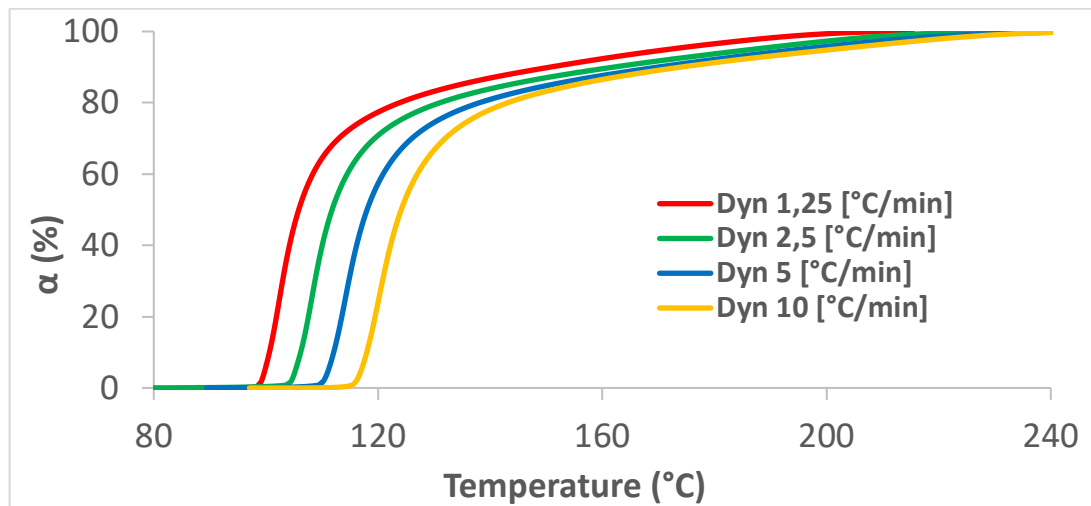


Figure 35. Comparison degrees of conversion (α) versus temperature for thermal curing of the net epoxy formulation. Heating rate of 1.25, 2.5, 5, 10 ($^{\circ}C/min$) are shown.

Table 3. Summary of the DSC dynamic analysis of ES100CI1-0.1 formulations for different heating rate 1.25, 2.5, 5, 10 ($^{\circ}C/min$). Δh (J/g) is the reaction heat released during the thermal curing. Δh_A (J/g) is the average reaction heat calculated on overall measurement.

$\beta(^{\circ}C/min)$	Δh (J/g)	Δh (kJ/eq)
1.25	616.9	81.8
2.5	630.9	83.7
5	621.9	82.5
10	620.6	82.3
Average	622.6	82.6

The curing kinetics were analyzed the isoconversional integral method based on the Starink expression for the temperature integral [58,59], Equation 11. The main factors, evaluated in

the Table 4, were the activation energy E (in kJ/mol) and $\ln(g(\alpha)/k_0)$ (min^{-1}). The correlation coefficient r^2 has also been determined. The results indicate that the curing process has a very strong temperature dependence, with values of activation energy of ca. 140 kJ/mol up to conversions of 0.7, which are much higher than commonly reported values for cationic epoxy homopolymerization cycloaliphatic epoxides [62] or other epoxy curing systems [12]. This means that the reaction rate decreases substantially with decreasing temperature, while it becomes very high at elevated temperatures. This behavior is typical of latent curing systems. The quality of the experimental data and analysis was also high, as deduced from the values of r^2 . Using the data in Table 4, predictions of isothermal curing times can be made using Equation 9. An extrapolation to a curing temperature of 30 °C yields a stability (time to reach 5 % conversion) of many weeks. Although this extrapolation is subject to significant error, this agrees quite well with an experimental determination of the storage stability of epoxy formulations with this catalytic system [55].

Table 4. Kinetics parameters at different degrees of conversion, obtained using the Starink model, from experiments of pure epoxy formulation ES100CI1-0.1

α	E (kJ/mol)	$\ln(g(\alpha)/k_0)$ (min^{-1})	r^2
0.05	139.8	-43.2	0.9999
0.1	139.1	-42.9	1.0000
0.2	138.4	-42.5	0.9999
0.3	137.6	-42.1	0.9999
0.4	137.1	-41.8	0.9997
0.5	136.9	-41.5	0.9992
0.6	137.0	-41.3	0.9975
0.7	140.8	-41.9	0.9878
0.8	151.9	-43.9	0.9124
0.9	161.7	-43.3	0.8194
0.95	162.9	-41.1	0.9486

Validation of the dynamic data and the isoconversional methodology was performed by comparing the results of the predictions made by the isoconversional method with experimental isothermal curing processes determined with DSC. Figure 36 shows the rate curves determined at 90°C, 100°C, 110°C, 120°C. A striking feature of these curves is the fact that reaction rate is close to zero at the beginning of the curing process while, after a certain period, it increases sharply up to a peak in reaction rate. This can be associated with a latent behavior of the catalytic system. During the initial period, carbocations are being generated but blocked by available TEA. When TEA is exhausted, further activation of the catalyst produces a fast and sharp reaction. A strong temperature dependence, as suggested by the previous analysis, is reported. As seen in Figure 36, the reaction onset increases, and the reaction rate decreases by a factor of 4 approximately upon decreasing the curing temperature 10 °C.

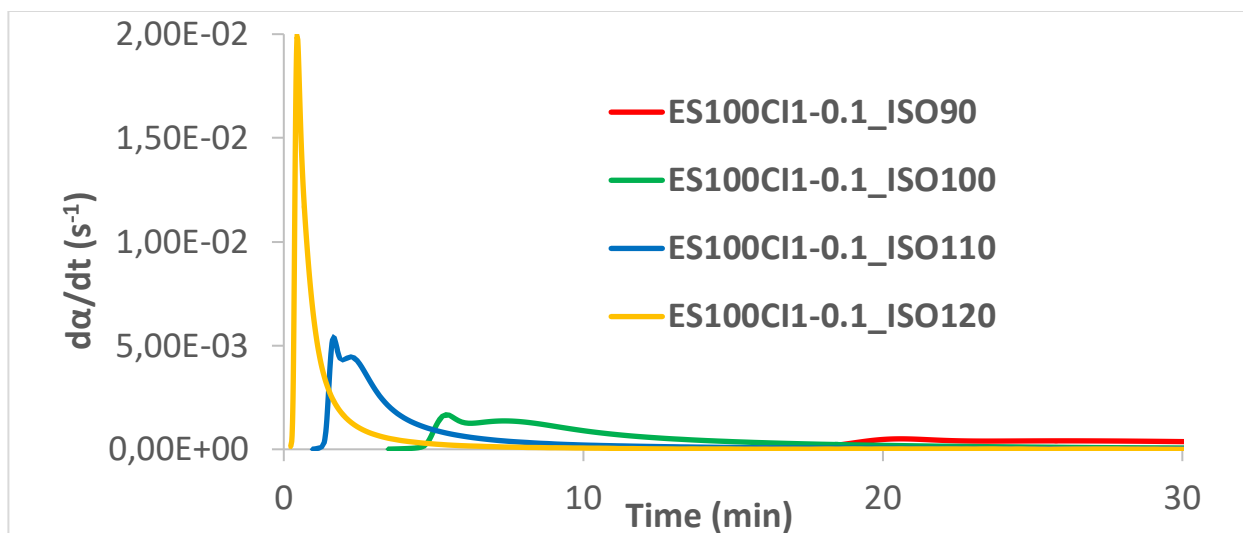


Figure 36. DSC isothermal analysis for the epoxy system ES100CI1.0.1. Evaluation rate of degree of conversion ($d\alpha/dt$) versus time during different isothermal trials 90, 100, 110, 120 °C.

The results of the calorimetric analysis of the isothermal DSC measurement are presented in the Table 5. It can be observed that the heat released during the isothermal curing process is clearly lower than the heat evolved during the dynamic scans (see Table 3). This suggested, in all cases, that the curing process was incomplete due to vitrification (as could be expected given the high T_g of these curing systems [55]). The values of the heat released Δh_{iso} do not follow a rational trend, however, for experimental reasons (i.e. difficulty to measure appropriately the reaction heat at too high or low temperatures). In consequence, dynamic scans at 10 °C/min were performed, and it can be observed that, the higher the isothermal curing temperature, the lower the residual heat Δh_{res} , therefore the higher the degree of cure in the isothermal step α_{iso} , as could be expected. The total reaction heat Δh_{tot} is about 620 J/g or 80 kJ/eq, except for the experiment at 120 °C, because of experimental or analysis error.

Table 5. Comparison of Isothermal DSC analysis at different temperatures 90, 100, 110, 120 °C. Δh_{iso} (J/g) is the reaction heat released during the isothermal experiment. Δh_{res} (J/g) is the residual heat generate during the dynamin analysis 10 (°C/min). Δh_{TOT} (J/g) is the total amount of heat produced during all the process. Δh_{TOT} (KJ/eq) is the heat liberated but calculated with an epoxy equivalent of 130 (g/eq). α_{iso} us the calculated degree of cure in the isothermal experiments determined on the basis of the residual heat.

T (°C)	Δh_{iso} (J/g)	Δh_{res} (J/g)	Δh_{tot} (J/g)	Δh_{tot} (KJ/eq)	α_{iso}
90	511.9	122.0	633.9	84.1	0.803
100	509.0	107.4	616.4	81.7	0.827
110	524.7	91.7	616.4	81.7	0.852
120	485.7	85.1	570.8	75.7	0.863

Taking into account the maximum conversion of epoxy groups during the isothermal curing stage, the experimental degree of conversion was calculated with the simulated isothermal curing processes making use of the parameters in Table 4 and Equation 9. As can be observed in Figure 37, the agreement between the experimental and predicted data are excellent,

therefore confirming the validity of the previous analysis. In the light of these results, the tentative prediction of storage time at lower temperatures becomes pore solid. Therefore, it can be concluded from this analysis that this cationic epoxy formulation has a significant thermal latency, as expected [55].

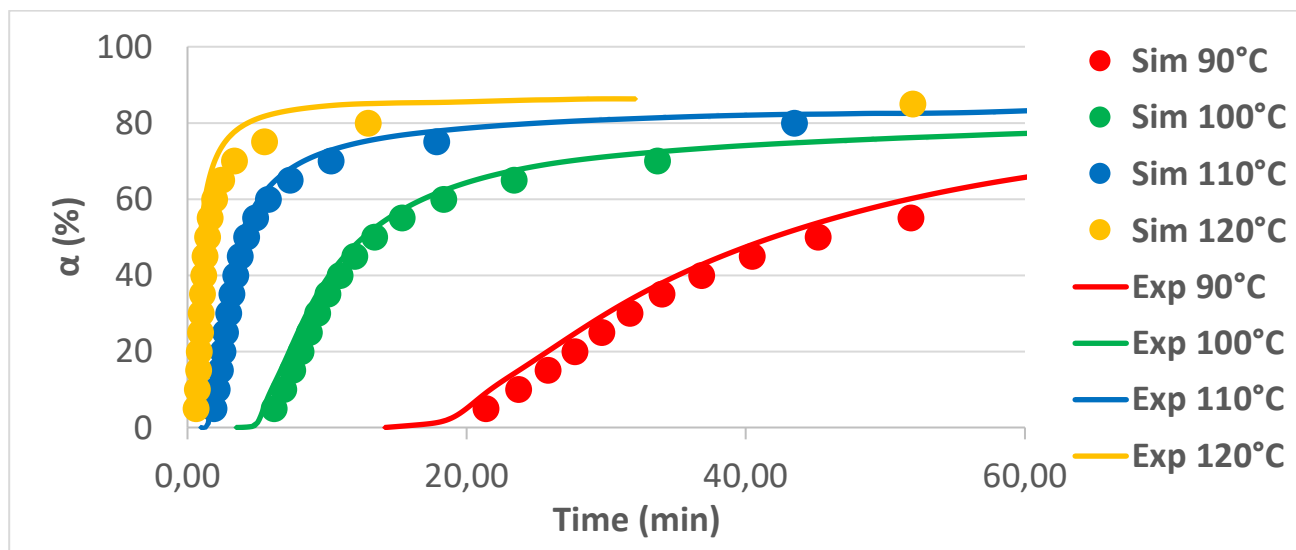


Figure 37. Kinetics analysis of net epoxy system. Experimental and simulated degree of conversion versus time for 90°C, 100°C, 110°C, 120°C isothermal trials. The solid lines represent the experimental data and the symbol correspond to the data calculated by using the parameters obtained with the Equation 11.

The FTIR spectra of the uncured and cured Epoxy system is determined in the Figure 38. The blue spectrogram is typical of the raw uncured epoxy formulation, showing a strong peak at 1730 cm^{-1} characteristic of the carbonyl ester group in the monomer structure and the absorption at ca. $750\text{-}800\text{ cm}^{-1}$ characteristic of the epoxy ring. The red curve shows the spectrum of a fully cured material, evidencing complete disappearance of the epoxy group at 800 cm^{-1} and appearance of a strong absorption at 1100 cm^{-1} typical of C-O-C ether bonds formed during the cationic homopolymerization.

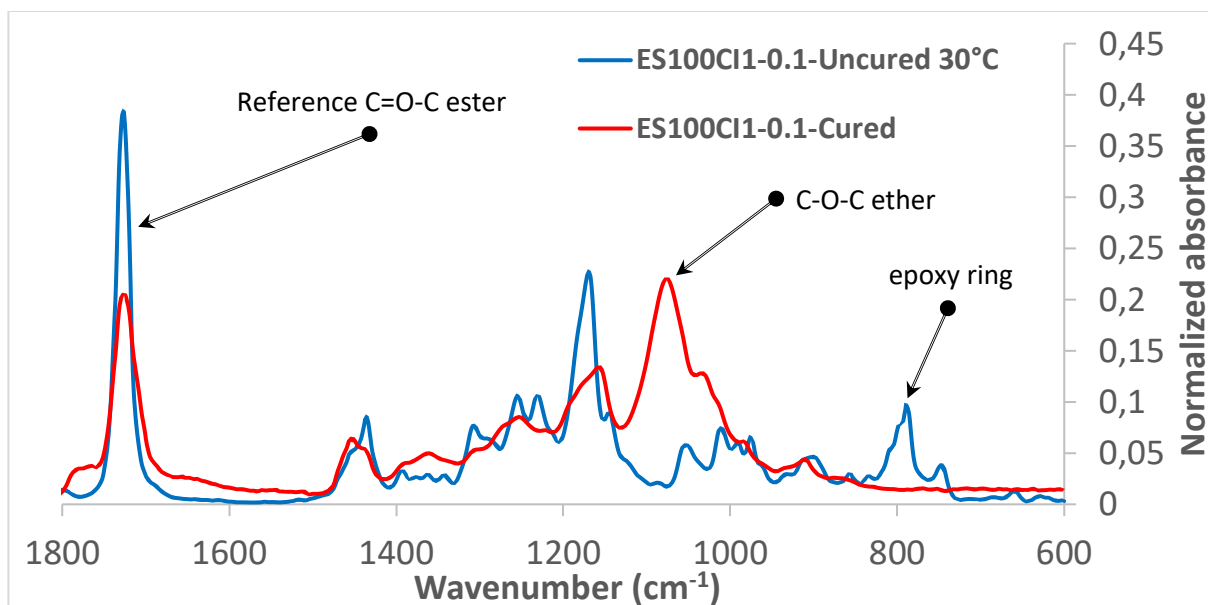


Figure 38. FTIR spectrometry results epoxy system ES100CI1-0.1. The red curve is referred to the cured formulation. The blue curve represents the uncured formulation. Detail of 600-1800 cm^{-1} absorption band are plotted.

It was not possible to determine with precision the glass transition temperature of fully cured materials using DSC or DMA, because of the difficult preparation of samples. At the tested thermal oven temperatures, very sharp reaction rate would take place, therefore producing an excessive accumulation of heat leading to extremely high curing temperatures causing degradation. It was attempted to determine the T_g after curing in the DSC but the high crosslinking density lead to an extremely broad relaxation making it difficult to determine the value of T_g with precision. In consequence, it was trusted the reported results for these formulations [55], suggesting a value of T_g close to or higher than 200 °C for the fully cured epoxy.

3.1.3 Feasibility of the dual-curing system

The results above suggest that it is possible to design a family of dual-curing systems based on the combination of different amounts of Spot-HT and ES (with the employed catalytic system). In more specific terms:

- From the kinetics point of view, the analysis of the individual Spot-HT and epoxy formulations suggests that the curing processes can be activated in a selective and sequential way. Irradiation at room temperature would be used to activate the acrylate homopolymerization (it was also verified that the curing process of the epoxy formulation was not activated using UV-light), while temperature would be used to activate the second curing reaction after completion of the first curing stage. The analysis also suggests that dual-curing formulations would have a significant latency and therefore storage stability.

- With respect to material properties, the large difference between the properties of the cured Spot-HT (T_g of ca. 49 °C) and the epoxy (T_g of ca. 200 °C) indicates that it is possible to design a family of materials with a wide range of properties, ranging from that of a flexible and tough material at room temperature to that of a highly rigid material at elevated temperatures, as observed for other dual-curing systems [63].

Therefore, in the following section of this thesis a family of dual-curing systems based on this combination will be explored. The effect and interaction between the different components will be tested. Additional components such as coupling agent (hydroxyethyl methacrylate, HEMA) will be tested.

3.2 Analysis of dual systems

3.2.1 Analysis of photo-curing stage

Epoxy monomer content

First of all, we tested the effect of the epoxy monomer on the photocuring kinetics. A range of formulations with varying epoxy content, ESxCI1-0.1, were prepared. Figure 39 and Figure 40 show the heat flow and the conversion during the photocuring stage. It can be observed that the addition of ES to the Spot-HT produces a decrease in the reaction rate during the photocuring stage, which becomes proportional to the Spot-HT content. Table 6 show that the heat released during the photocuring stage decreases with increasing epoxy content. It is noteworthy that the overall degree of conversion, relative to the extent of photocuring process (see Figure 40), show that the photocuring process is completed in nearly the same time regardless of the ES content. These results could be partially explained by the expected taking into account that only the acrylates would react in the photocuring stage, while epoxy groups would remain unreacted. However, the dilution effect caused by the addition of the epoxy component should be analyzed. One might expect that the mixture between Spot-HT and the epoxy would produce a dilution of both the acrylate and the photo-initiator, and therefore a stronger decelerating effect might be expected, according to the radical photopolymerization model outlined by Decker [29], assuming continuous irradiation, pseudo-steady state initiator concentration and bimolecular termination:

$$-\frac{dM}{dt} = k_p \cdot \left(\frac{\phi_i \cdot I_a}{k_t} \right)^{1/2} \cdot M$$

Where k_p and k_t are the propagation and termination rate constants, M is the concentration of monomer (acrylate), and $\phi_i \cdot I_a$ is the initiation rate expressed in terms of quantum yield of the photolysis (ϕ_i) and intensity absorbed and I_a . However, given that the dilution of Spot-HT facilitates light penetration [64], photolysis and photoinitiation rate would be somewhat enhanced therefore making up for the decrease in photo-initiator content.

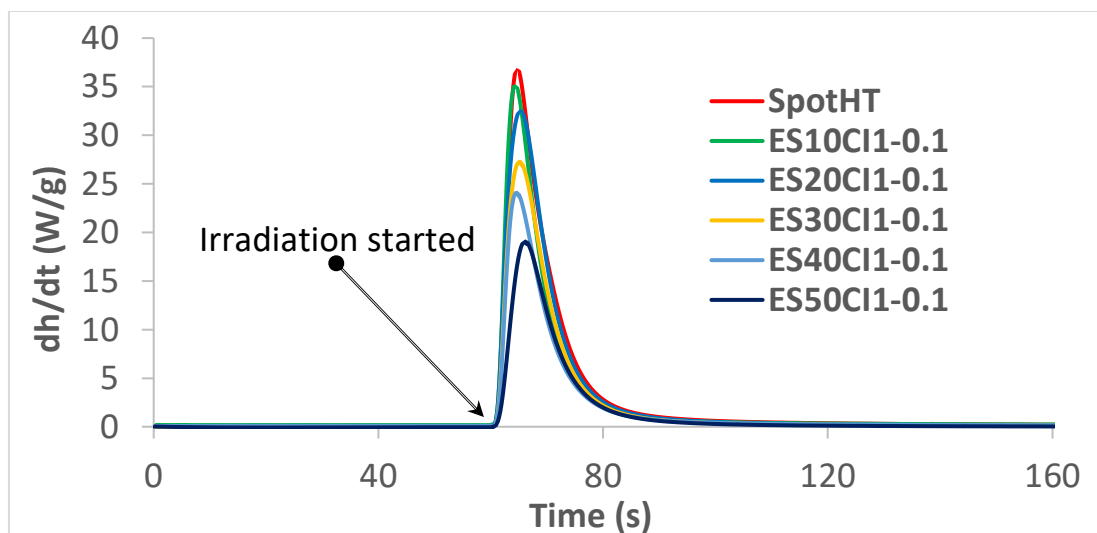


Figure 39. DSC photo-curing kinetics for different dual-system formulation ES_xCI1-0.1. Reaction heat for base-3D system and samples with 10%, 20%, 30%, 40%, 50% epoxy content into the formulation are shown at 10 (°C)/min heating rate respect to time.

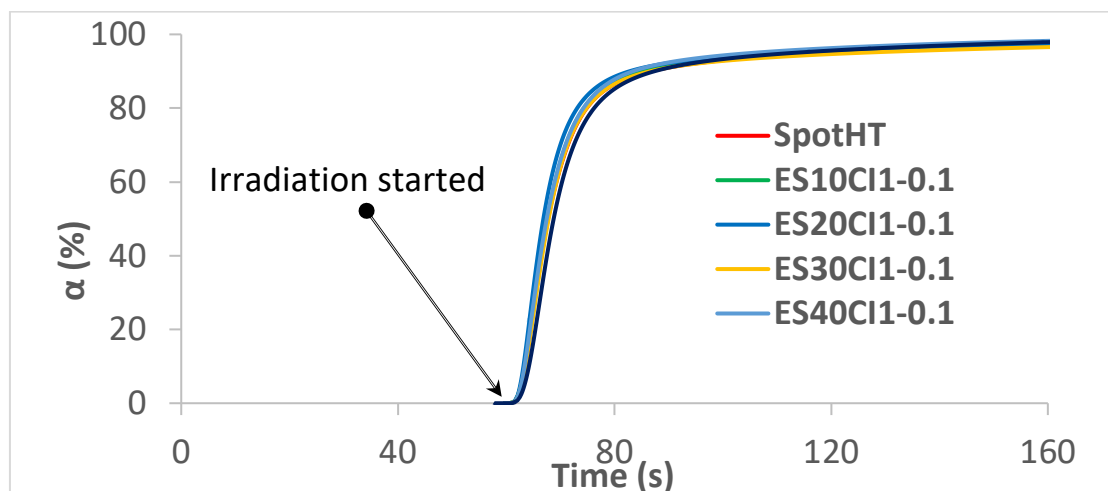


Figure 40. DSC photo-curing analysis for different dual-system formulation ES_xCI1-0.1. Simulated degrees of conversion (α) vs. time for Base-3D system and samples with 10%, 20%, 30%, 40%, 50% epoxy contents are charted.

Table 6. Summary of DSC analysis for the Spot-HT and different epoxy formulation ES_xCI1-0.1. Δh_{ISO} (J/g) is the isothermal reaction heat. Δh_{RES} (J/g) is the residual heat obtained from the dynamic experiment at 10 (°C)/min). Δh_{TOT} (J/g) is the total amount of heat produced during the curing reaction. T_{g1} (°C) is the glass transition temperature after photo-curing stage and T_{g2} (°C) is the glass transition temperature of the fully polymerized sample.

Formulation	Δh_{ISO} (J/g)	Δh_{RES} (J/g)	Δh_{TOT} (J/g)	T_{g1} (°C)	T_{g2} (°C)
Spot-HT	346.9	8.2	355.1	49	49
ES10CI10.1	323.7	63.5	387.2	31	65
ES20CI10.1	293.5	129.7	423.3	-9	78
ES30CI10.1	273.7	191.6	465.3	-25	92
ES40CI10.1	224.5	256.3	480.8	-36	97
ES50CI10.1	200.1	310.7	510.8	-42	110

The FTIR analysis of intermediate materials was carried out. In all cases it was shown that conversion of acrylate groups was complete, as observed in Figure 41 for ES30CI1-0.1 (30 wt.% epoxy), in agreement with the data reported in Table 6.

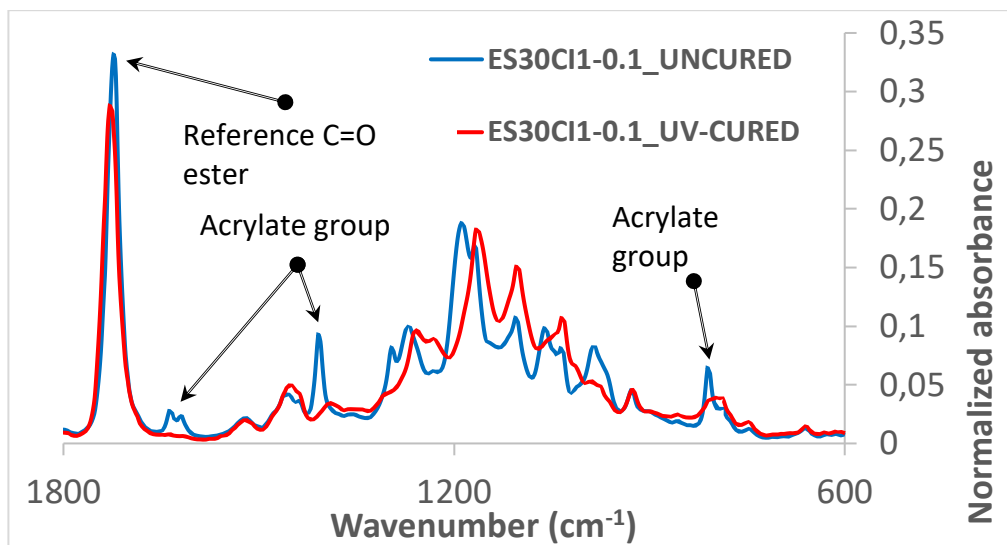


Figure 41. FTIR spectrometry results of ES30CI1-0.1 formulation. The red curve is referred to the UV-cured sample. The blue curve indicates the uncured formulation. Detail of 600-1800 cm⁻¹ absorption band are plotted.

Coupling agent content

It was hypothesized that the presence of a coupling such as HEMA would have a beneficial effect in terms of compatibility between the acrylate and the epoxy network in the final materials, given the possibility of the participation of the methacrylate group in the radical homopolymerization process of acrylate groups of Spot-HT and the participation of the hydroxyl group in HEMA as chain-transfer agent in the cationic epoxy homopolymerization [33].

The effect of using HEMA as coupling agent was examined on formulations containing 30 wt.% of epoxy component, that is, ES30CA_yCI1-0.1, where *y* is the HEMA content. The results of the analysis of the HEMA content on the photocuring stage are shown in Figure 42 and Figure 43, and also in Table 7. It can be seen that increasing HEMA content leads to a decrease of reaction rate and therefore a slower conversion of reactive groups. This effect is especially visible with a proportion of HEMA higher than 2 wt.%. The effect of the HEMA content on the total reaction heat during the photocuring stage is negligible, as seen in Table 7, which indicates that does not affect completion of cure in the photocuring stage. The effect on kinetics could be expected taking into consideration that the coupling agent used, HEMA, is a methacrylate, and the reaction rate of methacrylate polymerization is slower than of acrylates, because of the higher stability (and lower reactivity) of the tertiary radical formed during methacrylate homo-polymerization, in contrast with the highly active, secondary radical formed during acrylate homo-polymerization.

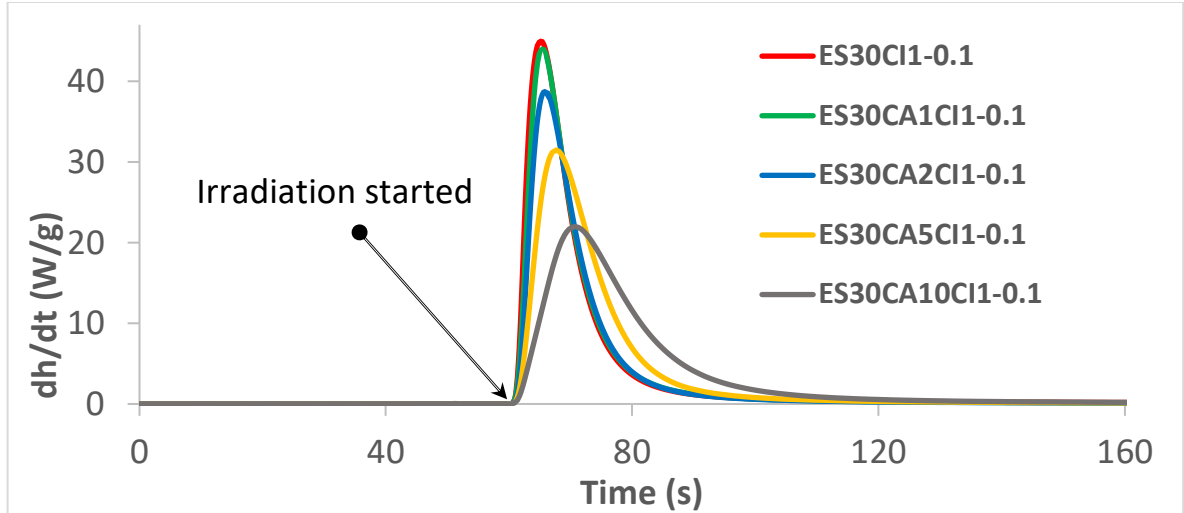


Figure 42. DSC photo-curing kinetics for ES30CAxCI1-0.1 formulation. Reaction heat for samples with 1%, 2%, 5%, 10% coupling agent content into the formulation are shown at 10 (°C)/min heating rate.

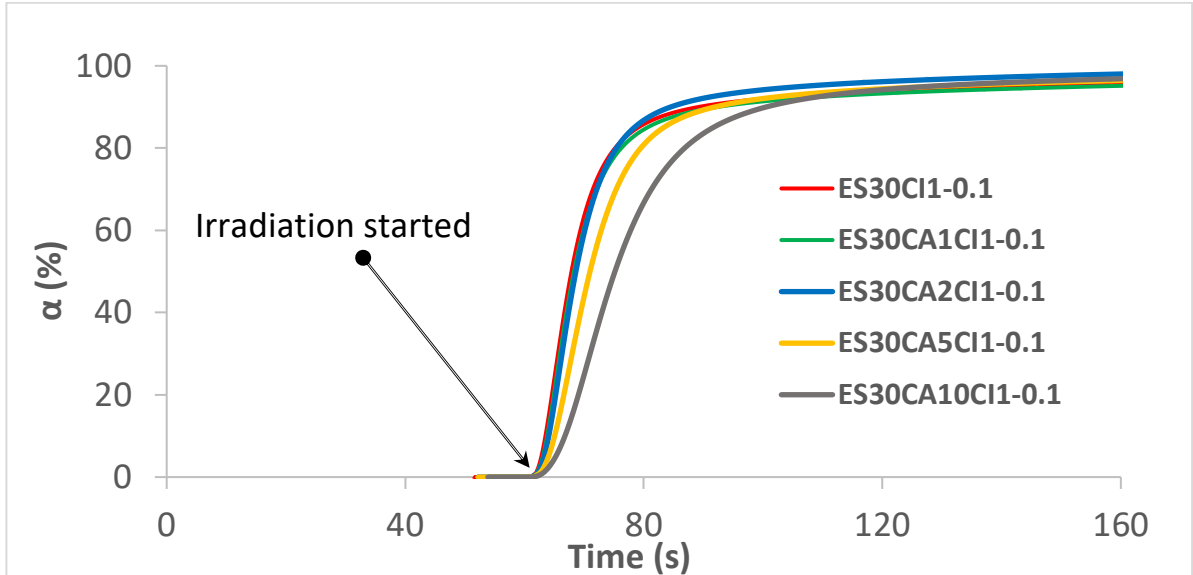


Figure 43 DSC photo-curing analysis. Simulated degrees of conversion (α) vs. time for ES30CAxCI1-0.1 formulation with 1%, 2%, 5%, 10% coupling agent contents are shown at 10 (°C)/min heating rate.

Table 7. DSC analysis of a given epoxy formulation for different coupling agent (CA) concentration. Δh_{ISO} (J/g) Is the heat released during the photo-curing stage. Δh_{RES} (J/g) Is the heat produced to complete the thermal curing process. Δh_{TOT} (J/g) Is the total quantity of heat developed during the dual-curing polymerization.

Formulation	Δh_{ISO} (J/g)	Δh_{RES} (J/g)	Δh_{TOT} (J/g)
ES30CI1-0.1	276.0	186.9	462.9
ES30CA1CI1-0.1	273.2	182.4	455.6
ES30CA2CI1-0.1	263.6	181.1	444.6
ES30CA5CI1-0.1	274.8	182.5	457.2
ES30CA10CI1-0.1	268.3	188.7	456.9

The results suggest that it is safe to use up to 2 wt. % of HEMA as coupling agent, because higher amounts would have a significant impact on kinetics and therefore it would be detrimental to the production rate in the 3D-printing stage. Given the small limiting amount of HEMA, it was decided not to proceed further with the use of HEMA in the following analyses. An acrylate-based coupling agent would be necessary if one wanted to increase compatibility without decreasing the rate. Hydroxyethyl acrylate (HEA) was also available in the laboratory, but was not considered because it was too volatile for practical use. The study of other coupling agent was left out of the scope of the work. In consequence, the main compositional parameter in the dual-curing systems studied will only be the epoxy monomer content.

Intermediate materials properties

The effect of the epoxy content on the intermediate materials was analyzed. A number of formulations were photocured in the UV oven and the intermediate materials were later analyzed. Figure 47 shows the dynamic scan at 10 °C/min determined with DSC, showing the increase in heat capacity step taking place during the glass transition of the different intermediate materials (with 10 to 50 wt.% epoxy content) in comparison with the Spot-HT. The numerical values of the T_g are also shown in Table 6 (intermediate material properties $T_{g,1}$). It can be observed that, upon increasing epoxy content, the glass transition is shifted to lower temperatures. This could be expected because the T_g of Spot-HT is 49 °C but that of the unreacted epoxy monomer is of about -70 °C (determined long ago within the research group). These results indicate that the intermediate materials would be relaxed and therefore soft at room temperature once photocured, in contrast with the neat Spot-HT material.

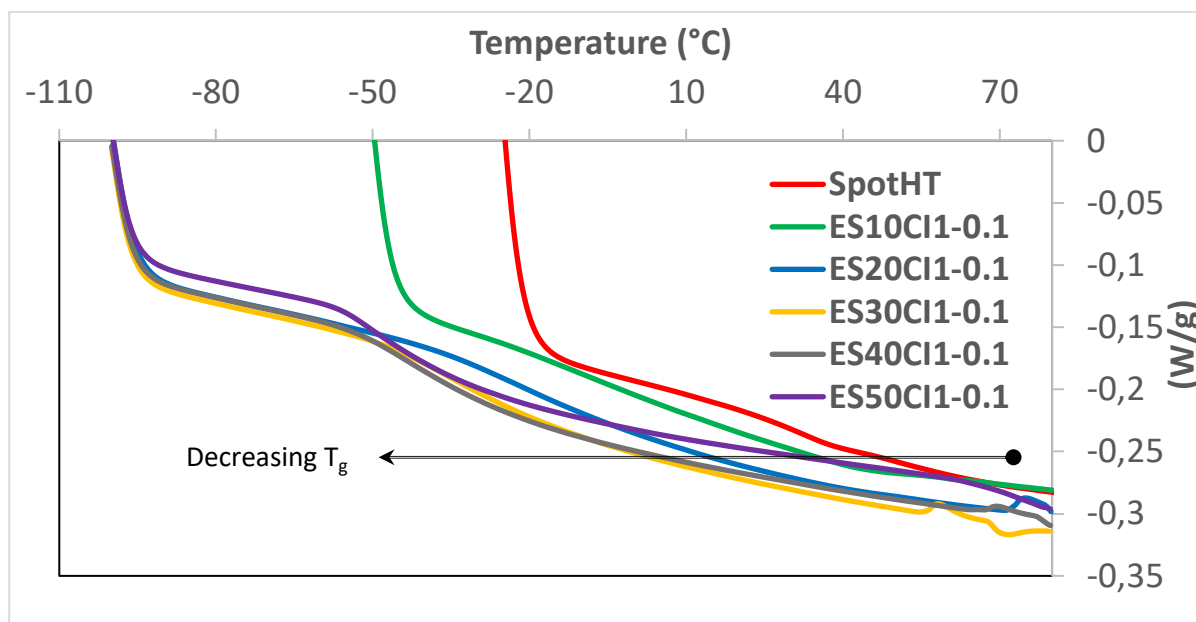


Figure 44. Effect of the epoxy content on the T_g of the intermediate materials after photocuring. Experiments carried out at 10 °C/min after photocuring in the UV oven.

A dynamic mechanical analysis of the photocured materials was carried out in order to analyze their structure and mechanical properties. The results are summarized in Figure 45,

Figure 46 and Table 8. As can be seen in the Figure 45 (storage modulus E') and Figure 46 (loss factor $\tan \delta$), the mechanical relaxation of the intermediate materials (given by the drop in storage modulus and peak in $\tan \delta$) shifts to lower temperatures upon increasing epoxy content. This is in agreement with the DSC results shown in Figure 47 and the decreasing glass transition temperatures reported on Table 6. It can also be observed that the relaxed storage modulus of the material decreases significantly with increasing epoxy content, because of the presence of unreacted epoxy monomer swelling the acrylate network. The decrease in modulus is connected with the dilution of the acrylate with epoxy, but also with a change in the network build-up process during the acrylate homo-polymerization, as reported in the literature [65]. Materials with an epoxy content above 30 wt.% are nearly fully relaxed at temperatures as low as room temperature, with a modulus in the range of 10-30 MPa (see Table 8). This indicates that the materials would be soft and relaxed after the 3D-printing process and during the thermal treatment to activate the second curing process. Table 8 also shows that the relaxation becomes broader with increasing epoxy content, as it is commonly reported for swollen networks [65].

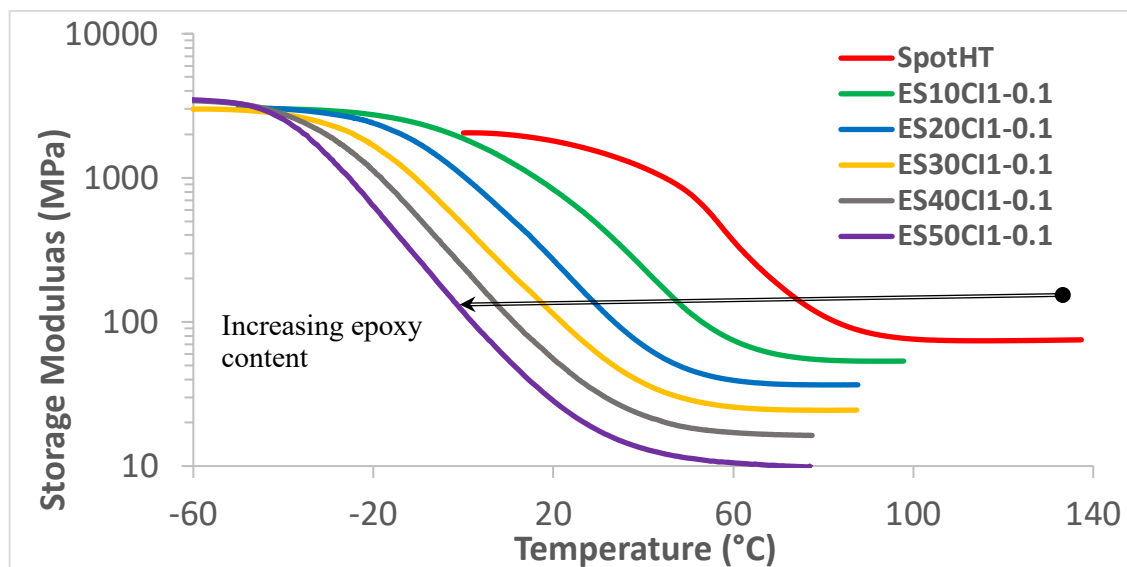


Figure 45. Results of the DMA dynamic analysis at 3 °C/min, 1 Hz and 0.05 % strain of Spot-HT and ES_xCI1-0.1 intermediate formulation. Storage Modulus is shown.

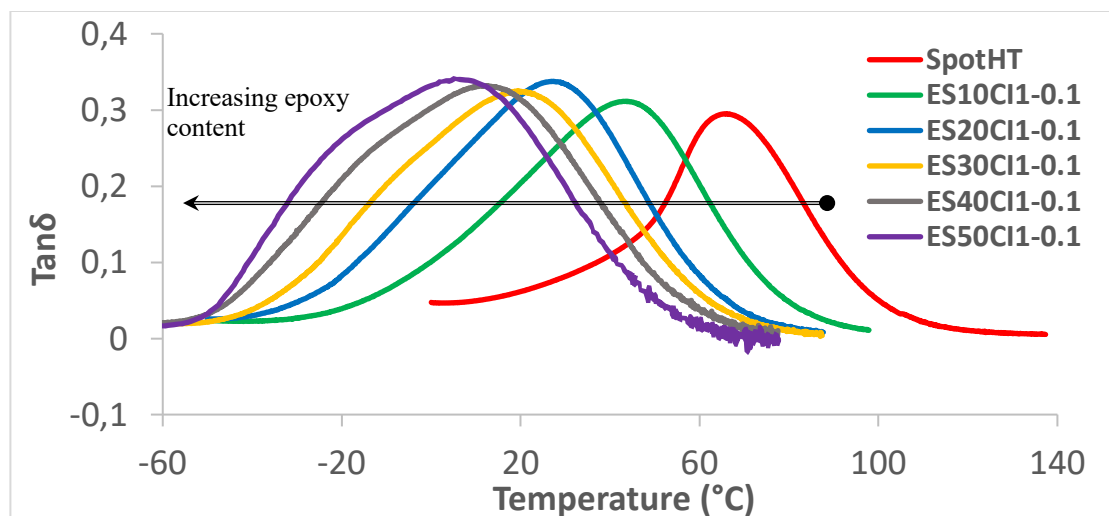


Figure 46. Results of the DMA dynamic analysis at 3 °C/min, 1 Hz and 0.05 % strain of Spot-HT and ESxCI1-0.1 intermediate formulation. $Tan\delta$ is plotted in the graph.

Table 8. Summary of DMA analysis of Spot-HT and ESxCI1-0.1 intermediate formulation. Storage modulus (E'), loss modulus (E''), and $Tan\delta$ trend are tabled.

Formulation	E' relaxed (MPa)	$Tan\delta$ peak T(°C)	$Tan\delta$ \uparrow height (°C)	$Tan\delta$ \Leftrightarrow width (°C)	E'' peak T(°C)
Spot-HT	74	66.5	0.269	34.5	40.9
ES10CI1-0.1	53	43.7	0.295	50.6	6.5
ES20CI1-0.1	37	21.2	0.322	52.5	-9.3
ES30CI1-0.1	25	19.5	0.314	59.4	-19.2
ES40CI1-0.1	17	11.5	0.317	63.5	-30.1
ES50CI1-0.1	8	5,1	0.335	65.4	-35.1

Further analyses were carried out to verify the degree of cure and analyze the material properties after the photocuring stage. First of all, we determined the soluble fraction of the photocured material in dichloromethane under normal boiling and full reflux conditions. The results of the analysis are shown in Table 9. It can be observed that the insoluble residual weight fraction decreases upon increasing the epoxy content. The results are reasonable, given that the epoxy monomer would not participate in the photocuring process, and confirms that reaction of acrylates in the photocuring stage is quantitative. The experimental results agree well with the theoretical residual weight calculated from the composition of the formulation, as seen in the table, and evidence the formation of an acrylate network after photocuring in all cases. The results suggest there is a larger soluble fraction than the theoretical due to a minor fraction of acrylate monomers unreacted by topological restrictions. The solid fraction was further analyzed by FTIR and DSC, confirming this hypothesis.

Table 9. Comparison between the experimental residual weight and the expected theoretical weight for the intermediate material.

Formulation	Experimental Residual weight (%)	Theoretical Residual weight (%)
Spot-HT	96.9	100
ES10CI1-0.1	85.5	88.2
ES20CI1-0.1	76.5	78.4
ES30CI1-0.1	69.9	68.6
ES40CI1-0.1	57.4	58.8
ES50CI1-0.1	48.1	49.0

The insoluble fraction of all the materials, which should correspond only to reacted acrylate network, were analyzed using FTIR and DSC. The results were almost identical in all cases. From the DSC analysis, it was observed that the T_g of the insoluble was of ca. 70 °C, around 20 °C higher than the T_g of the photocured Spot-HT formulation. Figure 47 compares the DSC traces of the cured Spot-HT and the solid filtrate of ES30CI1-0.1 (the quality of the data was better in this case, although the results were very similar in all the formulations). In spite in the uncertainty in the determination of the nominal value of T_g , the shift of the glass transition to higher temperatures is evident. This can be explained by the presence of either unreacted acrylate monomers in the cured Spot-HT material, or unreactive plasticizing agents, that are added to the formulation with the purpose of enhancing flexibility and toughness.

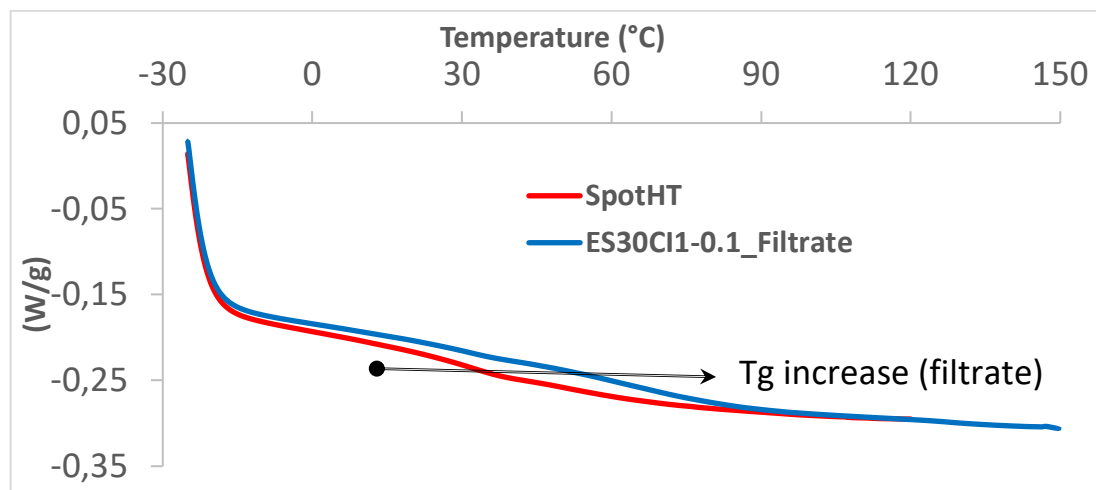

Figure 47. Dynamic DSC curves for investigated Spot-HT and ES30CI1-0.1_Filtrate system. Rising T_g is shown at 10 (°C/min) heating rate.

Figure 48 compares the FTIR spectra of the solid filtrate and liquid extract from the analysis of the sample containing the highest epoxy content. It could be observed the solid filtrate is almost identical to the cured Spot-HT material (see Figure 31), showing no traces or acrylate nor epoxy groups, while the liquid extract is almost identical to the pure unreacted epoxy monomer (see Figure 38), which confirms that the first reaction is quantitative and selective, in agreement with previous results. Comparison of the FTIR spectra of Spot-HT and a solid

filtrate evidenced there was a small amount remaining unreacted acrylate groups (the results are not shown because the difference between the spectra are difficult to appreciate), therefore confirming the above hypothesis on the higher T_g of the solid filtrate.

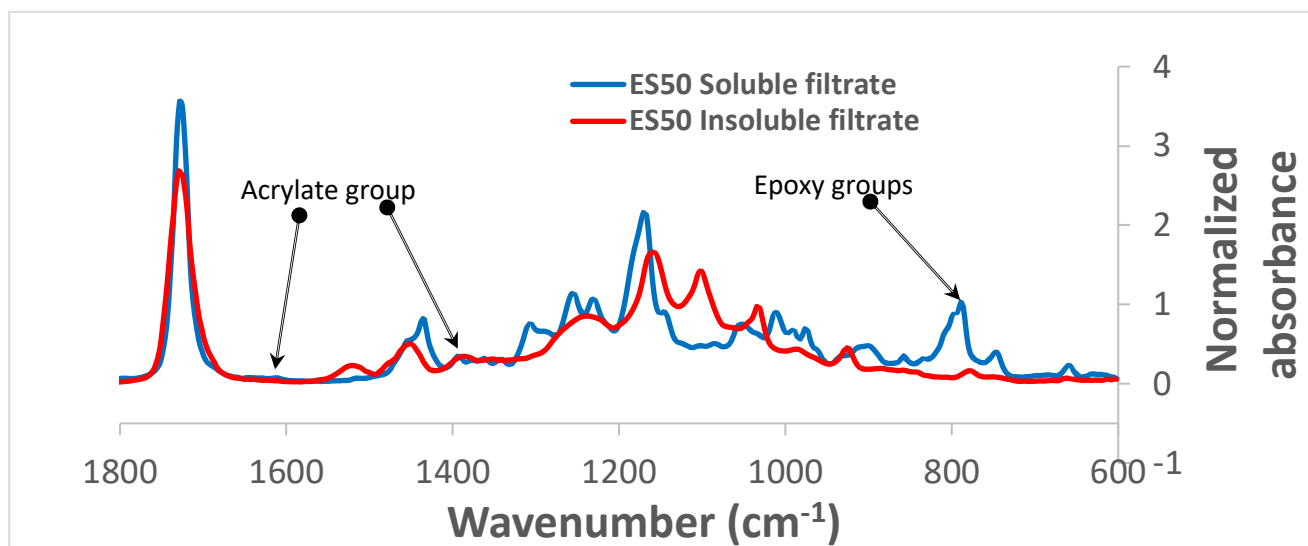


Figure 48. FTIR spectra of soluble extract and insoluble filtrate after solubility analysis of ES50CI1-0.1 in dichloromethane.

3.2.2 Analysis of thermal curing stage

Effect of epoxy content on curing kinetics

First of all, the effect of the epoxy content on the thermal curing stage after the photocuring was examined. As is can be seen in the Figure 49, the result heat flow developed during the thermal-polymerization increase with the rising of the epoxy concentration. The maximum heat released corresponds to the pure epoxy formulation and that behavior was expected taking into consideration the composition of the formulation and the results of the initial analysis. The same behavior is observed in the Figure 50 where is reported the degree of conversion (α) versus the temperature during the dynamic curing. An improved conversion is achieved with the rising of epoxy content. Given that the concentration of CI in the formulation was identical in all cases, the decrease in reaction rate with increasing dilution in the Spot-HT formulation can be explained, first of all, by the dilution of epoxy groups within the formulation. However, it is hypothesized that the significant presence of ester groups in the formulation coming from the structure of the Spot-HT material or other species, can further slowdown the curing process. Crivello reported on the negative interaction of ester groups in the cationic homopolymerization of cycloaliphatic epoxides [66]. Indeed, it was verified that the ester:epoxy ratio was higher for formulations with decreasing epoxy content. Other species such as polyether structures are also known to produce a delay on the curing process by the formation of dormant species [34].

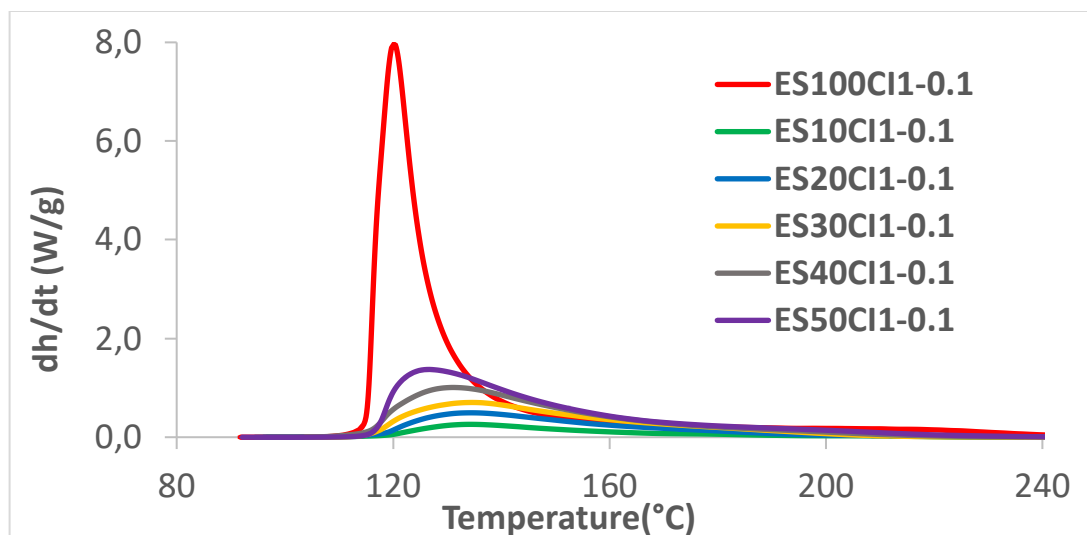


Figure 49. DSC thermal-curing analysis for different ESxCI1-0.1 dual-systems. Reaction heat for the net epoxy formulation and samples with 10%, 20%, 30%, 40%, 50% epoxy contents are shown at 10 (°C)/min heating rate.

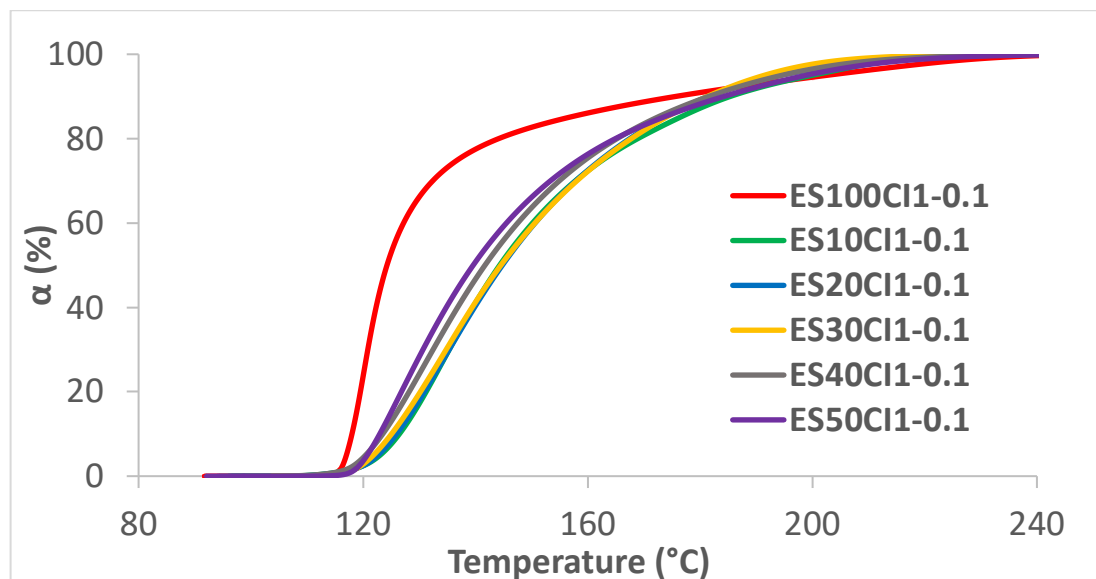


Figure 50. DSC dynamic measurement. Comparison of degrees of conversion (α) versus temperature during the thermal-curing process for different epoxy content. Heating rate of 10 (°C/min) shown.

Table 10 shows the effect of the epoxy content effects on the heat evolved during the thermal, second curing stage. As can be seen, the higher the epoxy content the higher the heat released. In fact, the values reported in J/g are nearly proportional to the epoxy wt.% of the formulations. The calculated heat released per epoxy equivalent was found to be around 82-85 kJ/eq, which is very similar to the previously reported values for the cationic homopolymerization of this epoxy monomer [61].

Table 10. Comparison of DSC evaluation of net epoxy system ES100CI1-0.1 and of ESxCI1-0.1 formulations. Δh_{exp} (J/g) is the heat released in the dynamic heating 10 °C/min based on the sample's weight. Δh_{exp} (kJ/eq) is the heat liberated but calculated with an epoxy equivalent of 130 (g/eq).

Formulation	Δh_{exp} (J/g)	Δh_{exp} (kJ/eq)
ES100CI1-0.1	620	82
ES10CI1-0.1	63.5	84
ES20CI1-0.1	129.7	86
ES30CI1-0.1	189.3	84
ES40CI1-0.1	256.3	85
ES50CI1-0.1	310.7	82

Evidence of completion of the curing process was obtained with FTIR. Figure 51 compares the FTIR spectra of the intermediate, UV-cured ES30CI1-0.1 material (blue) and fully cured material (red). It can be clearly observed that the peak at 750-800 cm^{-1} , associated with the epoxy ring, disappears completely after the thermal treatment. In addition, it was observed the appearance of the peak at 1100 cm^{-1} characteristic of the C-O-C bonds of the epoxy homopolymer network. Therefore, the presence of an already reacted acrylate network does not produce any relevant restriction to complete reaction of epoxy groups.

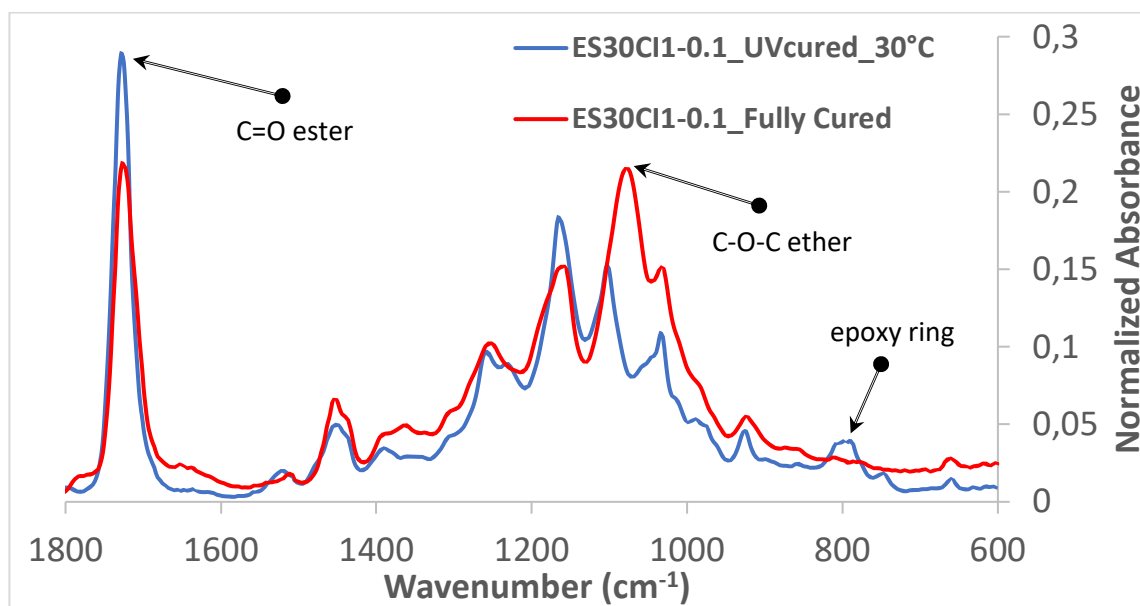


Figure 51. FTIR spectrometry results of dual-system ES30CI1-0.1. The blue curve is referred to the UV-cured sample and the red curve indicates the fully polymerized formulation. Detail of 600-1800 cm^{-1} absorption band is plotted.

Kinetics analysis of ES30CI1-0.1

The kinetics analysis were carried out to determine the second dual-curing stage of the epoxy formulation ES30CI1-0.1. As is possible to see in the following graphs, the rate degree of conversion da/dt (s^{-1}) and the degree of conversion were evaluated at different heating rates, 1.25, 2.5, 5, 10 ($^{\circ}\text{C}/\text{min}$).

Figure 52 shows that increasing heating rates shift the curing process to higher temperatures, as expected and as observed in the analysis of the pure epoxy system. Table 11 shows that the heat evolved at each heating rate was, in all cases, around 180 J/g and 80 kJ/eq, which could be expected taking into consideration experimental error and uncertainty in the analysis.

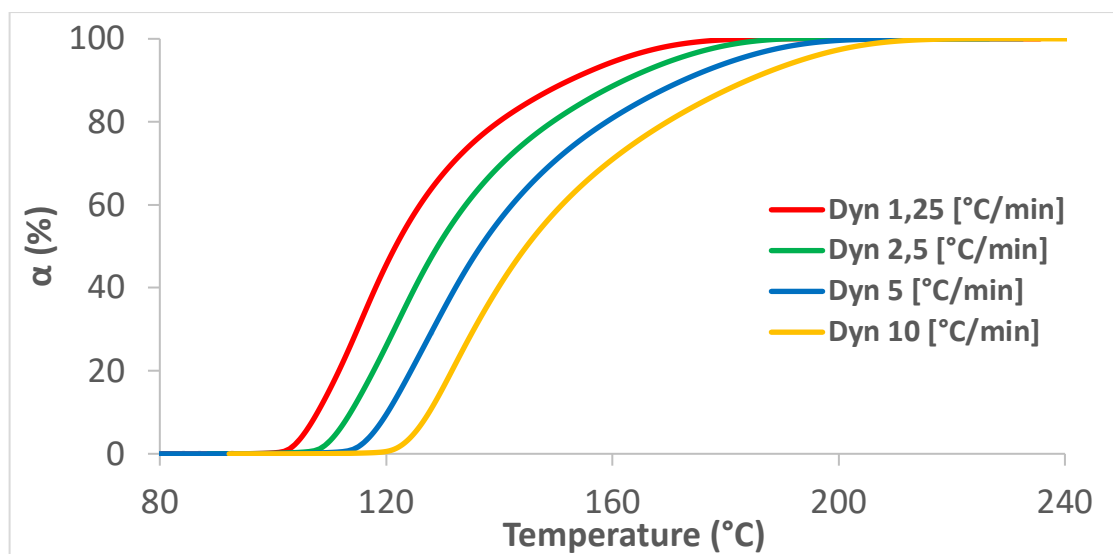


Figure 52. Comparison degree of conversion (α) versus temperature for the epoxy formulation ES30CI1-0.1. Heating rate of 1.25, 2.5, 5, 10 ($^{\circ}\text{C}/\text{min}$) are shown.

Table 11. Summary of the DSC dynamic analysis of ES30CI1-0.1 formulations for different heating rate 1.25, 2.5, 5, 10 ($^{\circ}\text{C}/\text{min}$).

β ($^{\circ}\text{C}/\text{min}$)	Δh (J/g)	Δh (kJ/ee)
1.25	169.3	74.8
2.5	178.9	79.1
5	183.6	81.2
10	189.3	83.7
Average	180.3	79.7

We applied the same methodology for the analysis of the curing kinetics and determination of kinetic parameters (integral iso-conversional methodology, Equation 11) as in the case of the pure epoxy system. The results of this analysis are shown in Table 12. The activation energy is slightly lower than in the case of the neat epoxy (see Table 4), but the kinetic parameters still reflect a strong temperature dependence. The validity of these parameters was also tested by comparing isothermal simulations at 110, 120 and 130 $^{\circ}\text{C}$ (using Equation 9 and the data in Table 12). Such validation is important, because it illustrates the possibility of predicting optimized curing schedules for the thermal curing stage after the 3D-printing. In this case, it can be observed that this thermal post-curing stage would be nearly complete within 2 hours at 130 $^{\circ}\text{C}$, which are rather mild and easily attainable processing conditions. In addition, extrapolated predictions down to room temperature indicate that the 3D-printed

specimens would be stable for several weeks, indicating that they could be safely transported or stored at convenience before the final treatment takes place.

Table 12. Kinetics parameters at different degrees of conversion, obtained using the Starink model, from experiments of epoxy formulation ES30CI1-0.1.

α	E (kJ/mol)	\ln (g/k0) (min ⁻¹)	r_2
0.05	127.8	-126.0	0.9980
0.1	127.4	-124.9	0.9986
0.2	128.4	-125.2	0.9995
0.3	126.8	-123.2	0.9999
0.4	122.4	-118.5	1.0000
0.5	116.8	-112.7	1.0000
0.6	110.3	-106.0	0.9999
0.7	103.9	-99.5	0.9999
0.8	99.6	-95.0	0.9998
0.9	99.7	-95.0	0.9997
0.95	100.5	-95.8	0.9995

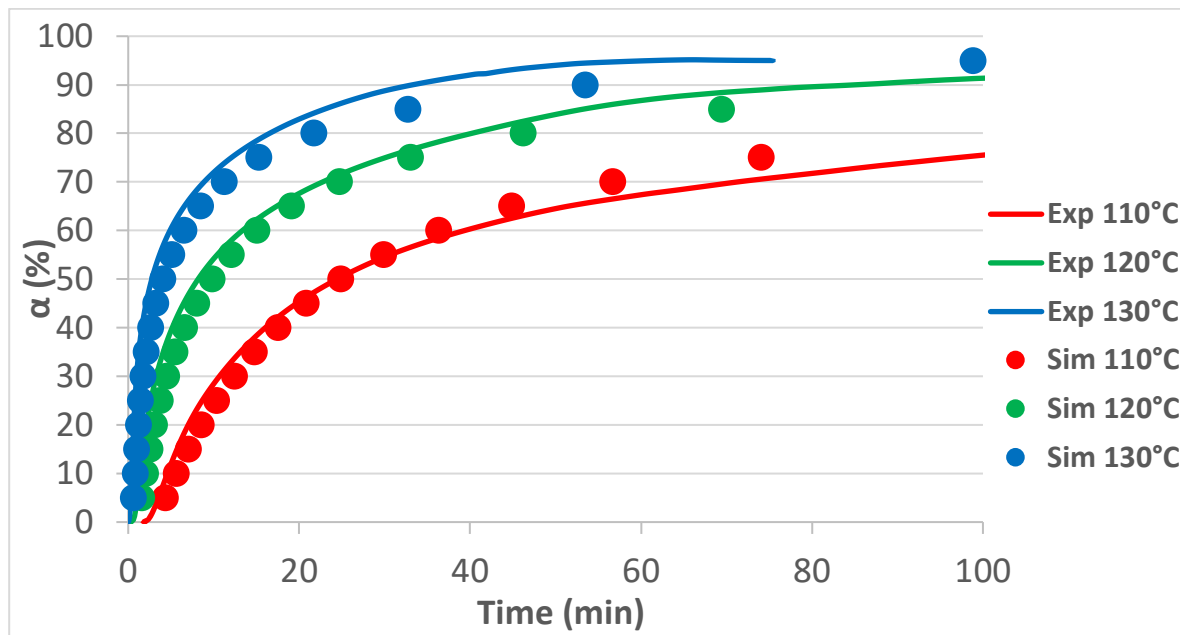


Figure 53. Kinetics analysis for the epoxy formulation ES30CI1-0.1. Experimental and simulated degree of conversion (α) versus time for, 110°C, 120°C, 130°C isothermal trials. The solid lines represent the experimental data and the symbol correspond to the simulated data.

Analysis of the crosslinking process

From the previous analysis, it was observed that the second thermal treatment would be complete under mild temperature conditions and reasonable curing times. The DMA analysis of the intermediate materials revealed that it was possible to obtain materials with different mechanical properties, given by the relative contributions of the acrylate network and unreacted epoxy monomer. It was hypothesized that the acrylate network structure would remain stable during the heating process prior to the activation of the second thermal treatment and during the second process, and therefore the 3D-printed objects would have mechanical and dimensional stability during the second thermal treatment. Therefore, it was attempted to monitor the crosslinking process of UV-cured materials under DMA, and monitored also under the same conditions under DSC, in order to compare the evolution of the mechanical properties with the evolution of the degree of cure.

Figure 54 shows the monitoring of the crosslinking process of ES30CI1-0.1 formulation with DMA at a constant heating rate of 3 °C/min. At the beginning of the graph, it can be observed the end of the relaxation process, a decrease of $\tan \delta$ down to a value of 0 and the stabilization of the storage modulus E' down to a value of 28 MPa (see Table 8). Upon further heating, the values of $\tan \delta$ and E' remain fairly constant, suggesting that the material is mechanically stable and under equilibrium, in the relaxed state. At around 120 °C, it is observed that E' starts to increase gradually up to 70 MPa, indicating that a crosslinking process is taking place, while $\tan \delta$ remains fairly constant and close to 0. After the analysis, it was observed that the shape of the sample was unaltered, that is, it had retained its dimensional stability throughout the entire crosslinking process.

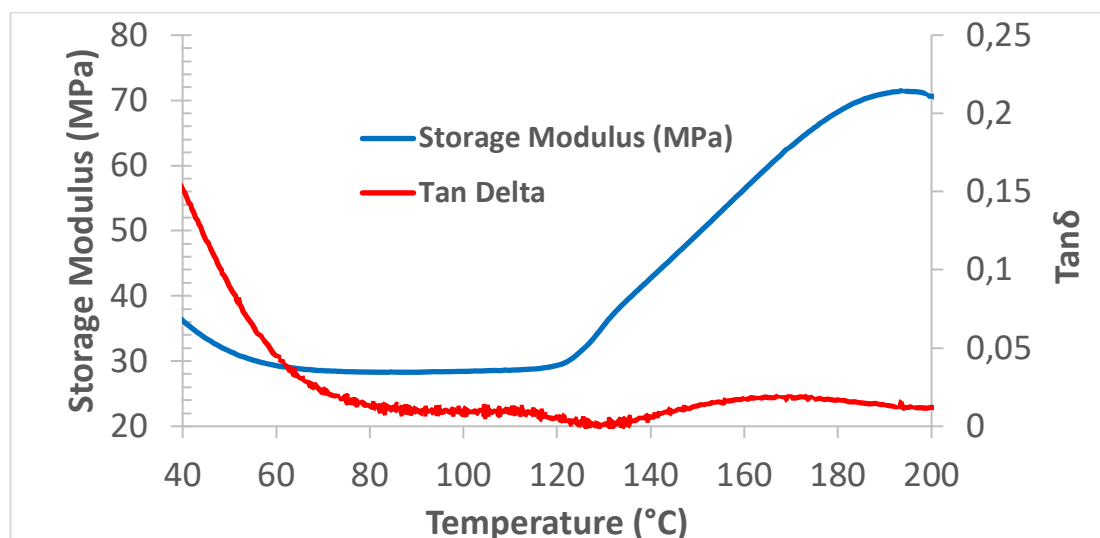


Figure 54. DMA analysis for ES30CI1-0.1 intermediate photo-cured material. E' (blue curve) and $\tan \delta$ (red curve) are plotted during the cross-linking process at constant heating rate of 3 °C/min, frequency of 1 Hz and 0.05 % strain.

These results were compared with the curing of a DSC sample at the same heating rate. Figure 55 compares the evolution of the DSC conversion with the evolution of the storage modulus E' . It can be observed that the crosslinking process starts at a DSC conversion of about 20-25 %. This conversion could be associated with the conversion at gelation of the cationic homopolymerization process. Taking into account the experimental uncertainty associated with the real sample temperature during the DMA and DSC analyses, this result is reasonable

taking into consideration that gelation during homopolymerization of pure cycloaliphatic epoxy formulations takes place at about 15 % epoxy conversion [67] and that gelation during homopolymerization of other epoxy monomers takes place between 20-30 % conversion [34,68].

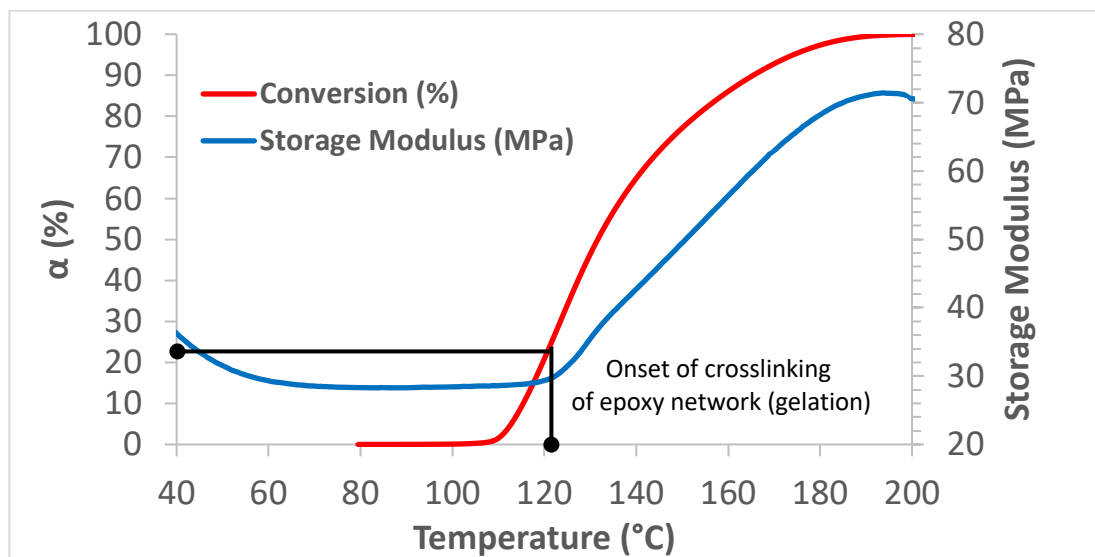


Figure 55. Comparison between DSC and DMA measurement for epoxy formulation ES30C11-0.1. Degree of conversion (α) vs. storage modulus (E') for the intermediate material are charted.

The same comparison was made for a different curing programme, more similar to the application of a thermal treatment of a 3D-printed sample inside an oven: a heating at 3 °C/min up to 120 °C, followed by isothermal curing at 120 °C for 1 h, heating at 3 °C/min up to 180 °C and dwelling at that temperature until the end of the curing process. The results are shown in Figure 56. It can be observed that the crosslinking process is nearly complete when the sample reaches 180 °C in the second heating step, and that the total thermal treatment lasts about 2 hours. The evolution of the DSC conversion and modulus follow parallel trends, showing also the same conversion at gelation.

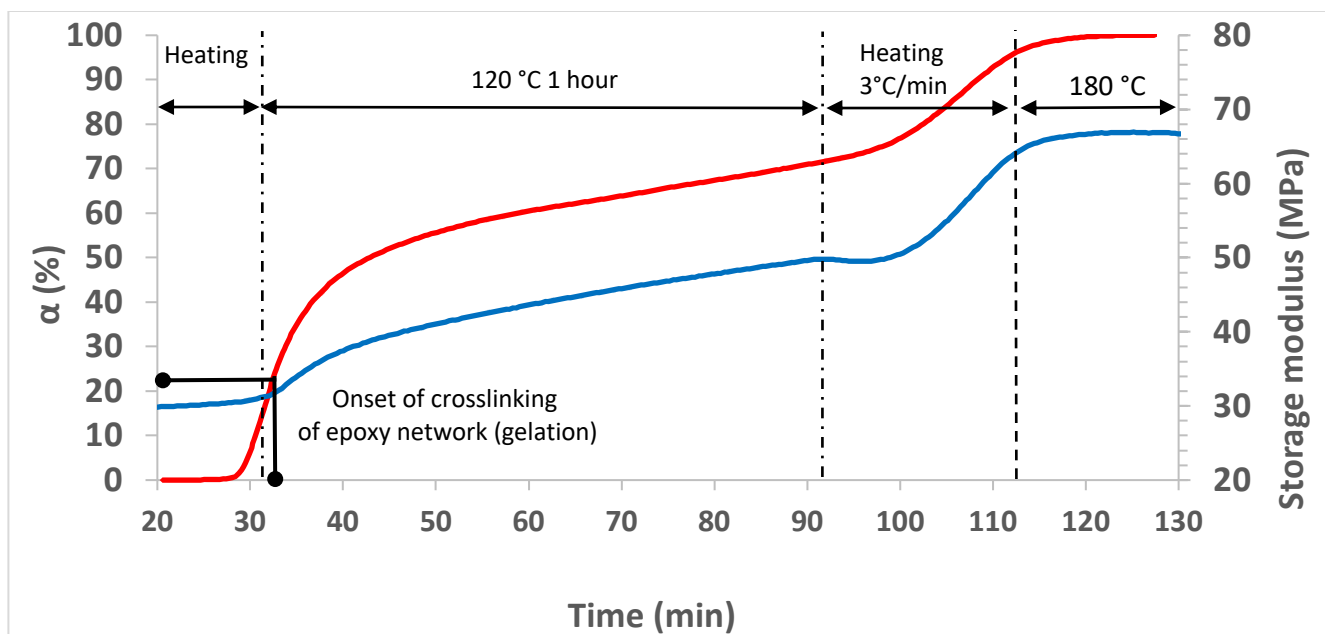


Figure 56. DMA and DSC analysis with same heating scheduled program. Degree of conversion and E' vs. time for ES30CI1-0.1 final curing formulation.

It should be commented that this relatively long thermal treatment in a oven would not be a processing bottleneck, because a large amount of 3D-printed samples can be processed at the same time in a conventional convective oven to complete the curing process.

Properties of fully cured sample

Fully cured materials were prepared by application of the following thermal treatment to UV-cured samples: heating up 120 °C, 1 hour at 120 °C, heating up to 180 °C, 1 hour at 180 °C. This way, it was ensured that the curing of all samples would be complete. The cured samples were then analyzed using different techniques.

Figure 57 shows the DSC traces at 10 °C/min of the fully cured materials. Although the superposition between the different curves makes observation difficult, it is observed a shifting of the glass transition to higher temperatures with increasing epoxy content. The nominal values of T_g are reported in Table 6 (on page 65). This could be expected, taking into consideration the high glass transition of the pure epoxy homopolymer [55]. Moreover, the higher the epoxy content, the higher the difference between the intermediate and final materials, as reported for other dual-curing systems [63]. This indicates the substantial change in material properties caused by the second curing process, the thermally activated cationic epoxy homopolymerization.

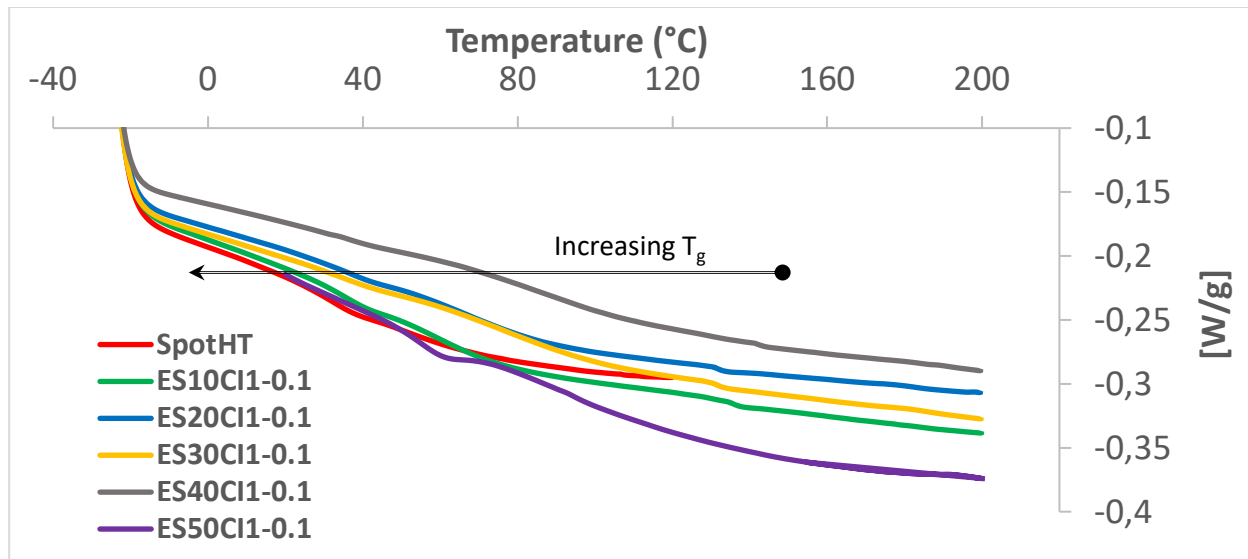


Figure 57. DSC thermal-curing analysis for the Spot-HT and ES_xCI1-0.1 final formulation. T_g variations for samples with 10%, 20%, 30%, 40%, 50% epoxy content are shown at 10 (°C/min) heating rate.

The materials were analyzed by DMA, and the results were represented in Figure 58, Figure 59 and Table 13. The effect of increasing epoxy content on the properties of the fully cured materials become more evident. The mechanical relaxation is now shifted to higher temperatures with increasing epoxy content. This is logical taking into account that the cationic homo-polymerization, of the epoxy group leads to a tightly crosslinked network structure with a high glass transition temperature [55]. In addition, the figures and Table 13 show that the mechanical relaxation broadens with increasing epoxy content, which is typical for materials with increasing crosslinking density [5]. There is no clear effect of the epoxy content on the relaxed modulus, all the more taking into account that complete relaxation of materials was not observed, especially for higher epoxy content (further heating might have induced some thermal degradation).

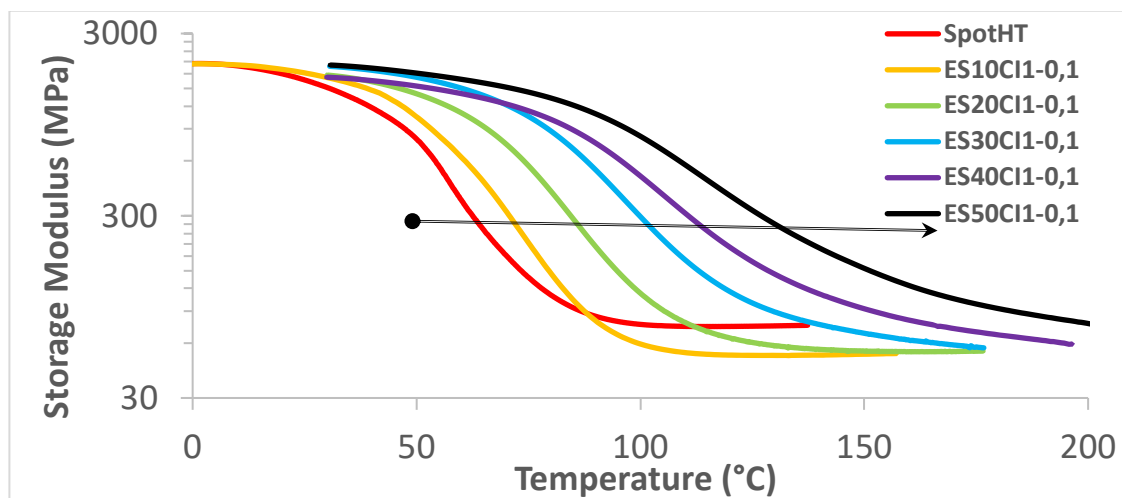


Figure 58. Results of the DMA dynamic analysis at 3°C/min, 1 Hz and 0.05% strain of Spot-HT and ES_xCI1-0.1 final formulation. Storage Modulus (E') is plotted.

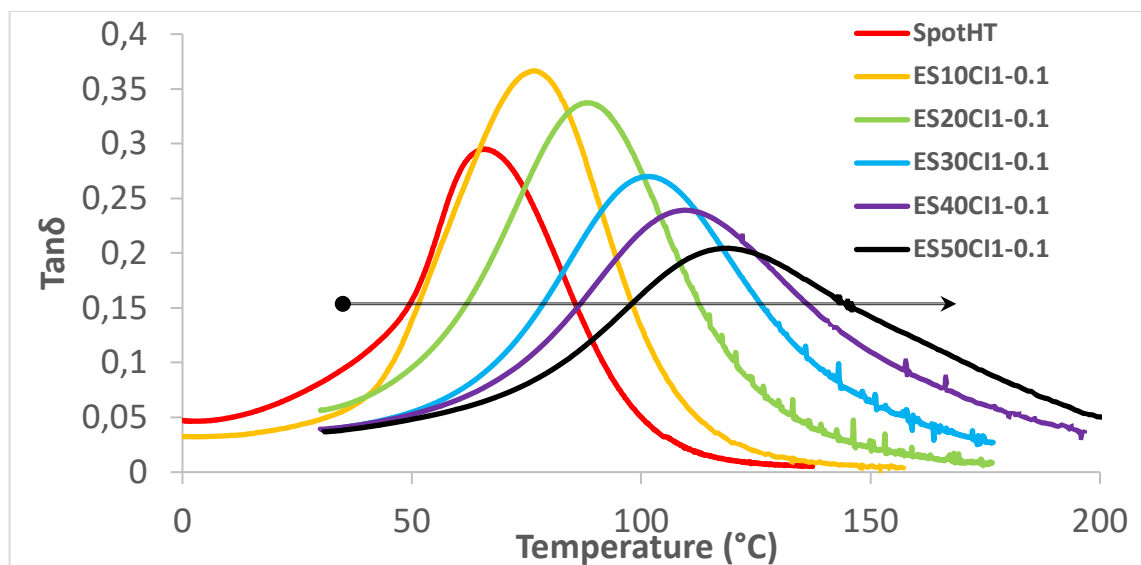


Figure 59. Results of the DMA dynamic analysis at 3°C/min, 1 Hz and 0.05% strain of Spot-HT and ESxCI1-0.1 final formulation. $Tan\delta$ is plotted in the graph.

Table 13. Summary of DMA analysis of Spot-HT and ESxCI1-0.1 fully cured formulation.

Formulation	E' relaxed (MPa)	$Tan\delta$ peak T(°C)	$Tan\delta$ \uparrow height (°C)	$Tan\delta$ \leftrightarrow width (°C)	E'' peak T(°C)
Spot-HT	75	66.5	0.269	34.5	40.9
ES10CI1-0.1	52	77.1	0.349	39.6	56.7
ES20CI1-0.1	59	88.8	0.301	42.5	68,7
ES30CI1-0.1	74	101,3	0.237	48.2	81.5
ES40CI1-0.1	96	109.5	0.201	56.7	88.9
ES50CI1-0.1	104	118.0	0.170	72.3	96.9

In order to highlight the changes in the network structure caused by the epoxy homopolymerization, Figure 60 compares the storage modulus (E') and $\tan \delta$ after the first UV-curing process and the second thermal step for the reference formulation ES30CI1-0.1. It can be observed a significant shifting of the mechanical relaxation caused by the cationic epoxy homopolymerization taking place during the thermal treatment, and an increase in relaxed modulus due to the formation of new crosslinks.

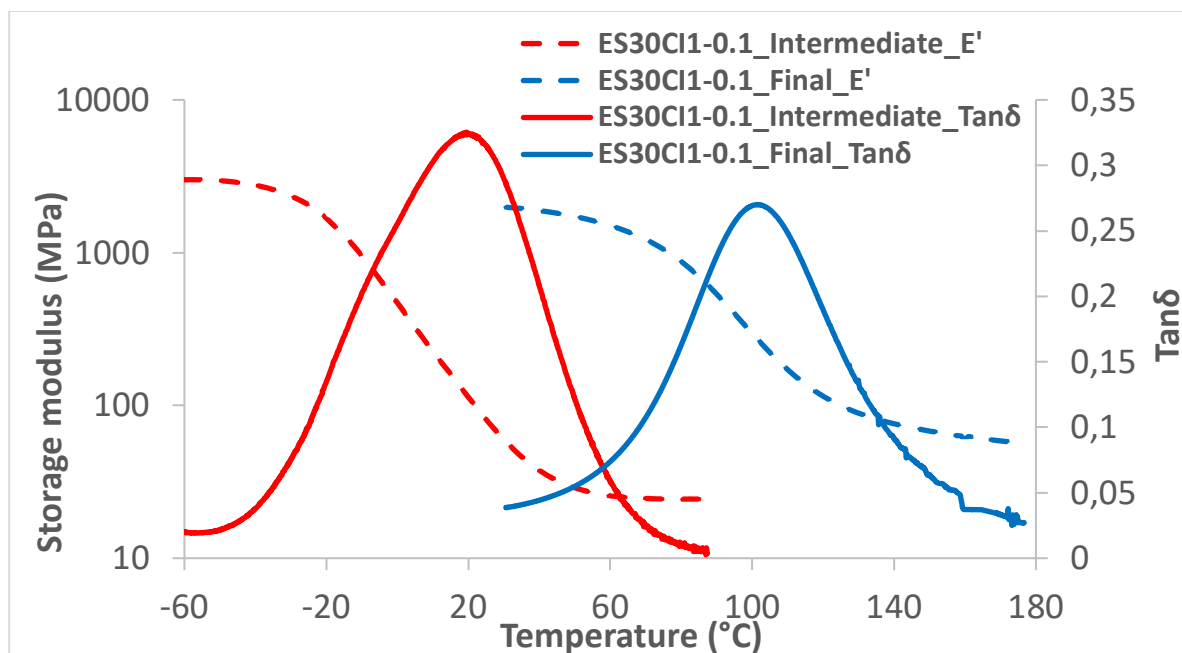


Figure 60. DMA measurement of epoxy ES30CI1-0.1 formulation. Comparison between storage modulus (E') and $Tan\delta$ for the UV-cured (red curves) and fully-cured (blue curves) samples.

The soluble fraction of the fully-cured materials was also determined by normal boiling under full reflux conditions in dichloromethane. As seen in Table 14, the insoluble fraction is close to unity in all cases and increasing with increasing epoxy content. Therefore, adding the epoxy monomer results in fully cured materials having very little or no low molecular weight soluble fraction and lower risk of VOC emission, which makes them safer from the environmental point of view.

Table 14. Comparison between the experimental residual weight and the expected theoretical weight for the fully cured material.

Formulation	Experimental Residual Weight (%)	Theoretical Residual Weight (%)
Spot-HT	96.9	100
ES10CI1-0.1	96.7	100
ES20CI1-0.1	98.1	100
ES30CI1-0.1	98.3	100
ES40CI1-0.1	99.5	100
ES50CI1-0.1	99.8	100

The fully cured samples were also analyzed by thermogravimetric analysis (TGA), The TGA results are presented in Figure 61. As can be observed, it was not observed any relevant difference between the cured materials in terms of thermal stability nor any trend with respect to the epoxy content. All the materials are highly stable up to 200-250 °C, showing temperatures of 5 wt.% loss around 320-340 °C in all cases. These results also evidence that the thermal treatment up to 180 °C is safe from the stability point of view, so that the materials are not damaged during processing.

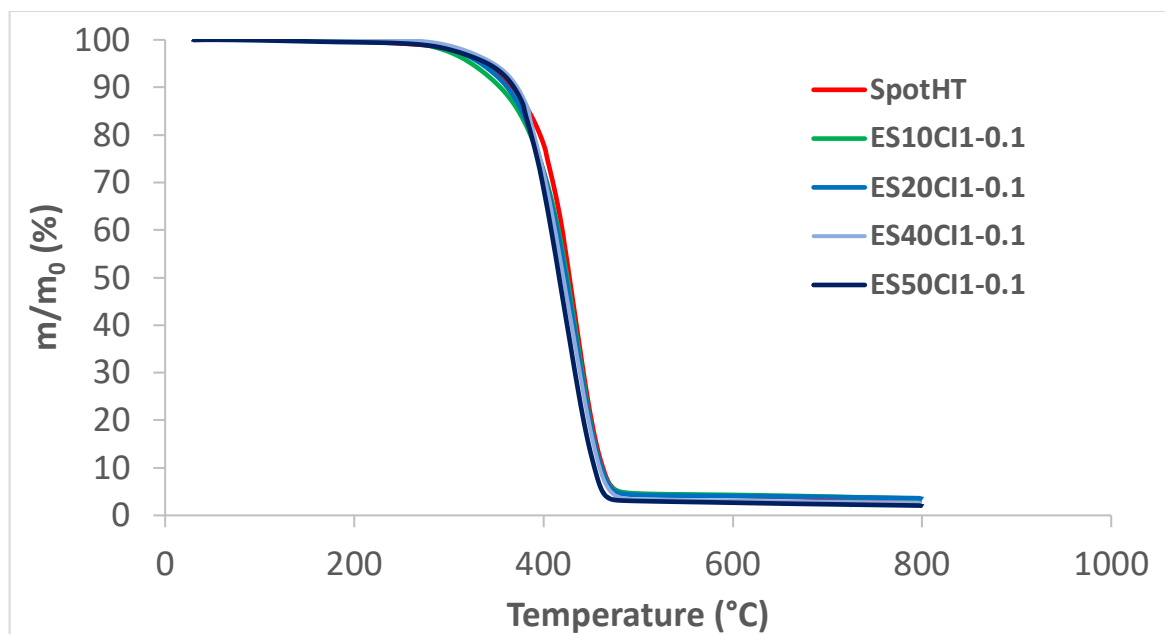


Figure 61. Thermogravimetric analysis for different epoxy ESxCI1-0.1 formulation. Mass loss (m/m_0) is plotted with respect to the temperature.

3.2.3 Analysis of storage stability

In order to determine the applicability of the dual-curing formulations, it is essential to analyze the storage stability of the uncured formulation and the UV-cured formulation. To begin with, storage stability of the acrylate component should be guaranteed as long as the mixture is kept under dark conditions, i.e. avoiding light exposure. For the epoxy component, it should be verified that the thermal latent catalyst is stable for a sufficient period of time in practical terms, and that both the photocuring process and subsequent thermal process are unaffected. This analysis has not been carried out in related works reported in the literature [53,54].

For that purpose, weekly analysis were carried on samples stored at 35 °C under suitable conditions, on the liquid, unreacted formulation (i.e. protected from sunlight) and on partially cured samples. Figure 62 shows the dynamic scans at 10 °C/min of UV-cured samples and stored at 35 °C. It can be observed that the exotherm corresponding to the epoxy reaction is hardly modified in 5 weeks. The onset of the curing process is slightly shifted to lower temperatures but, still, activation of the reaction takes place only above 100 °C. Isarn et al. [55], reported a storage stability of 16 weeks for an epoxy formulation using the same catalytic system, but in this case the storage stability seems to be lower. Table 15 compares the evolution of the recorded reaction heat during the UV-curing and subsequent thermal curing of the stored liquid, and of the thermal curing of the UV-curing formulation. In spite of the experimental uncertainty, it can be observed in all cases a change taking place after week 5-6, therefore indicating that the system has a limited pot life, as a consequence of some interaction between the components of the reaction mixture. In fact, some evidence gelation was observed on the liquid sample, caused mainly by epoxy homopolymerization.

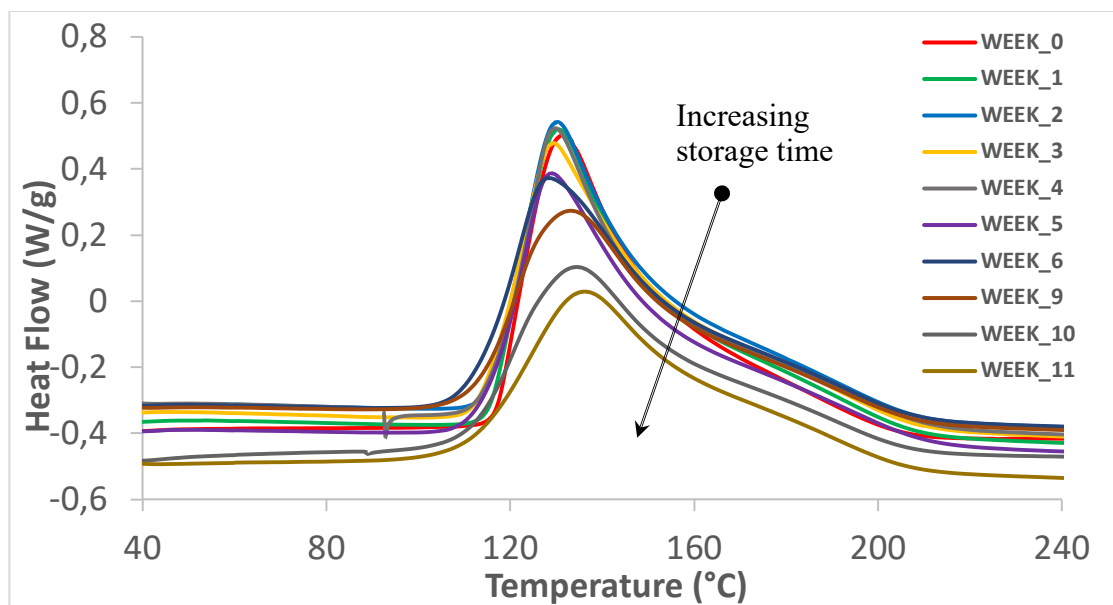


Figure 62. Weekly dynamic DSC analysis for ES30CI1-0.1 UV-cured reference sample. Different reaction heat are shown at 10 °C/min heating rate.

Table 15. DSC measurement for liquid and solid sample of epoxy formulation ES30CI1-0.1. Δh_{1st} is the heat released in the first isothermal UV-curing, Δh_{2nd} is the residual heat released in a subsequent heating process at 10 °C/min. Δh (J/g) is the heat produced during the dynamic final-curing process (10 °C/min).

Week n°	LIQUID		UV-cured
	Δh_{1st} (J/g)	Δh_{2st} (J/g)	Δh (J/g)
1	258.7	178.5	200.4
2	253.9	178.7	192.7
3	253.3	185.0	199.0
4	258.0	186.6	194.6
5	248.9	161.7	194.1
6	212	142.8	177.9
9	124.5	68.5	156.6
10	184.6	102.6	151.5
11	191.2	89.8	136.3

However, it was not examined in detail what was the effect of storage on kinetics on the photocuring process. This is of utmost practical importance, because the 3D-printing process would be affected by any change in the process. Although these preliminary results suggest that these materials could be distributed as 2-pot component which, once prepared, would be stable for a few weeks, further analyses should be carried out in the future in order to indicate exactly the applicability of this dual-curing system.

4 CONCLUSION

A novel dual-curing system was developed starting from an acrylate-based commercially available 3D-printing formulation (Spot-HTTM), modified by addition of an epoxy monomer and a latent thermal cationic initiator, in order to enhance the properties of the produced components. The dual-curing sequence consists of, first, a UV-curing stage in which the radical homopolymerization of acrylates takes place, followed by a thermal curing stage in which the cationic epoxy homopolymerization takes place.

A range of formulations with different epoxy content were prepared and the UV-curing and thermal curing steps were analyzed in detail. The properties of the intermediate and final materials were analyzed using a variety of techniques. It could be shown that the curing process was strictly sequential, with controlled and independent activation of both polymerization reactions, and that they proceeded to completion without interference of the other components. At the end of the first photopolymerization stage, an acrylate network is formed, swollen with varying amounts of unreacted epoxy monomers. As a consequence, increasing epoxy content produces a decrease in the intermediate glass transition temperature, resulting in almost relaxed, low-modulus materials but with mechanical and dimensionally consistency. The subsequent thermal treatment activates the cationic homopolymerization of epoxy groups. Increasing epoxy content, in contrast, produces a significant increase in the final glass transition temperature, producing final materials that are more suitable for applications demanding higher operating temperatures. Dimensional stability of the components was guaranteed during the thermal treatment, due to the mechanical consistency given by the existing acrylate network. Storage stability of the prepared liquid formulation and intermediate materials were analyzed, showing a stability period of about 5 weeks, which could be sufficient for practical application of the dual-curing system.

Definitively, the dual-curing provides the ability to design efficient formulation with reasonable storage stability of the uncured system and stable intermediate properties and custom-tailored final material with potential applicability in 3D-printing applications. Further work should be directed towards determining pot life with precision and practical application of these dual-curing systems in realistic processing environments. A detailed mechanical testing could be useful in order to envision the potential application of the fully-cured materials, after complete processing. Furthermore, material properties can be optimized by changing the composition of the acrylate formulation and the structure and content of the epoxy modifier.

5 BIBLIOGRAPHY

- [1] P.C. Painter, *Fundamentals of polymer science : an introductory text* / Paul C. Painter, Michael M. Coleman, Technomic, Lancaster [etc.] :, 1997. https://discovery.upc.edu/iii/encore/record/C__Rb1228268__Sfundamentals_of_polymer_science__Orightresult__U__X7?lang=cat (accessed February 6, 2019).
- [2] *Characterization analysis of polymers.*, Wiley-Interscience, Hoboken (N.J.) :, 2008. https://discovery.upc.edu/iii/encore/record/C__Rb1376690__Scharacterization_and_analysis_of_polymers__Orightresult__U__X7;jsessionid=C5E2BF68DDE92F514A83E38D0BC68445?lang=cat (accessed February 6, 2019).
- [3] P.T. Mather, X. Luo, I.A. Rousseau, Shape memory polymer research, *Annu. Rev. Mater. Res.* 39 (2009) 445–471. doi:10.1146/annurev-matsci-082908-145419.
- [4] E.A. Turi, *Thermal characterization of polymeric materials*, (1997).
- [5] J.-P. Pascault, H. Sautereau, J. Verdu, R. J.J Williams, *Thermosetting polymers*, Marcel Dekker, 2002.
- [6] Q. Guo, ed., *Thermosets. Structures, Properties and Application*, Elsevier, 2017. doi:<https://doi.org/10.1016/C2015-0-06205-0>.
- [7] J.P. Eloundou, M. Feve, J.F. Gerard, D. Harran, J.P. Pascault, Temperature dependence of the behavior of an epoxy-amine system near the gel point through viscoelastic study. 1. Low-Tg epoxy-amine system, *Macromolecules.* 29 (1996) 6907–6916. <http://dx.doi.org/10.1021/ma960287d>.
- [8] A. Hale, C.W. Macosko, H.E. Bair, Glass transition temperature as a function of conversion in thermosetting polymers, *Macromolecules.* 24 (1991) 2610–2621. doi:10.1021/ma00009a072.
- [9] R.A. Venditti, J.K. Gillham, Relationship between the glass transition temperature (Tg) and fractional conversion for thermosetting systems, *J. Appl. Polym. Sci.* 64 (1997) 3–14. [http://dx.doi.org/10.1002/\(SICI\)1097-4628\(19970404\)64:1%3C3::AID-APP1%3E3.0.CO;2-S](http://dx.doi.org/10.1002/(SICI)1097-4628(19970404)64:1%3C3::AID-APP1%3E3.0.CO;2-S).
- [10] J.P. Pascault, R.J.J. Williams, Glass transition temperature versus conversion relationships for thermosetting polymers, *J. Polym. Sci. Part B Polym. Phys.* 28 (1990) 85–95. <http://dx.doi.org/10.1002/polb.1990.090280107>.
- [11] S. Montserrat, J.G. Martin, The isothermal curing of a diepoxide-cycloaliphatic diamine resin by temperature modulated differential scanning calorimetry, *J. Appl. Polym. Sci.* 85 (2002) 1263–1276. <http://dx.doi.org/10.1002/app.10792>.
- [12] D. Santiago, X. Fern?ndez-Francos, X. Ramis, J.M. Salla, M. Sangermano, Comparative curing kinetics and thermal-mechanical properties of DGEBA thermosets cured with a hyperbranched poly(ethyleneimine) and an aliphatic triamine, *Thermochim. Acta.* 526 (2011). doi:10.1016/j.tca.2011.08.016.
- [13] S. Corezzi, D. Fioretto, G. Santucci, J.M. Kenny, Modeling diffusion-control in the cure kinetics of epoxy-amine thermoset resins: An approach based on configurational entropy, *Polymer (Guildf).* 51 (2010) 5833–5845. <http://www.sciencedirect.com/science/article/B6TXW-51696XJ-2/2/7bbb36de42e9202cd975bb76c8d084a3>.
- [14] M.T. Aronhime, J.K. Gillham, Time-Temperature-Transformation (TTT) Cure Diagram of Thermosetting Polymeric Systems, in: Springer-Verlag, Berlin, West Ger, 1986: pp. 83–113.

- [15] X. Ramis, J.M. Salla, Time-temperature transformation (TTT) cure diagram of an unsaturated polyester resin, *J. Polym. Sci. Part B Polym. Phys.* 35 (1997) 371–388. [http://dx.doi.org/10.1002/\(SICI\)1099-0488\(19970130\)35:2%3C371::AID-POLB13%3E3.0.CO;2-F](http://dx.doi.org/10.1002/(SICI)1099-0488(19970130)35:2%3C371::AID-POLB13%3E3.0.CO;2-F).
- [16] E. Ruiz, F. Trochu, Multi-criteria thermal optimization in liquid composite molding to reduce processing stresses and cycle time, *Compos. Part A Appl. Sci. Manuf.* 37 (2006) 913–924. doi:<https://doi.org/10.1016/j.compositesa.2005.06.010>.
- [17] M.A. Tasdelen, M.U. Kahveci, Y. Yagci, Telechelic polymers by living and controlled/living polymerization methods, *Prog. Polym. Sci.* 36 (2011) 455–567. doi:10.1016/j.progpolymsci.2010.10.002.
- [18] P. Vancaeter, E.J. Goethals, Telechelic polymers - New developments, *Trends Polym. Sci.* 3 (1995) 227–233.
- [19] Y. Shudo, A. Izumi, T. Takeuchi, T. Nakao, M. Shibayama, Dynamic light scattering study of the curing mechanisms of novolac-type phenolic resins, *Polym. J.* 47 (2015) 428. <https://doi.org/10.1038/pj.2015.15>.
- [20] J.R. Fried, *Polymer science and technology* / Joel R. Fried, Prentice Hall, Upper Saddle River :, 2014. [https://discovery.upc.edu/iii/encore/record/C__Rb1476010__Spolymer science and technology__Orightresult__U__X7?lang=cat](https://discovery.upc.edu/iii/encore/record/C__Rb1476010__Spolymer%20science%20and%20technology__Orightresult__U__X7?lang=cat) (accessed February 7, 2019).
- [21] S. Pichaud, X. Duteurtre, A. Fit, F. Stephan, A. Maazouz, J.P. Pascault, Chemorheological and dielectric study of epoxy-amine for processing control, *Polym. Int.* 48 (1999) 1205–1218. [http://dx.doi.org/10.1002/\(SICI\)1097-0126\(199912\)48:12%3C1205::AID-PI285%3E3.0.CO;2-Z](http://dx.doi.org/10.1002/(SICI)1097-0126(199912)48:12%3C1205::AID-PI285%3E3.0.CO;2-Z).
- [22] B.A. Rozenberg, Kinetics, Thermodynamics and Mechanism of Reactions of Epoxy Oligomers with Amines, *Adv. Polym. Sci.* 75 (1986) 113–165.
- [23] L. Matějka, S. Pokorný, K. Dušek, Acid curing of epoxy resins. A comparison between the polymerization of diepoxide-diacid and monoepoxide-cyclic anhydride systems, *Die Makromol. Chemie.* 186 (1985) 2025–2036. doi:10.1002/macp.1985.021861006.
- [24] M.S. Heise, G.C. Martin, J.T. Gotro, Characterization of imidazole-cured epoxy-phenol resins, *J. Appl. Polym. Sci.* 42 (1991) 1557–1566. <http://dx.doi.org/10.1002/app.1991.070420609>.
- [25] J.E. Boulden, N.B. Cramer, K.M. Schreck, C.L. Couch, C. Bracho-Troconis, J.W. Stansbury, C.N. Bowman, Thiol-ene-methacrylate composites as dental restorative materials, *Dent. Mater.* 27 (n.d.) 267–272. doi:10.1016/j.dental.2010.11.001.
- [26] D. Guzmán, X. Ramis, X. Fernández-Francos, A. Serra, New catalysts for diglycidyl ether of bisphenol A curing based on thiol–epoxy click reaction, *Eur. Polym. J.* 59 (2014). doi:10.1016/j.eurpolymj.2014.08.001.
- [27] G. González, X. Fernández-Francos, À. Serra, M. Sangermano, X. Ramis, Environmentally-friendly processing of thermosets by two-stage sequential aza-Michael addition and free-radical polymerization of amine-acrylate mixtures, *Polym. Chem.* 6 (2015) 6987–6997. doi:10.1039/c5py00906e.
- [28] D.P. Nair, N.B. Cramer, J.C. Gaipa, M.K. McBride, E.M. Matherly, R.R. McLeod, R. Shandas, C.N. Bowman, Two-Stage Reactive Polymer Network Forming Systems, *Adv. Funct. Mater.* 22 (2012) 1502–1510. doi:10.1002/adfm.201102742.
- [29] C. Decker, Kinetic Study and New Applications of UV Radiation Curing, *Macromol. Rapid Commun.* 23 (2002) 1067–1093. <http://dx.doi.org/10.1002/marc.200290014>.
- [30] W.D. Cook, Thermal aspects of the kinetics of dimethacrylate photopolymerization, *Polymer (Guildf.)* 33 (1992) 2152–2161.

- <http://www.sciencedirect.com/science/article/B6TXW-48DYJ8T-8F/2/a6c14a394f8d37426e8a2bcd9ba23e96>.
- [31] J.M. Salla, X. Ramis, Comparative study of the cure kinetics of an unsaturated polyester resin using different procedures, *Polym. Eng. Sci.* 36 (1996) 835–851. <http://dx.doi.org/10.1002/pen.10471>.
- [32] T.F. Scott, W.D. Cook, J.S. Forsythe, Photo-DSC cure kinetics of vinyl ester resins. I. Influence of temperature, *Polymer (Guildf)*. 43 (2002) 5839–5845. <http://www.sciencedirect.com/science/article/B6TXW-46P9MWW-6/2/5923aeaeaeda8027ad5d973cd889ef17>.
- [33] P. Kubisa, S. Penczek, Cationic activated monomer polymerization of heterocyclic monomers, *Prog. Polym. Sci.* 24 (1999) 1409–1437. [http://dx.doi.org/10.1016/S0079-6700\(99\)00028-3](http://dx.doi.org/10.1016/S0079-6700(99)00028-3).
- [34] L. Matejka, P. Chabanne, L. Tighzert, J.P. Pascault, Cationic polymerization of diglycidyl ether of bisphenol a, *J. Polym. Sci. Part A Polym. Chem.* 32 (1994) 1447–1458. <http://dx.doi.org/10.1002/pola.1994.080320806>.
- [35] M. Sangermano, N. Razza, J.V. Crivello, Cationic UV-curing: Technology and applications, *Macromol. Mater. Eng.* (2014). doi:10.1002/mame.201300349.
- [36] M.D. Soucek, J. Chen, Model for the effects of water on the cationic UV-curing of cyclohexyl epoxides, *J. Coatings Technol.* 75 (2003) 49–58.
- [37] M. Sangermano, G. Malucelli, R. Bongiovanni, A. Priola, Photopolymerization of oxetane based systems, *Eur. Polym. J.* 40 (2004) 353–358. <http://dx.doi.org/10.1016/j.eurpolymj.2003.09.026>.
- [38] I.E. Dell’Erba, R.J.J. Williams, Homopolymerization of Epoxy Monomers Initiated by 4- (Dimethylamino)pyridine, *Polym. Eng. Sci.* 46 (2006) 351–359. doi:10.1002/pen.
- [39] X. Fernandez-Francos, W.D. Cook, A. Serra, X. Ramis, G.G. Liang, J.M. Salla, Crosslinking of mixtures of DGEBA with bislactone initiated by tertiary amines. IV. Effect of hydroxyl groups on initiation and curing kinetics, *Polymer (Guildf)*. 51 (2010) 26–34. doi:10.1016/j.polymer.2009.11.013.
- [40] X. Fernandez-Francos, Theoretical modeling of the effect of proton donors and regeneration reactions in the network build-up of epoxy thermosets using tertiary amines as initiators, *Eur. Polym. J.* 55 (2014) 35–47. doi:10.1016/j.eurpolymj.2014.03.022.
- [41] S.K. Ooi, W.D. Cook, G.P. Simon, C.H. Such, DSC studies of the curing mechanisms and kinetics of DGEBA using imidazole curing agents, *Polymer (Guildf)*. 41 (2000) 3639–3649. [http://dx.doi.org/10.1016/S0032-3861\(99\)00600-X](http://dx.doi.org/10.1016/S0032-3861(99)00600-X).
- [42] A.-L. Brocas, C. Mantzaridis, D. Tunc, S. Carlotti, Polyether synthesis: From activated or metal-free anionic ring-opening polymerization of epoxides to functionalization, *Prog. Polym. Sci.* 38 (2013) 845–873. doi:10.1016/J.PROGPOLYMSCI.2012.09.007.
- [43] J. V Crivello, Cationic polymerization — Iodonium and sulfonium salt photoinitiators BT - Initiators — Poly-Reactions — Optical Activity, in: Springer Berlin Heidelberg, Berlin, Heidelberg, 1984: pp. 1–48.
- [44] J.-P. Fouassier, J.F. Rabek, eds., *Radiation curing in polymer science and technology*, Springer, 1993.
- [45] J.-P. Fouassier, *Photoinitiation, Polymerization and Photocuring - Fundamentals and Applications*, Hanser Publishers, 1995.
- [46] G.G. Odian, *Principles of polymerization*, 4th ed., Wiley, 2004.
- [47] C. Decker, A.D. Jenkins, *Kinetic approach of oxygen inhibition in ultraviolet- and*

- laser-induced polymerizations, *Macromolecules*. 18 (1985) 1241–1244. doi:10.1021/ma00148a034.
- [48] R. Liska, M. Schuster, R. Inführ, C. Turecek, C. Fritscher, B. Seidl, V. Schmidt, L. Kuna, A. Haase, F. Varga, H. Lichtenegger, J. Stampfl, Photopolymers for rapid prototyping, *J. Coatings Technol. Res.* 4 (2007) 505–510. doi:10.1007/s11998-007-9059-3.
- [49] J. Bonada, A. Muguruza, X. Fernández-Francos, X. Ramis, Optimisation procedure for additive manufacturing processes based on mask image projection to improve Z accuracy and resolution, *J. Manuf. Process.* 31 (2018). doi:10.1016/j.jmapro.2018.01.004.
- [50] A. Vitale, T.J. Cabral, Frontal Conversion and Uniformity in 3D Printing by Photopolymerisation, *Materials (Basel)*. 9 (2016). doi:10.3390/ma9090760.
- [51] X. Ramis, X. Fernández-Francos, S. De La Flor, F. Ferrando, À. Serra, Click-based dual-curing thermosets and their applications, in: Q. Guo (Ed.), *Thermosets 2nd Ed. Struct. Prop. Appl.*, Elsevier, 2017.
- [52] C. Decker, F. Masson, R. Schwalm, Dual-Curing of Waterborne Urethane-Acrylate Coatings by UV and Thermal Processing, *Macromol. Mater. Eng.* 288 (2003) 17–28. doi:10.1002/mame.200290029.
- [53] M. Invernizzi, G. Natale, M. Levi, S. Turri, G. Griffini, UV-Assisted 3D Printing of Glass and Carbon Fiber-Reinforced Dual-Cure Polymer Composites, *Materials (Basel)*. 9 (2016). doi:58310.3390/ma9070583.
- [54] G. Griffini, M. Invernizzi, M. Levi, G. Natale, G. Postiglione, S. Turri, 3D-printable CFR polymer composites with dual-cure sequential IPNs, *Polymer (Guildf)*. 91 (2016) 174–179. doi:10.1016/j.polymer.2016.03.048.
- [55] I. Isarn, F. Gamardella, L. Massagués, X. Fernández-Francos, A. Serra, F. Ferrando, New epoxy composite thermosets with enhanced thermal conductivity and high T_g obtained by cationic homopolymerization, *Polym. Compos.* (2018). doi:10.1002/pc.24774.
- [56] S. Nakano, T. Endo, Thermal cationic curing with benzylammonium salts - 2, *Prog. Org. Coatings*. 28 (1996) 143–148. doi:10.1016/0300-9440(95)00612-5.
- [57] S. Vyazovkin, N. Sbirrazzuoli, Isoconversional kinetic analysis of thermally stimulated processes in polymers, *Macromol. Rapid Commun.* 27 (2006) 1515–1532. <http://dx.doi.org/10.1002/marc.200600404>.
- [58] M.J. Starink, The determination of activation energy from linear heating rate experiments: a comparison of the accuracy of isoconversion methods, *Thermochim. Acta*. 404 (2003) 163–176. <http://www.sciencedirect.com/science/article/B6THV-48CNP3P-4/2/b47beaf7452967da445e0cf5a17bfdb0>.
- [59] D. Santín, O. Konuray, X. Fernández-Francos, X. Ramis, Kinetics analysis and simulation of sequential epoxy dual-curing systems with independent thermal activation, *Thermochim. Acta*. 673 (2019) 158–168. doi:10.1016/J.TCA.2019.01.023.
- [60] A.O. Konuray, A. Ruiz, J.M. Morancho, J.M. Salla, X. Fernández-Francos, À. Serra, X. Ramis, Sequential dual curing by selective Michael addition and free radical polymerization of acetoacetate-acrylate-methacrylate mixtures, *Eur. Polym. J.* 98 (2018). doi:10.1016/j.eurpolymj.2017.11.003.
- [61] X. Fernandez, J.M. Salla, A. Serra, A. Mantecón, X. Ramis, Cationic copolymerization of cycloaliphatic epoxy resin with a spirobis lactone with lanthanum triflate as initiator: I. Characterization and shrinkage, *J. Polym. Sci. Part A Polym. Chem.* 43 (2005). doi:10.1002/pola.20801.

- [62] X. Fernandez, X. Ramis, J.M. Salla, Cationic copolymerization of cycloaliphatic epoxy resin with an spirobis lactone with lanthanum triflate as initiator: Kinetics of the curing process, *Thermochim. Acta.* 438 (2005). doi:10.1016/j.tca.2005.07.012.
- [63] O. Konuray, N. Areny, J.M. Morancho, X. Fernández-Francos, À. Serra, X. Ramis, Preparation and characterization of dual-curable off-stoichiometric amine-epoxy thermosets with latent reactivity, *Polymer (Guildf).* 146 (2018) 42–52. doi:10.1016/j.polymer.2018.05.040.
- [64] G.A. Miller, L. Gou, V. Narayanan, A.B. Scranton, Modeling of photobleaching for the photoinitiation of thick polymerization systems, *J. Polym. Sci. Part A Polym. Chem.* 40 (2002) 793–808. <http://dx.doi.org/10.1002/pola.10162>.
- [65] M. Dušková-Smrčková, H. Valentová, A. Ďuračková, K. Dušek, Effect of Dilution on Structure and Properties of Polyurethane Networks. Pregel and Postgel Cyclization and Phase Separation, *Macromolecules.* 43 (2010) 6450–6462. doi:10.1021/ma100626d.
- [66] J. V Crivello, U. Varlemann, Structure and Reactivity Relationships in the Photoinitiated Cationic Polymerization of 3,4-Epoxy cyclohexylmethyl-3 prime ,4 prime -epoxycyclohexane Carboxylate, *ACS Symp. Ser.* 673 (1997) 82–94.
- [67] Y.-M. Kim, L. Kris Kostanski, J.F. MacGregor, Kinetic studies of cationic photopolymerizations of cycloaliphatic epoxide, triethyleneglycol methyl vinyl ether, and cyclohexene oxide, *Polym. Eng. Sci.* 45 (2005) 1546–1555. <http://dx.doi.org/10.1002/pen.20383>.
- [68] X. Fernandez-Francos, W.D. Cook, J.M. Salla, A. Serra, X. Ramis, Crosslinking of mixtures of DGEBA with 1,6-dioxaspiro[4,4]nonan-2,7-dione initiated by tertiary amines. III. Effect of hydroxyl groups on network formation., *Polym. Int.* 58 (2009) 1401–1410. doi:10.1002/pi.2675.

6 ACKNOWLEDGEMENTS

I would first like to thank my thesis advisor Dr. Marco Sangermano (Politecnico di Torino), Dr. Maria Angels Serra Albet (Universitat Rovira I Virgili), Dr. Xavier Ramis Juan (Universitat Politècnica de Catalunya), Dr. Xavier Fernández Francos (Universitat Politècnica de Catalunya) to provide me the chance to develop my project in their research group and the essential support, patience, helpfulness, needed.

The door to Prof. Xavier Fernández office was always open whenever I ran into a trouble spot or had a question about my research. He consistently allowed this paper to be my own work, but in the same time, steered me in the right direction whenever he thought I needed it.

Finally, I must express my very profound gratitude to my family. My parents, Cosimo Di Donato, Angela Raspaolo for supporting me with unfailing love, continuous encouragement and reassurance throughout my years of study and through this unforgettable thesis program. To my brother, Simone Di Donato which cared me unconditionally without ever leaving me alone. To my dearest friend, Giovanni Fiumanó, which ever boosted me.

In conclusion, the last thought to my sweet and lovable Melissa.

This triumph would not have been possible without them.

Thank you.

Di Donato Fabio

LIST OF FIGURES

Figure 1. Temperature scan versus Storage Modulus E' . Adapted from [2].....	25
Figure 2. Scheme of cross-linking network formation. Image adapted from [4].....	26
Figure 3. Viscosity (η) and Modulus vs. degree of conversion (α). Adapted from [5].....	27
Figure 4. $\tan\delta$ vs. time (t). Adapted from [6].....	28
Figure 5. Glass transition temperature vs. degree of conversion (α). Adapted from [4].....	29
Figure 6. CTT diagram. Adapted from [4].....	30
Figure 7. TTT diagram. Adapted from [6].....	30
Figure 8. Details of phenolic resins reaction. Adapted from [19].....	32
Figure 9. Polyurethanes scheme polymerization. Adapted from [20].....	33
Figure 13. Epoxy-Amine pathway reaction. Adapted from [5].....	33
Figure 14. Mechanism of the cationic ring-opening polymerization of epoxide monomers. Adapted from [35].....	36
Figure 16. Epoxy anionic polymerization steps. Adapted from [42].....	36
Figure 17. Dual-curing stages. Adapted from [51].....	40
Figure 18. Reaction scheme of click reaction. (A) Nucleophilic ring opening reaction, (B) Michael addition reaction, (C) Photochemical additions of thiols to alkenes and alkynes, and (D) Carbonyl addition of thiols to isocyanates. Adapted from [51].....	41
Figure 19. Chemical structures of reagents ES and CA, and of components of catalyst solution CI, TEA and PC.....	42
Figure 20. Mettler DSC-821e (left) and DSC-822e (right).....	44
Figure 21. DSC double scansion details. Adapted from [4].....	45
Figure 22. Sample preparation details.....	46
Figure 23. DMA typical scan. Adapted from [2].....	47
Figure 24. Dynamic mechanic analyzer TA instrument DMA Q800.....	47
Figure 25. Sample's accessories preparation.....	48
Figure 26. Vilber Lourmat UV-oven.....	48
Figure 27. Vertex 70 spectrometer Brukers and detail of ATR device.....	49
Figure 28. Mettler TGA/SDTA-851e Ultra-micro Balance.....	50
Figure 29. Crucibles for thermogravimetric analysis.....	50
Figure 30. ES50CII-0.1 after and before the soluble fraction analysis.....	51
Figure 31. Detail of the storage oil-bath.....	51
Figure 32. Isothermal DSC analysis (30°C) for the Spot-HT system. Degree of conversion (α) and rate of degree of conversion ($d\alpha/dt$) are charted respect the time.....	54
Figure 33. Dynamic DSC curves (10 °C/min) for investigated Spot-HT system. The blue curve is referred to the residual reaction heat after the dynamic-curing process. On the red curve is shown the T_g of Base-3D sample photo-cured in the UV-oven.....	55
Figure 34. Dynamic DSC measurement (10 °C/min) for Spot-HT system. As can be seen by the plotted peak, the reaction in triggered by the high temperature at 200°C to end at 250°C.....	55

Figure 35. FTIR spectrometry results of Spot-HT sample. The red curve is referred to the uncured formulation. The blue curve represents the cured formulation. Detail of 600-1800 cm^{-1} absorption band are plotted. 56

Figure 36. DMA analysis of UV-cured Spot-HT system at 3°C/min, frequency of 1 Hz and 0.05 % strain. ... 57

Figure 37. DSC measurement for the pure epoxy system. Rate of degrees of conversion ($d\alpha/dt$) versus temperature during the dynamic curing 10 (°C/min) for different TEA content ES100CI1-x are shown. 58

Figure 38. DSC dynamic measurement, for pure epoxy, at different heating rate of 1.25, 2.5, 5, 10 (°C/min). Evaluation rate of degrees of conversion ($d\alpha/dt$) versus temperature are plotted. 59

Figure 39. Comparison degrees of conversion (α) versus temperature for thermal curing of the net epoxy formulation. Heating rate of 1.25, 2.5, 5, 10 (°C/min) are shown. 59

Figure 40. DSC isothermal analysis for the epoxy system ES100CI1.0.1. Evaluation rate of degree of conversion ($d\alpha/dt$) versus time during different isothermal trials 90, 100, 110, 120 °C. 61

Figure 41. Kinetics analysis of net epoxy system. Experimental and simulated degree of conversion versus time for 90°C, 100°C, 110°C, 120°C isothermal trials. The solid lines represent the experimental data and the symbol correspond to the data calculated by using the parameters obtained with the Equation 11. 62

Figure 42. FTIR spectrometry results epoxy system ES100CI1-0.1. The red curve is referred to the cured formulation. The blue curve represents the uncured formulation. Detail of 600-1800 cm^{-1} absorption band are plotted. 63

Figure 43. DSC photo-curing kinetics for different dual-system formulation ESxCI1-0.1. Reaction heat for base-3D system and samples with 10%, 20%, 30%, 40%, 50% epoxy content into the formulation are shown at 10 (°C)/min heating rate respect to time. 65

Figure 44. DSC photo-curing analysis for different dual-system formulation ESxCI1-0.1. Simulated degrees of conversion (α) vs. time for Base-3D system and samples with 10%, 20%, 30%, 40%, 50% epoxy contents are charted. 65

Figure 45. FTIR spectrometry results of ES30CI1-0.1 formulation. The red curve is referred to the UV-cured sample. The blue curve indicates the uncured formulation. Detail of 600-1800 cm^{-1} absorption band are plotted. 66

Figure 46. DSC photo-curing kinetics for ES30CAxCI1-0.1 formulation. Reaction heat for samples with 1%, 2%, 5%, 10% coupling agent content into the formulation are shown at 10 (°C)/min heating rate. 67

Figure 47 DSC photo-curing analysis. Simulated degrees of conversion (α) vs. time for ES30CAxCI1-0.1 formulation with 1%, 2%, 5%, 10% coupling agent contents are shown at 10 (°C)/min heating rate. 67

Figure 48. Effect of the epoxy content on the T_g of the intermediate materials after photocuring. Experiments carried out at 10 °C/min after photocuring in the UV oven. 68

Figure 49. Results of the DMA dynamic analysis at 3 °C/min, 1 Hz and 0.05 % strain of Spot-HT and ESxCI1-0.1 intermediate formulation. Storage Modulus is shown. 69

Figure 50. Results of the DMA dynamic analysis at 3 °C/min, 1 Hz and 0.05 % strain of Spot-HT and ESxCI1-0.1 intermediate formulation. $\text{Tan}\delta$ is plotted in the graph. 70

Figure 51. Dynamic DSC curves for investigated Spot-HT and ES30CI1-0.1_Filtrate system. Rising T_g is shown at 10 (°C/min) heating rate. 71

Figure 52. FTIR spectra of soluble extract and insoluble filtrate after solubility analysis of ES50CI1-0.1 in dichloromethane. 72

Figure 53. DSC thermal-curing analysis for different ESxCI1-0.1 dual-systems. Reaction heat for the net epoxy formulation and samples with 10%, 20%, 30%, 40%, 50% epoxy contents are shown at 10 (°C)/min heating rate. 73

Figure 54. DSC dynamic measurement. Comparison of degrees of conversion (α) versus temperature during the thermal-curing process for different epoxy content. Heating rate of 10 (°C/min) shown. 73

Figure 55. FTIR spectrometry results of dual-system ES30CI1-0.1. The blue curve is referred to the UV-cured sample and the red curve indicates the fully polymerized formulation. Detail of 600-1800 cm ⁻¹ absorption band is plotted.	74
Figure 56. Comparison degree of conversion (α) versus temperature for the epoxy formulation ES30CI1-0.1. Heating rate of 1.25, 2.5, 5, 10 (°C/min) are shown.	75
Figure 57. Kinetics analysis for the epoxy formulation ES30CI1-0.1. Experimental and simulated degree of conversion (α) versus time for, 110°C, 120°C, 130°C isothermal trials. The solid lines represent the experimental data and the symbol correspond to the simulated data.	76
Figure 58. DMA analysis for ES30CI1-0.1 intermediate photo-cured material. E' (blue curve) and Tan δ (red curve) are plotted during the cross-linking process at constant heating rate of 3 °C/min, frequency of 1 Hz and 0.05 % strain.	77
Figure 59. Comparison between DSC and DMA measurement for epoxy formulation ES30CI1-0.1. Degree of conversion (α) vs. storage modulus (E') for the intermediate material are charted.	78
Figure 60. DMA and DSC analysis with same heating scheduled program. Degree of conversion and E' vs. time for ES30CI1-0.1 final curing formulation.	79
Figure 61. DSC thermal-curing analysis for the Spot-HT and ESxCI1-0.1 final formulation. T _g variations for samples with 10%, 20%, 30%, 40%, 50% epoxy content are shown at 10 (°C/min) heating rate.	80
Figure 62. Results of the DMA dynamic analysis at 3°C/min, 1 Hz and 0.05% strain of Spot-HT and ESxCI1-0.1 final formulation. Storage Modulus (E') is plotted.	80
Figure 63. Results of the DMA dynamic analysis at 3°C/min, 1 Hz and 0.05% strain of Spot-HT and ESxCI1-0.1 final formulation. Tan δ is plotted in the graph.	81
Figure 64. DMA measurement of epoxy ES30CI1-0.1 formulation. Comparison between storage modulus (E') and Tan δ for the UV-cured (red curves) and fully-cured (blue curves) samples.	82
Figure 65. Thermogravimetric analysis for different epoxy ESxCI1-0.1 formulation. Mass loss (m/m ₀) is plotted with respect to the temperature.	83
Figure 66. Weekly dynamic DSC analysis for ES30CI1-0.1 UV-cured reference sample. Different reaction heat are shown at 10 (°C/min) heating rate.	84

LIST OF TABLES

Table 1. Comparison of DSC evaluation of net epoxy system ES100CI1-0.1 and Spot-HT formulation. $\Delta h Jg$ is the heat released in the dynamic heating 10°C/min based on the sample's weight. $\Delta h (kJ/eq)$ is the heat liberated but calculated with an epoxy equivalent of 130 (g/eq).....	55
Table 2. Summary of reaction heat Δh (in J/g and kJ/eq) for pure epoxy formulation with different TEA content ES100CI1-x.	58
Table 3. Summary of the DSC dynamic analysis of ES100CI1-0.1 formulations for different heating rate 1.25, 2.5, 5, 10 (°C/min). $\Delta h (J/g)$ is the reaction heat released during the thermal curing. $\Delta hA (J/g)$ is the average reaction heat calculated on overall measurement.	59
Table 4. Kinetics parameters at different degrees of conversion, obtained using the Starink model, from experiments of pure epoxy formulation ES100CI1-0.1.....	60
Table 5. Comparison of Isothermal DSC analysis at different temperatures 90, 100, 110, 120 °C. $\Delta hISO (J/g)$ is the reaction heat released during the isothermal experiment. $\Delta hRES (J/g)$ is the residual heat generate during the dynamin analysis 10 (°C/min). $\Delta hTOT (J/g)$ is the total amount of heat produced during all the process. $\Delta hTOT (KJ/eq)$ is the heat liberated but calculated with an epoxy equivalent of 130 (g/eq). αiso us the calculated degree of cure in the isothermal experiments determined on the basis of the residual heat.....	61
Table 6. Summary of DSC analysis for the Spot-HT and different epoxy formulation ESxCI1-0.1. $\Delta hISO (J/g)$ is the isothermal reaction heat. $\Delta hRES (J/g)$ is the residual heat obtained from the dynamic experiment at 10 (°C/min). $\Delta hTOT (J/g)$ is the total amount of heat produced during the curing reaction. $T_{g1} (°C)$ is the glass transition temperature after photo-curing stage and $T_{g2} (°C)$ is the glass transition temperature of the fully polymerized sample.	65
Table 7. DSC analysis of a given epoxy formulation for different coupling agent (CA) concentration. $\Delta hISO (J/g)$ Is the heat released during the photo-curing stage. $\Delta hRES (J/g)$ Is the heat produced to complete the thermal curing process. $\Delta hTOT (J/g)$ Is the total quantity of heat developed during the dual-curing polymerization.....	67
Table 8. Summary of DMA analysis of Spot-HT and ESxCI1-0.1 intermediate formulation. Storage modulus (E'), loss modulus (E''), and $Tan\delta$ trend are tabled.	70
Table 9. Comparison between the experimental residual weight and the expected theoretical weight for the intermediate material.	71
Table 10. Comparison of DSC evaluation of net epoxy system ES100CI1-0.1 and of ESxCI1-0.1 formulations. $\Delta hexp Jg$ is the heat released in the dynamic heating 10 °C/min based on the sample's weight. $\Delta hexp kJeq$ is the heat liberated but calculated with an epoxy equivalent of 130 (g/eq).....	74
Table 11. Summary of the DSC dynamic analysis of ES30CI1-0.1 formulations for different heating rate 1.25, 2.5, 5, 10 (°C/min).	75
Table 12. Kinetics parameters at different degrees of conversion, obtained using the Starink model, from experiments of epoxy formulation ES30CI1-0.1.....	76
Table 13. Summary of DMA analysis of Spot-HT and ESxCI1-0.1 fully cured formulation.....	81
Table 14. Comparison between the experimental residual weight and the expected theoretical weight for the fully cured material.....	82
Table 15. DSC measurement for liquid and solid sample of epoxy formulation ES30CI1-0.1. $\Delta h1st$ is the heat released in the first isothermal UV-curing, $\Delta h2nd$ is the residual heat released in a subsequent heating process at 10 °C/min. $\Delta h Jg$ is the heat produced during the dynamic final-curing process (10 °C/min).....	84